

AD-A061 719

TENNESSEE UNIV SPACE INST TULLAHOMA
INVESTIGATION OF COANNULAR NOZZLES WITH CONVENTIONAL AND INVERT--ETC(U)
APR 78 B H GOETHERT, J R MAUS, W A DUNNILL DOT-FA72WA-3053

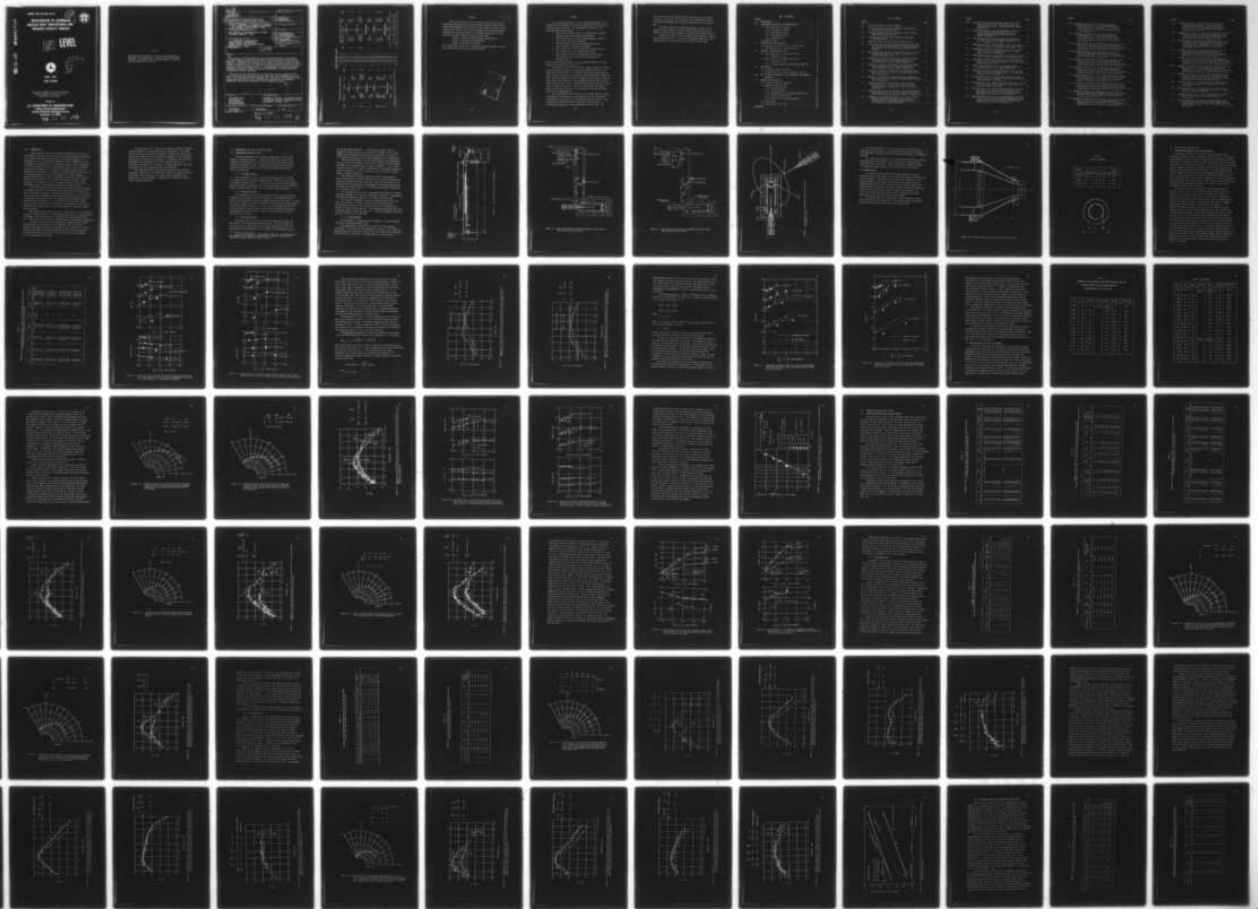
F/G 20/1

UNCLASSIFIED

FAARD-78-32

NL

1 OF 2
ADA
061719



REPORT NO. FAA-RD-78-32

12



**INVESTIGATION OF COANNULAR
NOZZLES WITH CONVENTIONAL AND
INVERTED VELOCITY PROFILES**

A

B. H. Goethert
J. R. Maus
W. A. Dunnill
I. Dathe
S. Venkitarama
L. Bates

LEVEL

AD A061719

DDC FILE COPY



APRIL 1978

FINAL REPORT

Document is available to the public through the
National Technical Information Service,
Springfield, Virginia 22161.

Prepared for

U.S. DEPARTMENT OF TRANSPORTATION

FEDERAL AVIATION ADMINISTRATION

Systems Research & Development Service

Washington, D.C. 20590

78 11 27 076

NOTICE

This document is disseminated under the sponsorship of the Department of Transportation in the interest of information exchange. The United States Government assumes no liability for its contents or use thereof.

| | | | |
|--|---|--|---|
| <p>18 19 Report FAA-RD-78-32</p> | <p>2. Government Accession No.</p> | <p>3. Recipient's Catalog No.</p> | |
| <p>4. Title and Subtitle Investigation of Coannular Nozzles With Conventional and Inverted Velocity Profiles,</p> | | <p>5. Report Date April 1978</p> | <p>6. Performing Organization Code</p> |
| <p>7. Author(s) B. H. / GOETHERT, J. R. / MAUS, W. A. / DUNNILL I. / DATHE, S. / VENKITARAMA L. BATES</p> | | <p>8. Performing Organization Report No.</p> | |
| <p>9. Performing Organization Name and Address THE UNIVERSITY OF TENNESSEE SPACE INSTITUTE TULLAHOMA, TENNESSEE 37388</p> | | <p>10. Work Unit No.</p> | <p>11. Contract or Grant No. DOT-FA72WA-3053</p> |
| <p>12. Sponsoring Agency Name and Address U.S. DEPARTMENT OF TRANSPORTATION FEDERAL AVIATION ADMINISTRATION SYSTEMS RESEARCH AND DEVELOPMENT SERVICE WASHINGTON, D.C. 20591</p> | | <p>13. Type of Report and Period Covered FINAL REPORT, SEPTEMBER 1976-APRIL 1978</p> | |
| <p>14. Sponsoring Agency Code ARD-550</p> | | <p>15. Supplementary Notes 12 14 pp.</p> | |
| <p>16. Abstract The results of the investigation of the noise characteristics of the exhaust jets from coannular nozzles with conventional and inverted velocity profiles are presented. Experiments were carried out on a series of coannular nozzles of equal primary and secondary area. The majority of acoustic tests were carried out holding either the total thrust or the total mass flow constant while varying the rates of secondary velocity to primary velocity. A limited number of tests were also made simulating the takeoff, cutback and approach conditions of the JT8D engine and corresponding inverted conditions. The results of this study show that at high thrust level the coannular flows with inverted velocity profiles are quieter than those with standard velocity profiles at the same thrust and the same mass flow. The acoustic differences are much greater when the velocity ratio is produced by differences in the stagnation temperature rather than by differences in the stagnation pressure.</p> | | | |
| <p>17. Key Words Aerodynamic Noise Aeroacoustics Noise Suppression Coannular Nozzles</p> | | <p>18. Distribution Statement Document is available to the public through the National Technical Information Service, Springfield, Virginia 22161</p> | |
| <p>19. Security Classif. (of this report) UNCLASSIFIED</p> | <p>20. Security Classif. (of this page) UNCLASSIFIED</p> | <p>21. No. of Pages 127</p> | <p>22. Price</p> |

387070
78 11 27 076 LB

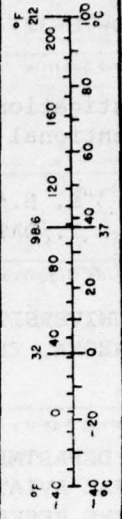
METRIC CONVERSION FACTORS

Approximate Conversions to Metric Measures

| Symbol | When You Know | Multiply by | To Find | Symbol |
|----------------------------|------------------------|----------------------------|---------------------|-----------------|
| LENGTH | | | | |
| in | inches | 2.5 | centimeters | cm |
| ft | feet | 30 | centimeters | cm |
| yd | yards | 0.9 | meters | m |
| mi | miles | 1.6 | kilometers | km |
| AREA | | | | |
| in ² | square inches | 6.5 | square centimeters | cm ² |
| ft ² | square feet | 0.09 | square meters | m ² |
| yd ² | square yards | 0.8 | square meters | m ² |
| mi ² | square miles | 2.6 | square kilometers | km ² |
| | acres | 0.4 | hectares | ha |
| MASS (weight) | | | | |
| oz | ounces | 28 | grams | g |
| lb | pounds | 0.45 | kilograms | kg |
| | short tons (2000 lb) | 0.9 | tonnes | t |
| VOLUME | | | | |
| tsp | teaspoons | 5 | milliliters | ml |
| Tbsp | tablespoons | 15 | milliliters | ml |
| fl oz | fluid ounces | 30 | milliliters | ml |
| c | cups | 0.24 | liters | l |
| pt | pints | 0.47 | liters | l |
| qt | quarts | 0.95 | liters | l |
| gal | gallons | 3.8 | liters | l |
| ft ³ | cubic feet | 0.03 | cubic meters | m ³ |
| yd ³ | cubic yards | 0.76 | cubic meters | m ³ |
| TEMPERATURE (exact) | | | | |
| °F | Fahrenheit temperature | 5/9 (after subtracting 32) | Celsius temperature | °C |

¹ 1 in = 2.54 (exact). For other exact conversions and more details, see NBS Mon. Publ. 286, Units of Weights and Measures, Price \$2.25, SD Catalog No. C-17-158.

| Symbol | When You Know | Multiply by | To Find | Symbol |
|----------------------------|-----------------------------------|-------------------|------------------------|-----------------|
| LENGTH | | | | |
| mm | millimeters | 0.04 | inches | in |
| cm | centimeters | 0.4 | inches | in |
| m | meters | 3.3 | feet | ft |
| m | meters | 1.1 | yards | yd |
| km | kilometers | 0.6 | miles | mi |
| AREA | | | | |
| cm ² | square centimeters | 0.16 | square inches | in ² |
| m ² | square meters | 1.2 | square yards | yd ² |
| km ² | square kilometers | 0.4 | square miles | mi ² |
| ha | hectares (10,000 m ²) | 2.5 | acres | |
| MASS (weight) | | | | |
| g | grams | 0.035 | ounces | oz |
| kg | kilograms | 2.2 | pounds | lb |
| t | tonnes (1000 kg) | 1.1 | short tons | |
| VOLUME | | | | |
| ml | milliliters | 0.03 | fluid ounces | fl oz |
| l | liters | 2.1 | pints | pt |
| l | liters | 1.06 | quarts | qt |
| l | liters | 0.26 | gallons | gal |
| m ³ | cubic meters | 35 | cubic feet | ft ³ |
| m ³ | cubic meters | 1.3 | cubic yards | yd ³ |
| TEMPERATURE (exact) | | | | |
| °C | Celsius temperature | 9/5 (then add 32) | Fahrenheit temperature | °F |



PREFACE

AD 24958
959
AD41982

This report describes part of the work carried out and results obtained by The University of Tennessee Space Institute under Contract Number DOT-FA72WA-3053. Earlier work on this contract has been reported in Report No. FAA-RD-75-162 entitled "Investigation of Feasible Nozzle Configurations for Noise Reduction in Turbofan and Turbojet Aircraft" consisting of three volumes subtitled as shown below:

Volume I Summary and Multi-Nozzle Configurations

Volume II Slot Nozzle Configurations

Volume III Shrouded Slot Nozzles

The present report deals with the research program on coannular nozzles with conventional and inverted velocity profiles.

| | |
|-----------------------|---------|
| ACCESSION NO. | |
| 478 | |
| 302 | |
| SEARCHED | INDEXED |
| SERIALIZED | FILED |
| DISTRICT HEADQUARTERS | |
| ADLITY CODES | |
| A | SPECIAL |

SUMMARY

An in-depth investigation of the noise characteristics of the exhaust jets from coannular nozzles with conventional and inverted profiles has been carried out. The investigation consisted of five principle phases listed below:

1. Reverberation Chamber Tests on a 2-inch nominal diameter coannular nozzle under cold flow conditions.
2. Free Field Tests on a 4-inch nominal diameter coannular nozzle under cold flow conditions.
3. Free Field Tests on the 4-inch diameter nozzle with either primary or secondary flow heated.
4. Free Field Tests on an 8-inch diameter coannular nozzle with either primary or secondary flow heated.
5. Laser Doppler Velocimeter measurements on the exhaust flow from the 4-inch nozzle with conventional and inverted profiles.

All tests were performed using circular coannular nozzles with equal primary and secondary area ($A_s/A_p = 1$).

The results of this study show that coannular flows with inverted velocity profiles are quieter than standard velocity profiles at the same thrust and mass flow. The acoustic differences between these two types of flow are much greater when the velocity differences between the inner and outer streams are caused by changes in the stagnation temperatures rather than by changes in the stagnation pressure ratios of the primary and secondary flows. The major differences in the sound fields occur at angles less than 45° from the jet axis, where the greatest noise is radiated, and result from a reduction of the peak frequency noise of the standard profile.

The reduction in noise obtained by the inverted velocity profile is thought to be largely due to the rapid decay of the maximum mean velocity that occurs compared to the standard velocity profiles. This implies that the source convection velocity is reduced with a corresponding reduction in sound radiated near the jet axis. The

fact that the effect is enhanced when the secondary flow is heated is due to the fact that the low density, high temperature secondary air loses its momentum more rapidly by mixing with the cold ambient air.

The noise reduction obtainable by mixing a standard profile coannular flow to produce a uniform velocity profile with the same thrust is less than that attainable by inverting the standard profile.

Standard jet noise scaling techniques can be applied to coannular flows with inverted velocity profiles to determine large scale noise levels from model tests provided the area ratios are the same.

TABLE OF CONTENTS

| CHAPTER | | |
|------------|---|-----|
| 1.0 | INTRODUCTION | 1 |
| 2.0 | EXPERIMENTAL FACILITIES AND MODEL NOZZLES. | 3 |
| | 2.1 Aeroacoustic Test Facilities. | 3 |
| | 2.1.1 Air Supply Systems | 3 |
| | 2.1.2 Reverberation Room | 3 |
| | 2.1.3 Free Field Facility. | 3 |
| | 2.1.4 Instrumentation. | 4 |
| | 2.2 Models Tested | 9 |
| 3.0 | ACOUSTIC DATA FOR COLD FLOW. | 12 |
| | 3.1 Reverberation Chamber Tests on 2-Inch Nozzle. | 12 |
| | 3.2 Free Field Data for Four-Inch Nozzle. | 24 |
| 4.0 | ACOUSTIC DATA FOR HEATED FLOW. | 37 |
| | 4.1 Free Field Results for Four-Inch Nozzle | 37 |
| | 4.1.1 JT8D Test Series | 51 |
| | 4.2 Free Field Tests on Eight-Inch Nozzle | 56 |
| | 4.2.1 JT8D Test Series | 59 |
| | 4.2.2 Constant Thrust and Constant Mass Flow Series. | 80 |
| 5.0 | DISCUSSION | 90 |
| | 5.1 Mechanism of Noise Reduction. | 90 |
| | 5.2 Noise Reduction Potential of Inverted Profiles. | 97 |
| 6.0 | FLUID DYNAMIC MEASUREMENTS FOR CONVENTIONAL AND INVERTED PROFILES. | 103 |
| 7.0 | SUMMARY AND CONCLUSIONS. | 119 |
| | 7.1 Overview of the Investigation | 119 |
| | 7.2 Summary of Major Results. | 120 |
| | 7.2.1 Cold Flow Results. | 120 |
| | 7.2.2 Hot Flow Results | 121 |
| | 7.2.3 Comparison with Synthesized and Mixed Flow | 122 |
| | 7.2.4 Effect of Nozzle Size. | 123 |
| | 7.2.5 Results of the LDV Measurements. | 123 |
| | 7.3 Conclusions | 124 |
| | 7.4 Limitations of the Study. | 124 |
| REFERENCES | | 126 |

LIST OF FIGURES

| FIGURE | | PAGE |
|--------|---|------|
| 2.1 | Free Field Facility Stilling Chambers | 5 |
| 2.2 | Free Field Facility Piping Arrangement for Hot Primary Flow and Cold Secondary Flow. | 6 |
| 2.3 | Free Field Facility Piping Arrangement for Cold Primary Flow and Hot Secondary Flow | 7 |
| 2.4 | Free-Field Facility Microphone Sweep Plan and Nozzle Coordinate System | 8 |
| 2.5 | Eight-Inch Nozzle and Free Field Transition Piece | 10 |
| 3.1 | Sound Power Level and Mass Flow Rate Versus Velocity Ratio for the 2-Inch Coannular Nozzle at Ambient Temperature and Constant Total Thrust/Unit Area (Reverberation Chamber). | 16 |
| 3.2 | Sound Power Level and Thrust Versus Velocity Ratio for the 2-Inch Coannular Nozzle at Ambient Temperature and Constant Total Mass Flow. | 17 |
| 3.3 | Comparison of Sound Power Spectra for Two Velocity Ratios at Constant Mass Flow and Constant Thrust for the 2-Inch Coannular Nozzle at Ambient Temperature. | 19 |
| 3.4 | Comparison of Sound Power Spectra for Two Velocity Ratios at Constant Mass Flow and Constant Thrust for the 2-Inch Coannular Nozzle at Ambient Temperature. | 20 |
| 3.5 | Comparison of Measured Sound Power Data with Synthesized Power and Fully Mixed Power for Constant Thrust Series with 2-Inch Nozzle. | 22 |
| 3.6 | Comparison of Measured Sound Power Data with Synthesized Power and Fully Mixed Power for Constant Mass for Series with 2-Inch Nozzle. | 23 |
| 3.7 | OASPL Directivities in the XZ Plane of the Four-Inch Coannular Nozzle for Two Velocity Ratios at Ambient Temperature and a Constant Thrust Per Unit Area of 11.10 lb/in^2 | 30 |
| 3.8 | OASPL Directivities in the XZ Plane of the 4-Inch Coannular Nozzle for Two Velocity Ratios at Ambient Temperature and a Constant Mass Flow Per Unit Area of $.37 \text{ lbs/sec in}^2$. | 31 |
| 3.9 | Comparison of Sound Pressure Spectra at $\theta = 30^\circ$ in the XZ Plane for Two Velocity Ratios of the Four-Inch Coannular Nozzle at Constant Thrust per Unit Area of 11.10 lbs/in^2 at Ambient Temperature. | 32 |

| FIGURE | PAGE |
|--------|---|
| 3.10 | Variation of Overall Sound Pressure Level at 30° and Mass Flow Per Unit Area with Velocity Ratio for Constant Thrust Series. (Four-Inch Nozzle, Ambient Temperature) 33 |
| 3.11 | Variation of Overall Sound Pressure Level at 30° and Thrust Per Unit Area with Velocity Ratio for Constant Mass Flow Series (Four-Inch Nozzle, Ambient Temperature) 34 |
| 3.12 | Correlation Sound Pressure Data with Jet Exit Velocity for Inner Circular Nozzle OASPL Standardized for $D_n = 4$ Inches and $R = 13$ feet. 36 |
| 4.1 | OASPL Directivities in the XZ Plane of the 4-Inch Coannular Nozzle at Elevated Temperatures and Constant Thrust. . . 42 |
| 4.2 | Comparison of Sound Pressure Spectra at $\theta = 30^\circ$ in the XZ Plane of the 4-Inch Coannular Nozzle at Constant Thrust and Elevated Temperature. 43 |
| 4.3 | OASPL Directivities in the XZ Plane of the 4-Inch Coannular Nozzle at Elevated Temperatures and Constant Thrust. . . 44 |
| 4.4 | Comparison of Sound Pressure Spectra at $\theta = 30^\circ$ in the XZ Plane of the 4-Inch Coannular Nozzle at Constant Thrust and Elevated Temperature 45 |
| 4.5 | OASPL in the XZ Plane of the 4-Inch Coannular Nozzle at Elevated Temperature and Constant Mass Flow. 46 |
| 4.6 | Comparison of Sound Pressure Spectra at $\theta = 30^\circ$ in the XZ Plane of the 4-Inch Coannular Nozzle at Constant Mass Flow and Elevated Temperature. 47 |
| 4.7 | Sound Pressure Level, Mass Flow, and Energy Input Versus Velocity Ratio for Constant Thrust/Area = 14.30 lb/in^2 (Four-Inch Nozzle, Hot Flow) 49 |
| 4.8 | Sound Pressure Level, Thrust, and Energy Input Versus Velocity Ratio for Constant Mass Flow/Area = 0.52 lb/sec in^2 , (Four-Inch Nozzle, Hot Flow) 50 |
| 4.9 | Comparative Directivities for Simulated Takeoff Conditions A and D for the JT8D Series with 4-Inch Nozzle at Mean Thrust Per Unit Area of 21.88 lb/in^2 and Mean Mass Flow Per Unit Area of $0.553 \text{ lb/sec in}^2$ 54 |
| 4.10 | Comparative Spectra at 30° for Simulated Takeoff Conditions A and D for the JT8D Series with 4-Inch Nozzle at Mean Thrust Per Unit Area of 21.88 lb/in^2 and Mean Mass Flow Per Unit Area of $0.553 \text{ lb/sec in}^2$ 55 |

4.11 Comparative Directivities for Simulated Approach
 Conditions C and F for the JT8D Series with the
 Four-Inch Nozzle at Mean Thrust Per Unit Area of
 12.10 lb/in² and Mean Mass Flow Per Unit Area of
 0.337 lb/sec in² 57

4.12 Comparative Spectra at 30° for Simulated Approach
 Conditions C and F for the JT8D Series with the
 Four-Inch Nozzle at Mean Thrust Per Unit Area of
 12.10 lb/in² and Mean Mass Flow Per Unit Area of
 0.337 lb/sec in² 58

4.13 Directivities for Simulated JT8D Takeoff Conditions A and D
 Comparing 8-Inch Nozzle Data with Scaled Four-Inch
 Nozzle Data at Mean Thrust Per Unit Area of 22.54 lb/in²
 and Mean Mass Flow Per Unit Area of 0.552 lb/sec in² . . . 62

4.14 Comparative Spectra of the 8-Inch Nozzle at 30° for
 Simulated JT8D Takeoff Conditions A and D at Mean
 Thrust Per Unit Area of 23.20 lb/in² and Mean Mass Flow
 Per Unit Area of 0.551 lb/sec in². 63

4.15 Comparison of 8-Inch Nozzle Spectra with Scaled Four-Inch
 Nozzle Spectra at 30° for Simulated JT8D Takeoff
 Condition A at Mean Thrust Per Unit Area of 22.58 lb/in²
 and Mean Mass Flow Per Unit Area of 0.555 lb/sec in² . . . 64

4.16 Comparison of 8-Inch Nozzle Spectra with Scaled Four-Inch
 Nozzle Spectra at 30° for Simulated JT8D Takeoff
 Condition D at Mean Thrust Per Unit Area of 22.50 lb/in²
 and Mean Mass Flow Per Unit Area of 0.549 lb/sec in² . . . 65

4.17 Comparative Spectra at $\theta = 90^\circ$ of the 8-Inch Coannular Nozzle
 for Simulated JT8D Takeoff Conditions A and D at Mean
 Thrust Per Unit Area of 23.20 lb/in² and Mean Mass
 Flow Per Unit Area of 0.551 lb/sec in² 66

4.18 Directivities for Simulated JT8D Cutback Conditions B and E
 Comparing Eight-Inch Nozzle Data with Scaled Four-Inch
 Nozzle Data at Mean Thrust Per Unit Area of 17.82 lb/in²
 and Mean Mass Flow Per Unit Area of 0.483 lb/sec in² . . . 69

4.19 Comparative Spectra of the Eight-Inch Nozzle at 30° for
 Simulated JT8D Cutback Conditions B and E at Mean Thrust
 Per Unit Area of 17.86 lb/in² and Mean Mass Flow Per
 Unit Area of 0.488 lb/sec in². 70

4.20 Comparison of Eight-Inch Nozzle Spectra with Scaled Four-Inch
 Nozzle Spectra at 30° for Simulated JT8D Cutback
 Condition B at Mean Thrust Per Unit Area of 17.82 lb/in²
 and Mean Mass Flow Per Unit Area of 0.484 lb/sec in² . . . 71

| | | |
|------|--|----|
| 4.21 | Comparison of Eight-Inch Nozzle Spectra with Scaled Four-Inch Nozzle Spectra at 30° for Simulated JT8D Cutback Condition E at Mean Thrust Per Unit Area of 17.82 lb/in^2 and Mean Mass Flow Per Unit Area of $0.482 \text{ lb/sec in}^2$ | 72 |
| 4.22 | Comparative Spectra at $\theta = 90^\circ$ of the Eight-Inch Coannular Nozzle for Simulated JT8D Cutback Conditions B and E at Mean Thrust Per Unit Area of 17.86 lb/in^2 and Mass Flow Per Unit Area of $0.488 \text{ lb/sec in}^2$ | 73 |
| 4.23 | Directivities for Simulated JT8D Approach Conditions C and F Comparing Eight-Inch Nozzle Data with Scaled Four-Inch Nozzle Data at Mean Thrust Per Unit Area of 11.90 lb/in^2 and Mean Mass Flow Per Unit Area of $0.358 \text{ lb/sec in}^2$ | 74 |
| 4.24 | Comparative Spectra of the Eight-Inch Nozzle at 30° for Simulated JT8D Approach Conditions C and F at Mean Thrust Per Unit Area of 11.70 lb/in^2 and Mean Mass Flow Per Unit Area of $0.380 \text{ lb/sec in}^2$ | 75 |
| 4.25 | Comparison of Eight-Inch Nozzle Spectra with Scaled Four-Inch Nozzle Spectra at 30° for Simulated JT8D Approach Condition C at Mean Thrust Per Unit Area of 11.85 lb/in^2 and Mean Mass Flow Per Unit Area of $0.385 \text{ lb/sec in}^2$ | 76 |
| 4.26 | Comparison of Eight-Inch Nozzle Spectra with Scaled Four-Inch Nozzle Spectra at 30° for Simulated JT8D Approach Condition F at Mean Thrust Per Unit Area of 11.95 lb/in^2 and Mean Mass Flow Per Unit Area of $0.332 \text{ lb/sec in}^2$ | 77 |
| 4.27 | Comparative Spectra at $\theta = 90^\circ$ of the Eight-Inch Coannular Nozzle for Simulated JT8D Approach Conditions C and F at Mean Thrust Per Unit Area of 11.70 lb/in^2 and Mean Mass Flow Per Unit Area of $0.380 \text{ lb/sec in}^2$ | 78 |
| 4.28 | Comparison of Noise from Conventional and Inverted Profiles for Four-Inch and Eight-Inch Nozzles for the JT8D Test Series. | 79 |
| 4.29 | OASPL Directivities in the XZ Plane of the 8-Inch Coannular Nozzle at Elevated Temperature and a Constant Thrust Per Unit Area of 18.1 lbs/in^2 | 83 |
| 4.30 | Comparative Spectra at $\theta = 30^\circ$ of the Eight-Inch Coannular Nozzle at a Constant Thrust Per Unit Area of 18.1 lbs/in^2 | 84 |
| 4.31 | Sound Pressure Level, Mass Flow, and Energy Input Versus Velocity Ratio for the Constant Thrust Series with the 8-Inch Coannular Nozzle. $\text{Th/A} = 18.1 \text{ lb/in}^2$, (Hot Flow, Table 4.5a). | 85 |

| FIGURE | PAGE |
|--------|--|
| 4.32 | OASPL Directivities in the XZ Plane of the Eight-Inch Coannular Nozzle at Elevated Temperatures and a Constant Mass Flow Per Unit Area of .36 lbs/sec in ² . . . 87 |
| 4.33 | Comparative Spectra of the Eight-Inch Nozzle at 30° for Test Conditions P and L at a Constant Mass Flow Per Unit Area of .36 lbs/sec in ² 88 |
| 4.34 | Sound Pressure Level, Thrust, and Energy Input Versus Velocity Ratio for the Constant Mass Flow Series with the 8-Inch Coannular Nozzle, $\dot{m}/A = 0.36 \text{ lb/sec in}^2$, (Hot Flow, Table 4.5a). 89 |
| 5.1 | Effects of Convection and Refraction on the Sound Radiated from Randomly Oriented Quadrupoles. 92 |
| 5.2 | Mean Velocity Data from Reference [12] (Cold Flow) 94 |
| 5.3 | Schematic of Flow-Acoustic Interaction for Conventional and Inverted Velocity Profiles. 96 |
| 5.4 | Relative Position of a Observer to Moving Aircraft 99 |
| 5.5 | Comparison of Static Directivities for Conventional and Inverted JT8D Conditions with Four-Inch Nozzle. 100 |
| 5.6 | Comparison of Estimated OASPL Directivities for Conventional and Inverted JT8D Conditions with a Forward Velocity of 300 ft/sec. 101 |
| 6.1 | Photograph of LDV System Mounted on the Free Field Facility. 104 |
| 6.2 | Photograph of Laser and Optics Mounted on Rail-Platform Assembly. 105 |
| 6.3 | Schematic Diagram of Laser Velocimeter Optics. 106 |
| 6.4 | Mean Velocity Profiles for Approach Condition C with Conventional Exit Velocity Profile. 109 |
| 6.5 | Turbulence Intensity Profiles for Approach Condition C with Conventional Exit Velocity Profile. 110 |
| 6.6 | Mean Velocity Profiles for Approach Condition F with Inverted Exit Velocity Profile. 112 |
| 6.7 | Turbulence Intensity Profiles for Approach Condition F with Inverted Exit Velocity Profile 113 |
| 6.8 | Comparison of Maximum Mean Velocities for Standard and Inverted Conditions (LDV Data). 114 |
| 6.9 | Comparison of Turbulence Velocities for Standard and Inverted Conditions (LDV Data). 115 |
| 6.10 | Decay of Maximum Velocity, Comparison of Standard and Inverted Configuration, Constant Thrust Series, 11.1 lb/in ² 117 |

LIST OF SYMBOLS

| | |
|-----------|--|
| A | Area |
| a_o | Ambient Speed of Sound |
| D | Diameter |
| M | Mach Number |
| \dot{m} | Mass Flow Rate |
| OASPL | Overall Sound Pressure Level, dB |
| P | Pressure |
| PWL | Sound Power Level |
| R | Radial Distance |
| r | Radial Coordinate Measured from x Axis |
| U | Local Mean Velocity |
| u' | Turbulence Velocity |
| V | Jet Exit Velocity |
| x,y,z | Coordinate Axes |
| θ | Polar Angle Measured from Flow Axis |
| ρ | Density |

Subscripts

| | |
|---|-----------------------|
| c | Convection |
| e | Exit |
| m | Mixed |
| n | Nozzle |
| o | Stagnation or Ambient |
| p | Primary |
| s | Secondary |
| t | Total |

1.0 INTRODUCTION.

A most successful method for reducing the exhaust noise levels of jet engines is based on the bypass principle, which provides for additional air to bypass the primary gas generator of the turbojet engine, have it energized by a fan, and afterwards exhausted into the atmosphere. It was considered to be essential that the bypass air exhaust into the atmosphere at velocities lower than those of the primary airflow. Since the exhaust velocity of the primary air is reduced by the energy transfer from the primary air to the bypass air through the turbofan system, the mean velocity of the engine exhaust is reduced in comparison to straight turbojet engines of equal thrust. Both the reduction of the mean exhaust velocity level and the low velocity of the bypass air combine to affect a large reduction of the exhaust jet noise. The bypass method has been applied, with great success, to most commercial subsonic aircraft of today.

Recent experiments (1,2) have shown that the usual method of keeping the exhaust velocity of the bypass air lower than that of the primary air does not necessarily produce the maximum noise attenuation. To the contrary, it was found that considerably greater noise attenuation could be achieved, in some cases, by having the bypass air deliberately exhaust with higher velocities than the primary air. In contrast to the "standard" exhaust velocity profile, that is with the bypass air exhausting with lower velocity than that of the primary air, the new scheme employs an "inverted" exhaust velocity profile.

The purpose of the research under the current contract is to investigate the noise reducing potential of bypass engines with inverted velocity profiles, to determine the optimum parameters for velocity and temperature profiles, and to shed light into the physical reasons behind the experimental observations.

In order to explore the relative merits of coannular nozzle systems, employing either the "standard" or the "inverted" velocity profile, a series of experimental studies was conducted in which gradually the velocity profile of the exhaust was changed from one extreme to the other extreme. The experiments were conducted for cold flow and for hot flow conditions up to air temperatures of 1,480°R.

Most experiments were conducted with coannular nozzles having an external diameter of 4-inches and 8-inches, respectively. With these nozzles, the sound pressure and the spectra at several key locations in the far-field around the nozzle exhaust were measured in the free-field aeroacoustic test stand at the Institute. In addition, some preliminary experiments were conducted with a 2-inch coannular nozzle in the reverberation chamber of the Institute. In these experiments, the total sound power and its frequency spectrum were determined.

Some experiments with the 4-inch and 8-inch nozzles simulated operational conditions of the JT8D engine, typical for takeoff, cut-back, and approach flight conditions. In these special experiments, the exhaust profile was established to simulate both "standard" as well as "fully inverted" conditions.

2.0 EXPERIMENTAL FACILITIES AND MODEL NOZZLES.

2.1 Aeroacoustic Test Facilities.

The UTSI aeroacoustic test facility is comprised of an air supply system, a reverberation room, an outdoor free field test stand, and the associated instrumentation. Since these facilities have been described in detail in Reference 3, only a brief description will be given in this report with emphasis on the special modifications which were required for the present study.

2.1.1 Air Supply System.

Air is supplied to the test facilities through a system of piping from three 250 ft³, high pressure storage tanks. Control of the air flow is achieved through the use of a 4-inch control valve and two dome regulators. A mass flow meter is installed in the piping upstream of the test facilities. Manual valves are used to direct the air to each of the test stands.

2.1.2 Reverberation Room.

The reverberation room is used to measure the total sound power level radiated by a jet without regard to directivity. The reverberation room used in this investigation is made of heavy plywood and is 8 ft long, 7 ft wide, and 6 1/2 ft high with a volume of 360 ft³. During testing the only opening is an 8-inch diameter exhaust duct. Air flow to the primary and secondary stilling chambers for the coannular nozzle tests is controlled by means of two independent throttling valves. Two 1/4 inch microphones are used to obtain the acoustic data.

2.1.3 Free Field Facility.

The outdoor free field facility is used to measure the spectra and directivity of the sound pressure levels of jets. The major elements of the free field test stand include the stilling chamber, which is 11 feet long and has an inside diameter of 25.75 inches, its supporting structure,

[†]After the experiments on the coannular nozzle for this investigation were completed, the Institute's reverberation chamber was replaced by a considerably larger chamber of 5600 ft³ volume.

and the microphone sweep arms. A kerosene fueled heater makes it possible to conduct tests at temperatures up to 1480°R. The stilling chamber may be raised and lowered from the horizontal to an angle of 35.5° above the horizontal to facilitate changes in test configurations.

Several modifications to the free field facility were necessary in order to conduct the coannular nozzle tests. An inner stilling chamber was added to the original chamber as shown in Figure 2.1. The acoustic liner was installed to attenuate unwanted noise. An additional section of piping was installed in order to supply air to the secondary stilling chamber as shown in Figure 2.2.

The experimental program required that tests be conducted for heated inner flow and cold outer flow and for the reverse conditions with the outer flow heated and the inner cold. Since only one stream of the supply air could be heated some rearrangement of the piping was necessary to produce the latter conditions. The piping arrangement for heated outer flow is shown in Figure 2.3.

For the high mass flow tests it was found that original fuel supply system was inadequate to attain the temperatures required. A supplementary fuel injection system was installed to alleviate this difficulty.

Two 1/4 inch microphones were used to obtain acoustic data at the free field facility. In order to obtain sound pressure levels at several angles relative to the nozzle exit one of the microphones was mounted on a motor driven sweep arm. The microphone sweep plane and nozzle coordinate system is shown in Figure 2.4. The second microphone, when used, was kept stationary in the YX plane.

2.1.4. Instrumentation.

The aeroacoustic instrumentation is composed of a flow measurement system and a sound measurement system.

Sound measurements are made with 1/4 inch B & K 4136 Condenser microphones. The signal from one microphone is fed into a B & K Frequency Analyzer Type 2112, and then recorded on the B & K Level Recorder Type 2305. The Aeroacoustics Laboratory is equipped with two of these systems.

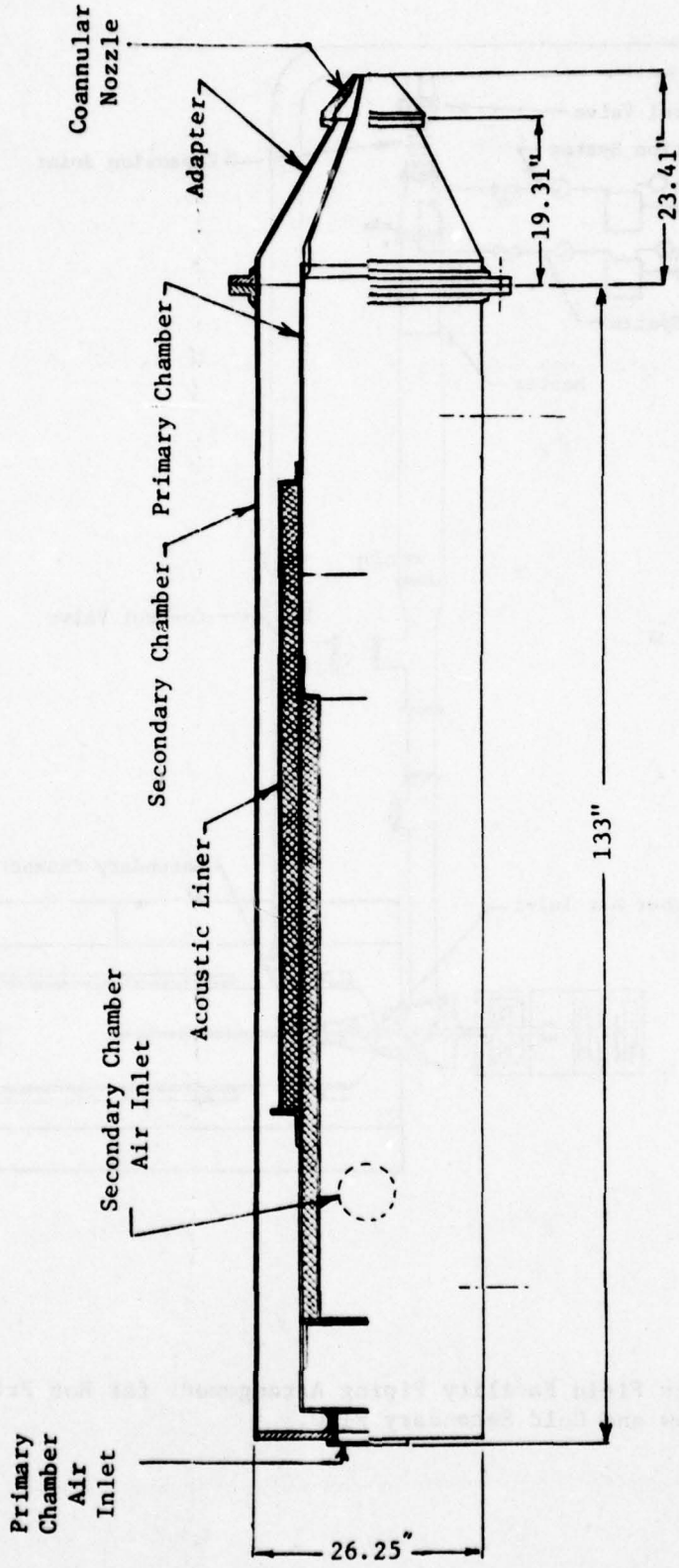


Figure 2.1. Free Field Facility Stilling Chambers.

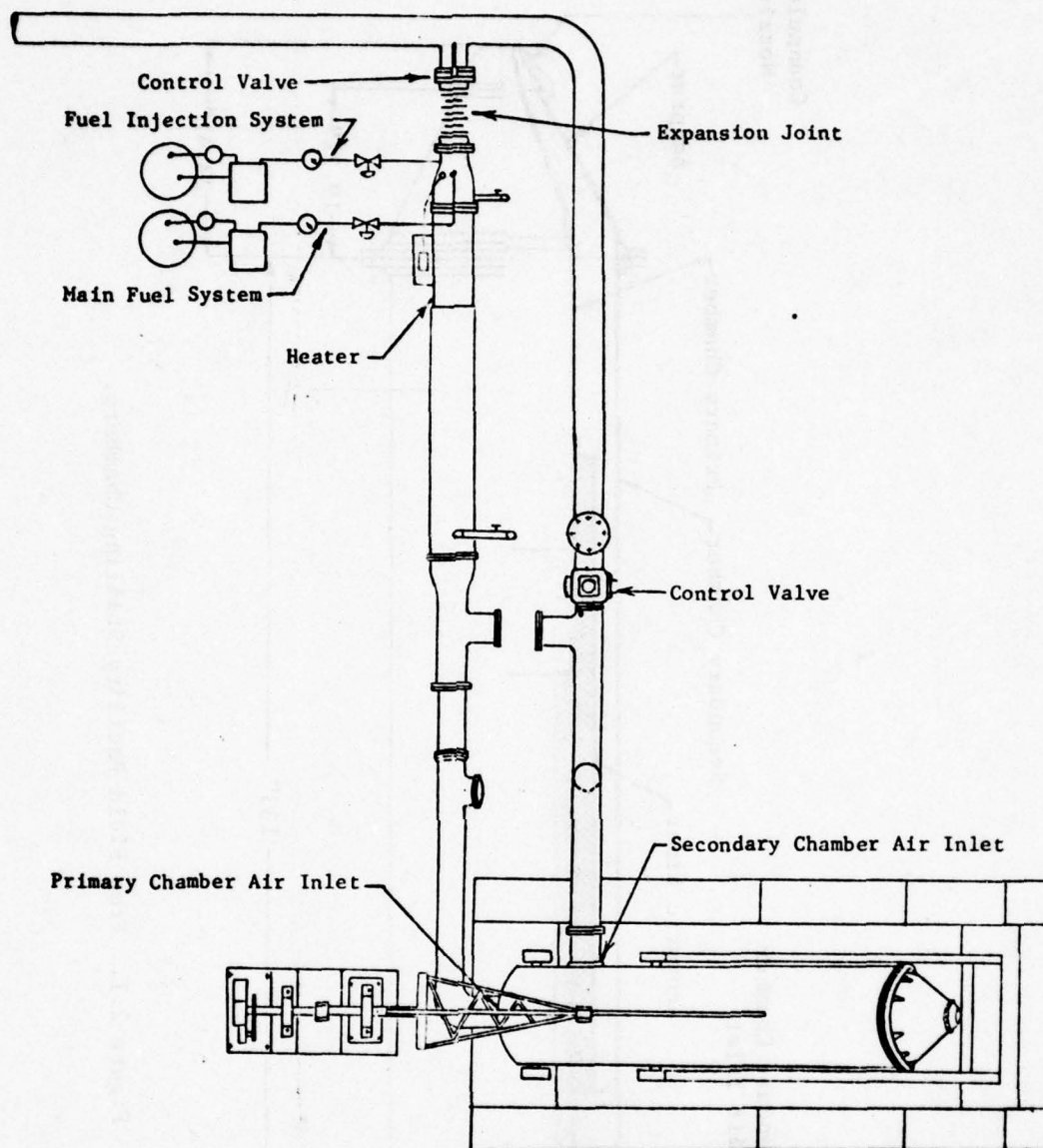


Figure 2.2. Free Field Facility Piping Arrangement for Hot Primary Flow and Cold Secondary Flow.

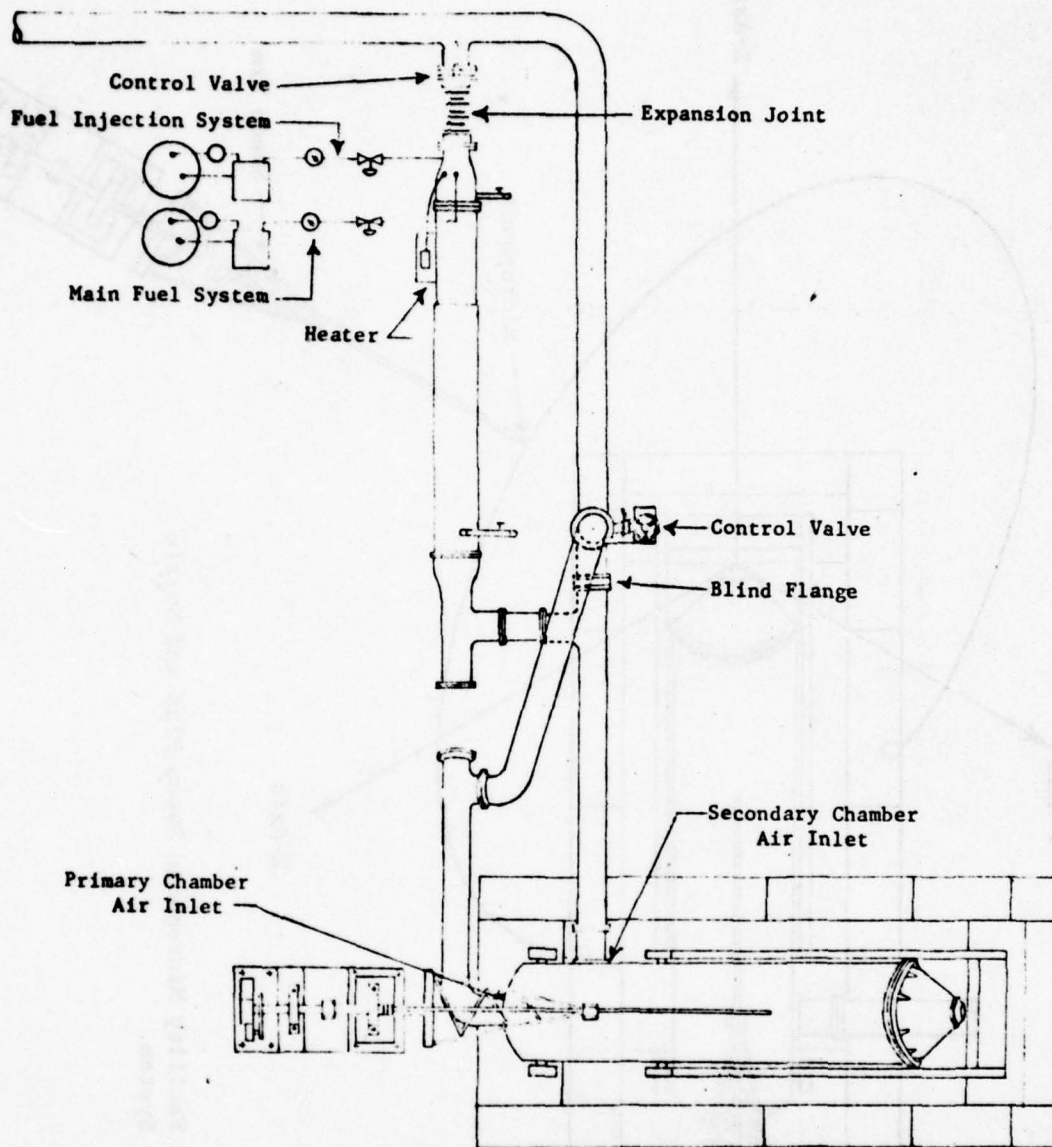


Figure 2.3. Free Field Facility Piping Arrangement for Cold Primary Flow and Hot Secondary Flow.

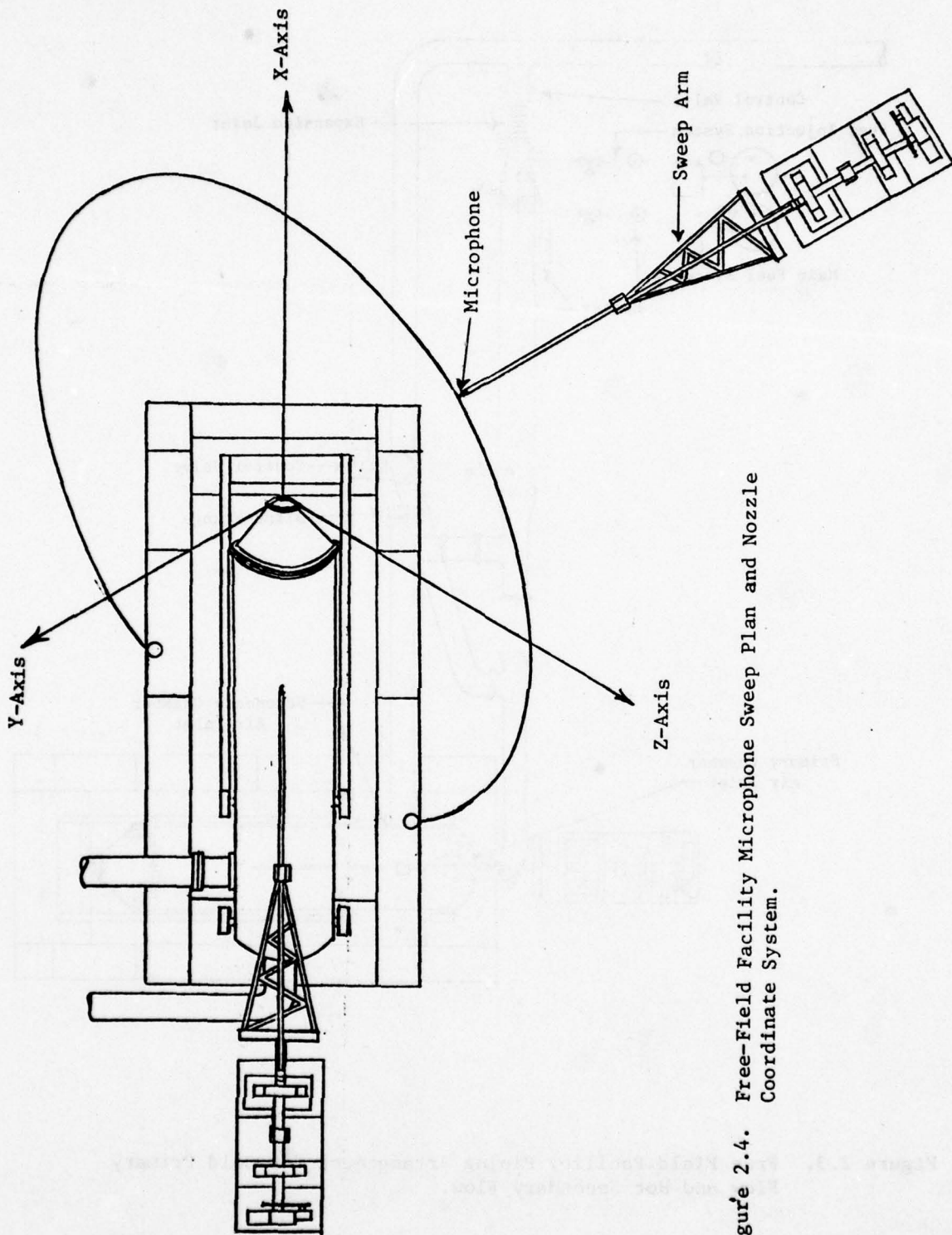


Figure 2.4. Free-Field Facility Microphone Sweep Plan and Nozzle Coordinate System.

The bulk flow conditions at the nozzle exit are determined by measuring stilling chamber pressures and temperatures and then applying one-dimensional, isentropic flow relations for the expansion to atmospheric pressure.

For some test conditions of the 4-inch nozzle, the velocity profiles were measured for both standard and inverted flow at several stations downstream of the nozzle exit. These measurements, conducted by means of a Laser Velocimeter are reported in Section 6.0 of this report.

2.2 Models Tested.

Acoustic tests were carried out on three different coannular, coplanar nozzles. Each nozzle is of the same basic design, differing only by a scale factor. In this report the nozzles are referred to by the nominal diameter of the larger circular nozzle. The inner and outer diameters were fixed so that the exit area for the inner (primary) and outer (secondary) streams were the same. Figure 2.5 shows the dimensions of the 8-inch nozzle and the manner in which it was mounted on the free field facility stilling chamber. Table 2.1 gives the pertinent dimensions for the nozzles used in this test program.

The two-inch nozzle was tested only in the reverberation chamber and only under cold flow conditions. The 4-inch and 8-inch nozzles were tested in the free field facility with cold and hot flow.

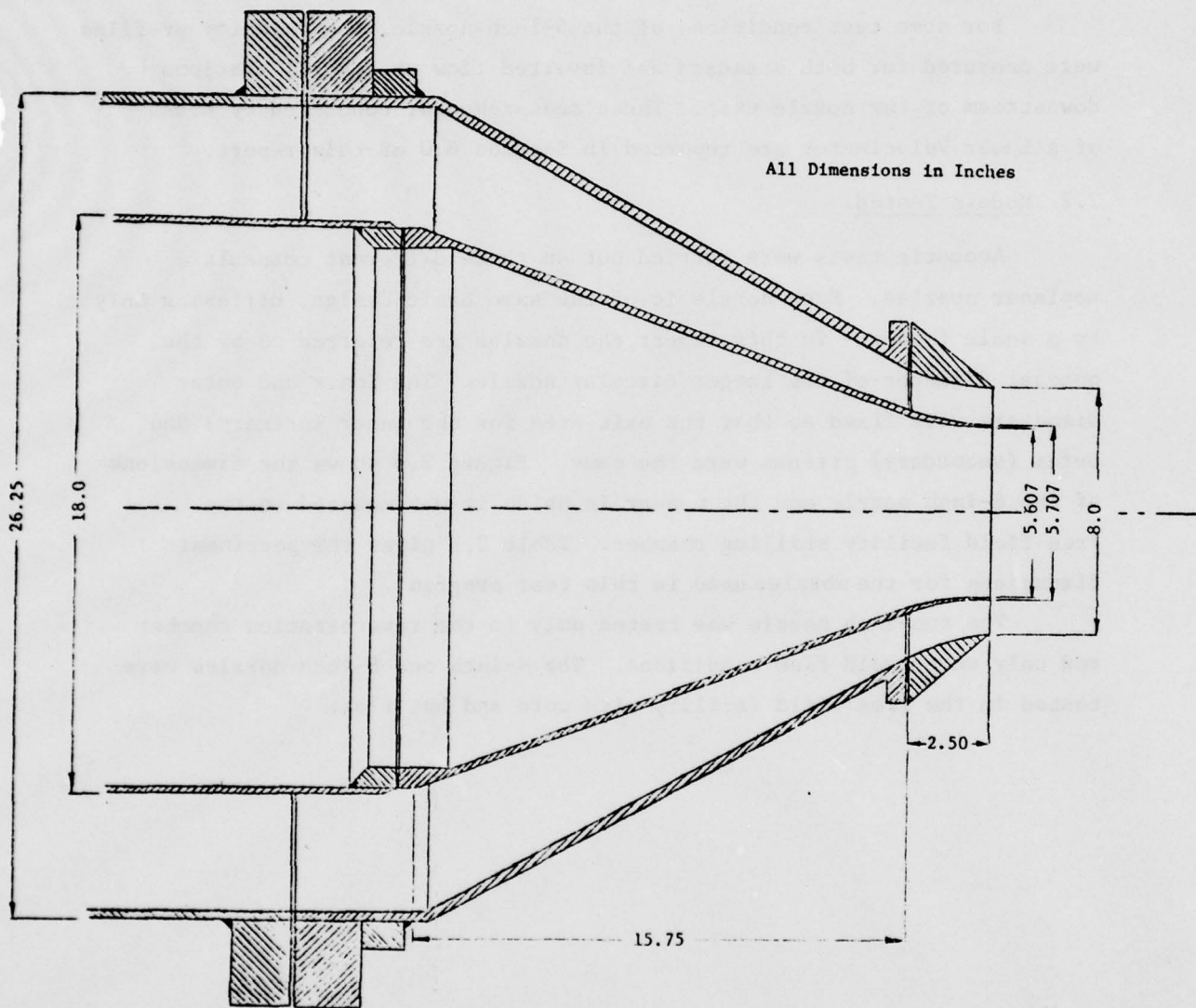
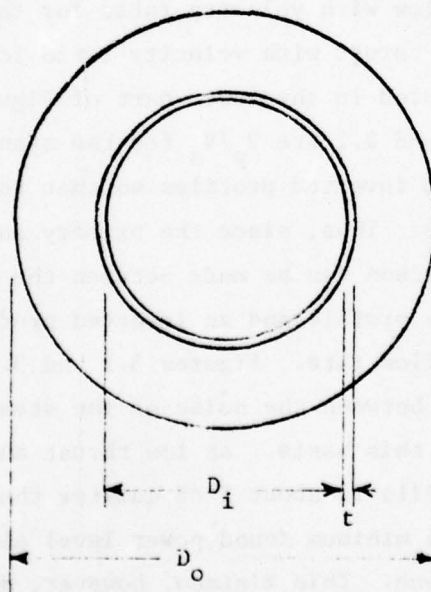


Figure 2.5. Eight Inch Nozzle and Free Field Transition Piece.

TABLE 2.1

NOZZLE PARAMETERS

| NOZZLE | D_o inches | D_i inches | t inches | A_p, A_s inches ² |
|--------|-----------------|-----------------|---------------|-----------------------------------|
| 2-INCH | 2.220 | 1.550 | .02 | 1.88 |
| 4-INCH | 4.0 | 2.778 | .05 | 6.06 |
| 8-INCH | 8.0 | 5.607 | .05 | 24.69 |



3.0 ACOUSTIC DATA FOR COLD FLOW.

3.1 Reverberation Chamber Tests on 2-Inch Nozzle.

The initial tests with the coannular nozzles were made in the reverberation chamber on the 2-inch nozzle with both primary and secondary stream unheated. Several test series were carried out varying the velocity ratio of the secondary and primary streams while maintaining either constant total thrust or constant total mass flow. In these test series, the velocity ratio was changed by varying the pressure ratios, that is the exit Mach numbers, of the primary and secondary streams. The test conditions and acoustic results for these test series are summarized in Tables 3.1 and 3.2. Table 3.1 gives the test conditions and results for the constant thrust test series and Table 3.2 shows similar information for the constant total mass flow series. The sound power level (PWL) values in these tables were obtained from microphone measurements in the chamber as corrected for the chamber's acoustic characteristics.

The results of these test series are presented graphically in Figures 3.1 and Figures 3.2 where the sound power level is plotted as a function of velocity ratio for values of constant total thrust or constant total mass flow. The lower portion of Figure 3.1 shows the variation of total mass flow with velocity ratio for the constant thrust series. The variation of thrust with velocity ratio for the constant mass flow series is presented in the lower part of Figure 3.2. The abscissa for Figures 3.1 and 3.2 are V_p/V_s for the standard velocity profiles and V_s/V_p for the inverted profiles so that the velocity ratio is always greater than one. Thus, since the primary and secondary areas are equal, a direct comparison can be made between the sound produced by a conventional velocity profile and an inverted profile with the same thrust and the same mass flow rate. Figures 3.1 and 3.2 show that there is very little difference between the noise of the standard and inverted profiles when compared on this basis. At low thrust and low mass flow rate the conventional profile is about 2 dB quieter than the inverted. In both of these figures, the minimum sound power level always occurs at or near a velocity ratio of one. This minimum, however, must be viewed with some care since for the constant thrust curves the mass flow rate is a maximum at this condition, and for the constant mass flow curves the thrust is a minimum.

TABLE 3.1
 SUMMARY OF FLOW PARAMETERS AND ACOUSTIC RESULTS FOR THE CONSTANT THRUST SERIES FOR THE TWO-INCH
 COANNULAR NOZZLE AT AMBIENT TEMPERATURE

| M_p | M_s | V_s/V_p | Th/A_t | \dot{m}_t/A_t lb/sec in ² | \dot{m}_s/\dot{m}_p | PWL dB |
|-------|-------|-----------|--------------------------|---|-----------------------|-----------|
| .30 | .64 | 2.09 | 4.87 lb/in ² | .280 | 2.22 | 106.74 |
| .40 | .58 | 1.42 | | .291 | 1.47 | 105.15 |
| .45 | .54 | 1.20 | | .296 | 1.21 | 103.88 |
| .49 | .51 | 1.03 | | .299 | 1.03 | 102.67 |
| .60 | .36 | .62 | | .288 | .59 | 102.92 |
| .65 | .27 | .43 | | .276 | .39 | 105.39 |
| .7 | 0 | 0 | | .274 | 0 | 110.17 |
| .3 | .86 | 2.70 | 8.26 lb/in ² | .366 | 2.99 | 117.15 |
| .5 | .76 | 1.48 | | .395 | 1.53 | 113.93 |
| .64 | .64 | 1.00 | | .401 | 1.00 | 111.17 |
| .7 | .57 | .83 | | .398 | .80 | 111.83 |
| .8 | .42 | .55 | | .379 | .50 | 113.81 |
| .9 | 0 | 0 | | .290 | 0 | 118.86 |
| .45 | .97 | 2.01 | 11.09 lb/in ² | .436 | 2.29 | 119.75 |
| .55 | .91 | 1.59 | | .449 | 1.74 | 118.75 |
| .65 | .84 | 1.26 | | .458 | 1.32 | 116.67 |
| .75 | .75 | 1.00 | | .462 | 1.01 | 114.80 |
| .84 | .65 | .79 | | .458 | .76 | 116.15 |
| .91 | .55 | .63 | | .449 | .58 | 117.98 |
| .97 | .45 | .50 | | .436 | .44 | 119.13 |
| .70 | .98 | 1.34 | 14.30 lb/in ² | .527 | 1.46 | 120.73 |
| .75 | .94 | 1.22 | | .527 | 1.28 | 120.29 |
| .85 | .85 | 1.00 | | .528 | .99 | 120.01 |
| .90 | .80 | .90 | | .528 | .87 | 119.17 |
| .95 | .73 | .80 | | .522 | .75 | 120.28 |

TABLE 3.1a
 SUMMARY OF TEST CONDITIONS AND COMPUTED MIXED FLOW CONDITIONS FOR CONSTANT THRUST
 SERIES TH/A = 8.26 lb/in² FOR THE 2-INCH COANNULAR NOZZLE (A_N = .0218 ft²)

| M _P | M _S | P ^{op} lb/ft ² abs | P ^{os} lb/ft ² abs | P ^{om} lb/ft ² | T ^{op} °R | T ^{os} °R | T ^{om} °R | V _s /V _p | A _m ft ² | PWL _{mix} dB |
|----------------|----------------|---|---|---------------------------------------|-----------------------|-----------------------|-----------------------|--------------------------------|-----------------------------------|--------------------------|
| .3 | .86 | 2177 | 3296 | 3015 | 479 | 479 | 479 | 2.70 | .0165 | 115.4 |
| .5 | .76 | 2428 | 2985 | 2763 | 479 | 481 | 480 | 1.48 | .0207 | 112.1 |
| .64 | .64 | 2694 | 2699 | 2696 | 480 | 484 | 482 | 1.00 | .0220 | 111.0 |
| .7 | .57 | 2839 | 2556 | 2714 | 482 | 487 | 484 | .83 | .0216 | 111.4 |
| .8 | .42 | 3120 | 2302 | 2852 | 487 | 495 | 490 | .55 | .0190 | 113.8 |
| .9 | 0 | 3462 | 2045 | 3462 | 492 | — | 492 | 0 | .0110 | 120.6 |

TABLE 3.2

SUMMARY OF FLOW PARAMETERS AND ACOUSTIC RESULTS FOR THE CONSTANT MASS FLOW SERIES
FOR THE TWO-INCH COANNULAR NOZZLE WITH COLD FLOW

| M_p | M_s | V_s/V_p | Th/A_T | \dot{m}_T/A_T | \dot{m}_s/\dot{m}_p | PWL dB |
|-------|-------|-----------|-------------------------|------------------------|-----------------------|-----------|
| .30 | .53 | 1.77 | 3.71 lb/in ² | .25 | 1.83 | 102.83 dB |
| .42 | .42 | 1.00 | 3.43 | lb/sec in ² | 1.00 | 98.03 |
| .50 | .34 | .70 | 3.63 | | .68 | 97.32 |
| .60 | .23 | .40 | 4.09 | | .37 | 102.43 |
| .70 | .13 | .20 | 5.02 | | .18 | 108.53 |
| .80 | 0 | 0 | 6.36 | | 0 | 114.67 |
| .35 | .82 | 2.24 | 7.84 | .36 | 2.48 | 113.11 |
| .45 | .73 | .159 | 7.31 | | 1.68 | 111.24 |
| .59 | .60 | 1.01 | 7.00 | | 1.01 | 107.63 |
| .70 | .49 | .71 | 7.19 | | .67 | 108.81 |
| .80 | .37 | .49 | 7.70 | | .44 | 112.58 |
| .95 | .20 | .23 | 9.36 | | .20 | 119.16 |
| .45 | .99 | 2.07 | 11.83 | .46 | 2.37 | 120.86 |
| .55 | .91 | 1.58 | 11.20 | | 1.74 | 119.21 |
| .65 | .82 | 1.24 | 10.87 | | 1.29 | 115.93 |
| .73 | .74 | 1.01 | 10.74 | | 1.00 | 114.81 |
| .81 | .65 | .82 | 10.87 | | .78 | 115.09 |
| .91 | .55 | .64 | 11.22 | | .58 | 117.92 |
| .99 | .46 | .50 | 11.89 | | .43 | 120.13 |
| .70 | .98 | 1.35 | 14.46 | .52 | 1.46 | 120.42 |
| .75 | .94 | 1.23 | 14.31 | | 1.28 | 119.66 |
| .84 | .85 | 1.01 | 14.22 | | 1.00 | 119.43 |
| .90 | .79 | .90 | 14.25 | | .86 | 119.12 |
| .95 | .73 | .81 | 14.31 | | .74 | 120.17 |

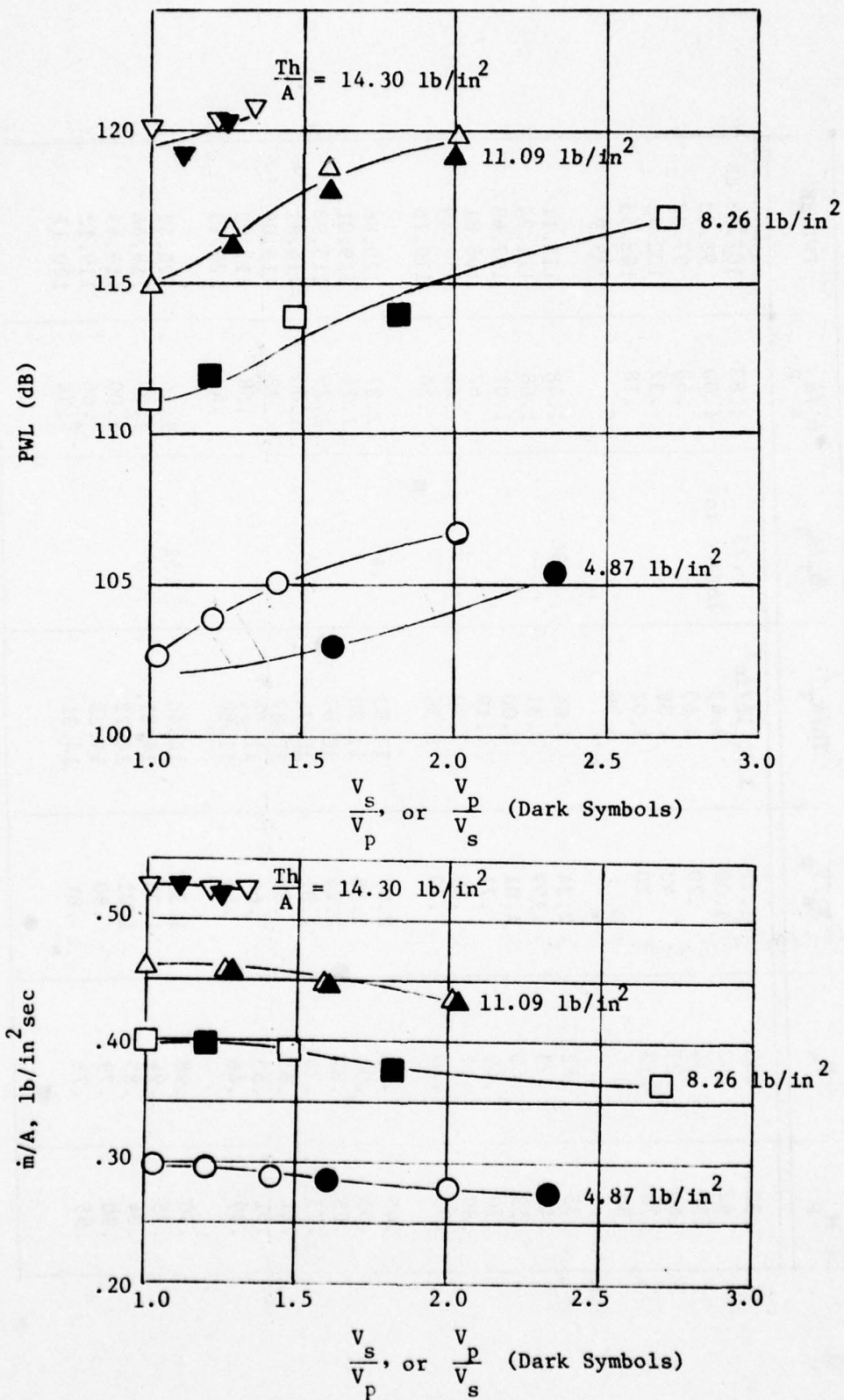


Figure 3.1 Sound Power Level and Mass Flow Rate Versus Velocity Ratio for the 2-Inch Coannular Nozzle at Ambient Temperature and Constant Total Thrust/Unit Area. (Reverberation Chamber).

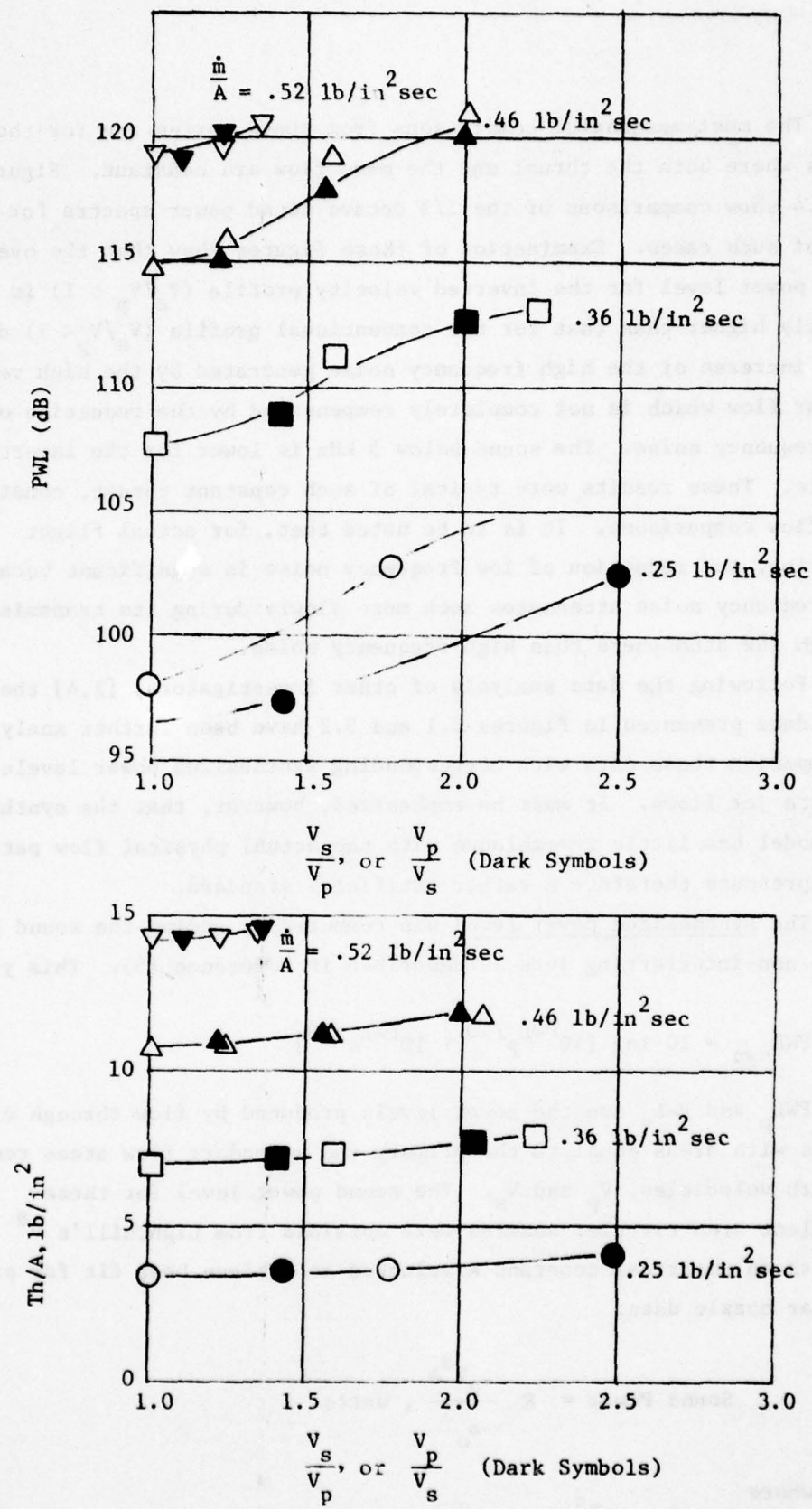


Figure 3.2. Sound Power Level and Thrust Versus Velocity Ratio for the 2-Inch Coannular Nozzle at Ambient Temperature and Constant Total Mass Flow.

The most meaningful comparisons from these series are for those points where both the thrust and the mass flow are constant. Figures 3.3 and 3.4 show comparisons of the 1/3 octave sound power spectra for two pair of such cases. Examination of these figures show that the overall sound power level for the inverted velocity profile ($V_s/V_p > 1$) is slightly higher than that for the conventional profile ($V_s/V_p < 1$) due to an increase of the high frequency noise generated by the high velocity annular flow which is not completely compensated by the reduction of low-frequency noise. The sound below 5 kHz is lower for the inverted profile. These results were typical of such constant thrust, constant mass flow comparisons. It is to be noted that, for actual flight condition, the reduction of low frequency noise is significant because low-frequency noise attenuates much more slowly during its transmission through the atmosphere than high frequency noise.

Following the data analysis of other investigators, [1,4] the sound power data presented in Figures 3.1 and 3.2 have been further analyzed by comparing these data with corresponding synthesized power levels of separate jet flows. It must be emphasized, however, that the synthesized flow model has little resemblance with the actual physical flow patterns, and represents therefore a rather artificial standard.

The synthesized power level was computed by adding the sound power of two non-interfering jets as described in Reference (5). This yields

$$PWL_{syn} = 10 \log [10^{PWL_p/10} + 10^{PWL_s/10}]$$

where PWL_p and PWL_s are the power levels produced by flow through circular nozzles with areas equal to the primary and secondary flow areas respectively and with velocities, V_p and V_s . The sound power level for these equivalent area circular nozzles were obtained from Lighthill's V^8 law with an empirical constant K selected to achieve best fit for previous circular nozzle data:

$$\text{Sound Power} = K \frac{\rho_0 V^8 A}{a_0^5}, \text{ watts}$$

where
 $K = 5 \times 10^{-5}$.

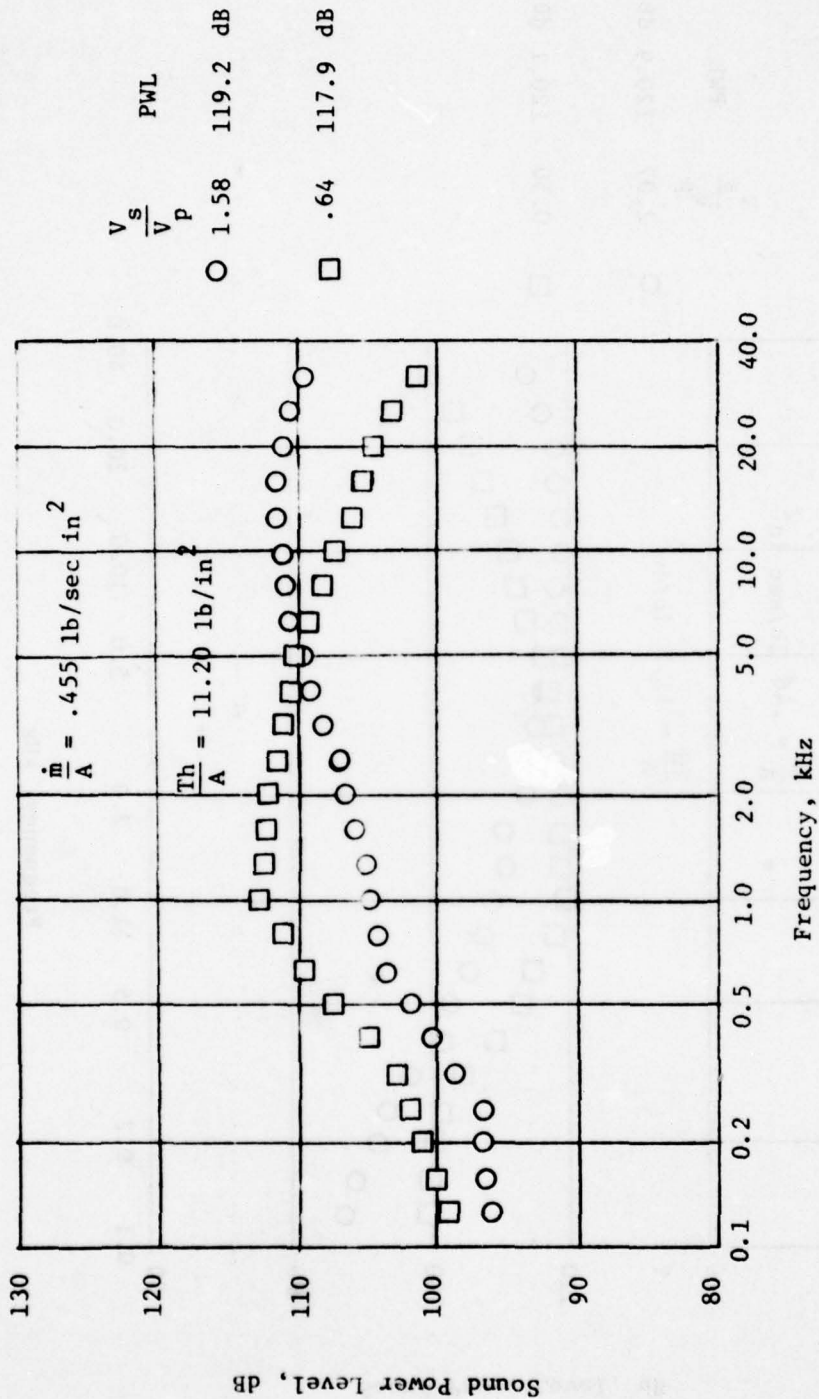


Figure 3.3. Comparison of Sound Power Spectra for Two Velocity Ratios at Constant Mass Flow and Constant Thrust for the 2-Inch Coannular Nozzle at Ambient Temperature.

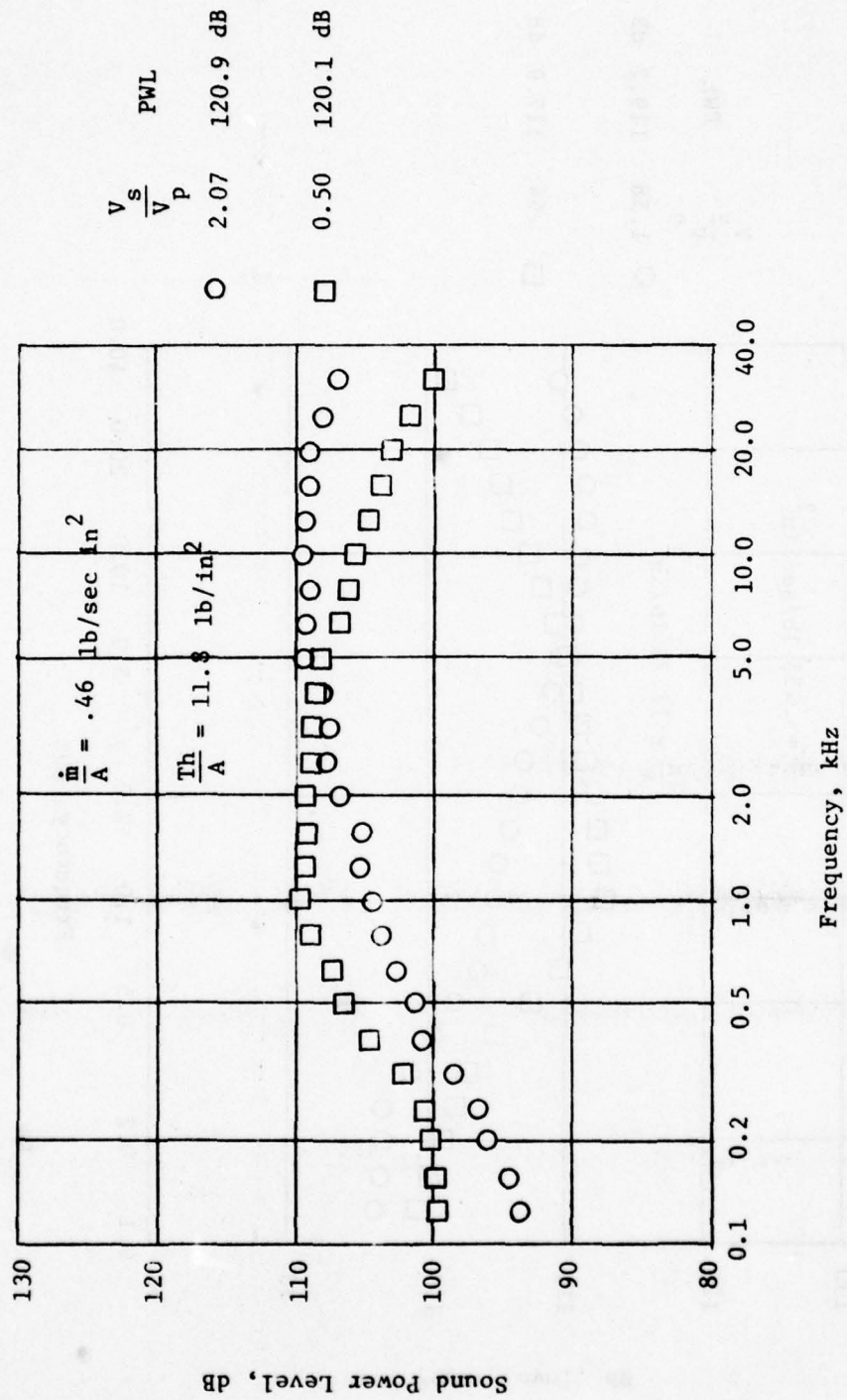


Figure 3.4. Comparison of Sound Power Spectra for Two Velocity Ratios at Constant Mass Flow and Constant Thrust for the 2-Inch Coannular Nozzle at Ambient Temperature.

Sound power data from the inner circular nozzle of the coannular nozzle were compared with this correlation and very good agreement was found. It is noted that for the synthesized method, both mass flow and thrust are kept constant for the test nozzle and the synthesized nozzle. Furthermore, the experimental data were compared with the data of fully mixed flow.

The fully mixed flow was computed by assuming that the stagnation pressure and temperature of the mixed flow is given by a weighted average of the primary and secondary flows:

$$\dot{m}_T p_{om} = \dot{m}_p p_{op} + \dot{m}_s p_{os}$$

$$\dot{m}_T T_{om} = \dot{m}_p T_{op} + \dot{m}_s T_{os}$$

where

$$\dot{m}_T = \dot{m}_p + \dot{m}_s$$

The exit velocity V_m can be computed from p_{om} and T_{om} . The nozzle exit area is then calculated to satisfy

$$\dot{m}_T = \rho_m A V_m$$

From the nozzle exit velocity and exit area, the sound power level of the mixed flow can be calculated from the correlation above.

The use of a mass weighed averaged for the stagnation pressure of the mixed flow is an approximation to a more exact mixing calculation using the one-dimensional momentum equation. It should be noted that this calculation does not maintain the same thrust between the mixed flow and the experimental conditions. The differences are small, however, with the calculated mixed flow generally having thrust differing from experimental conditions by no more than three percent. Table 3.1a gives a summary of the test conditions and the mixed flow conditions for the constant thrust series with $Th/A = 8.26 \text{ lb/in}^2$.

The results of the comparisons of the coannular flow with the synthesized power level and the power level of a fully mixed jet are shown in Figures 3.5 and 3.6. Because the curves on Figure 3.5 refer to

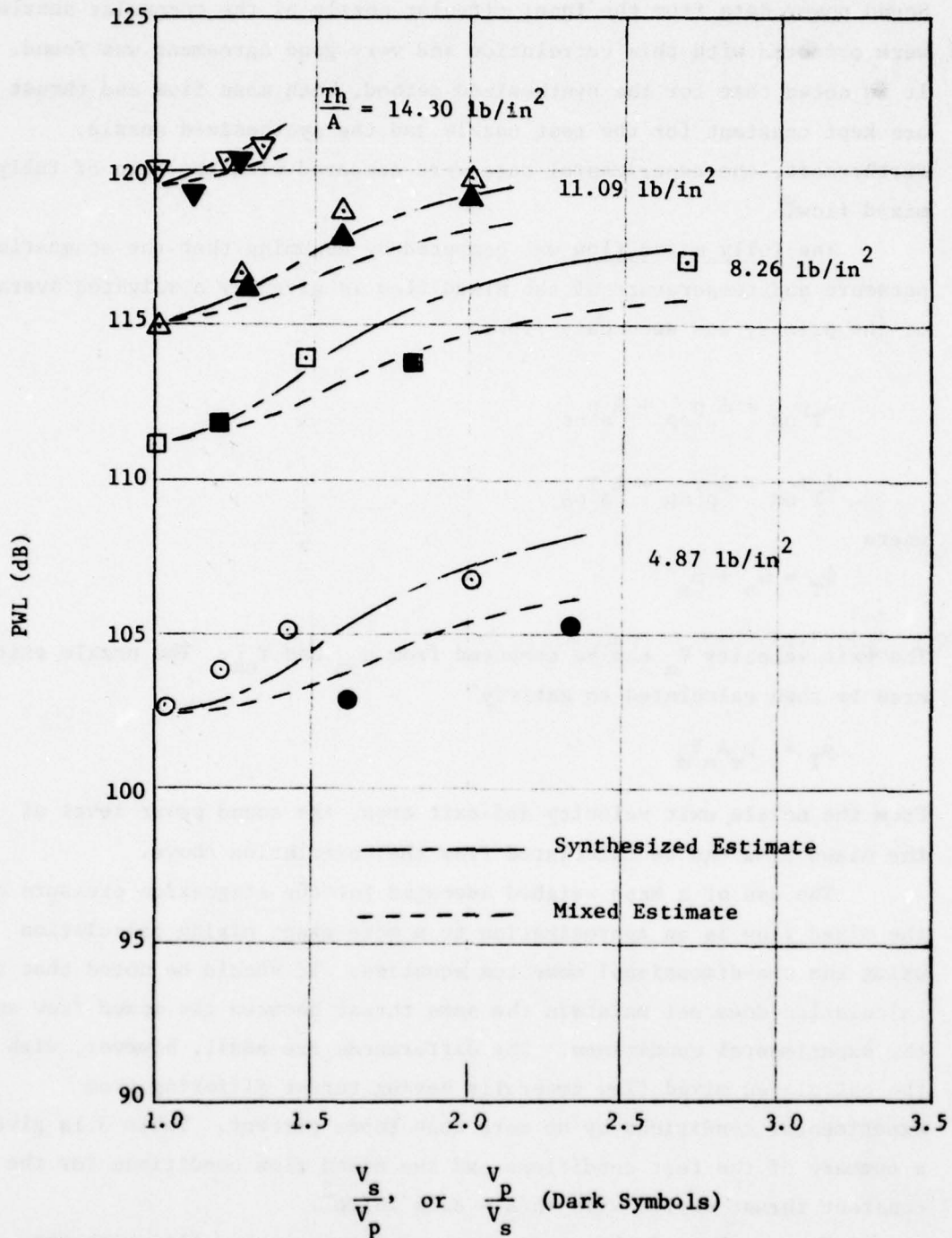


Figure 3.5. Comparison of Measure Sound Power Data with Synthesized Power and Fully Mixed Power for Constant Thrust Series with 2-Inch Nozzle.

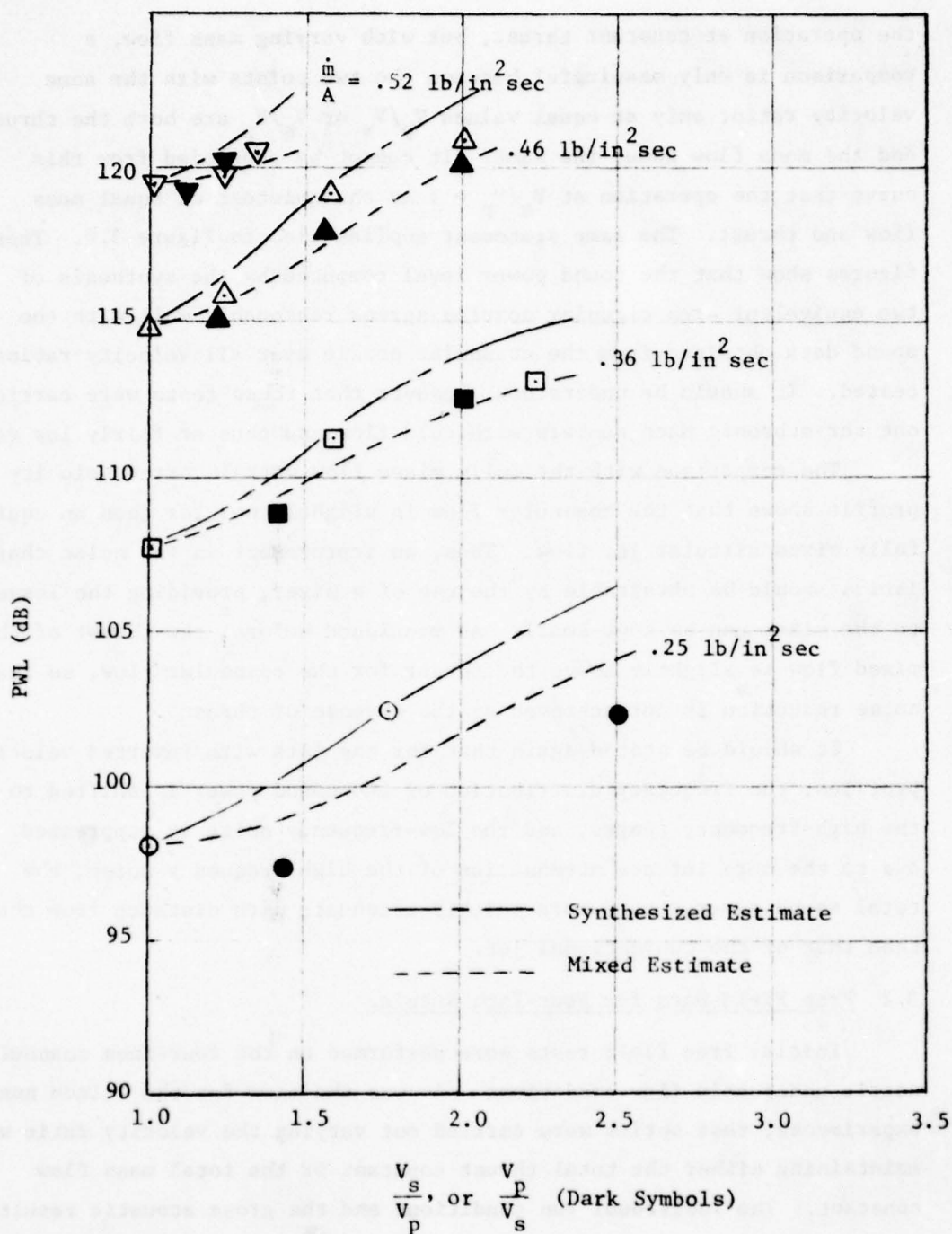


Figure 3.6. Comparison of Measured Sound Power Data with Synthesized Power and Fully Mixed Power for Constant Mass Flow Series with 2-Inch Nozzle.

the operation at constant thrust, but with varying mass flow, a comparison is only meaningful between the two points with the same velocity ratio; only at equal values V_p/V_s or V_s/V_p are both the thrust and the mass flow about the same. It cannot be concluded from this curve that the operation at $V_s/V_p = 1$ is the quietest at equal mass flow and thrust. The same statement applies also to Figure 3.6. These figures show that the sound power level computed by the synthesis of two equivalent area circular nozzles agrees reasonably well with the sound data obtained from the coannular nozzle over all velocity ratios tested. It should be understood, however that these tests were carried out for subsonic Mach numbers with cold flow and thus at fairly low velocity.

The comparison with the fully mixed flow with inverted velocity profile shows that the coannular flow is slightly noisier than an equivalent fully mixed circular jet flow. Thus, an improvement in the noise characteristics should be obtainable by the use of a mixer, providing the losses due to the mixer can be kept small. As mentioned before, the thrust of the mixed flow is slightly above the thrust for the coannular flow, so that the noise reduction is not achieved at the expense of thrust.

It should be stated again that for the jets with inverted velocity profiles, the frequency distribution of the sound power is shifted to the high-frequency ranges, and the low-frequency noise is suppressed. Thus, due to the more intense attenuation of the high-frequency noise, the total sound power should more quickly attenuate with distance from the jet than that of the conventional jet.

3.2 Free Field Data for Four-Inch Nozzle.

Initial free field tests were performed on the four-inch coannular nozzle under cold flow conditions. As was the case for the 2-inch nozzle experiments, test series were carried out varying the velocity ratio while maintaining either the total thrust constant or the total mass flow constant. The individual run conditions and the gross acoustic results are summarized for the constant thrust series in Table 3.3. Similar information for the constant mass flow series is presented in Table 3.4. In these tests the velocity ratio at higher thrust and mass flow levels was limited by choking of the convergent coannular nozzles. In the few cases where primary or secondary Mach numbers greater than one are shown, these are in fact, indications of choking with a slightly supercritical pressure ratio.

TABLE 3.3

SUMMARY OF FLOW PARAMETERS AND ACOUSTIC RESULTS FOR THE
 CONSTANT THRUST SERIES FOR THE FOUR-INCH
 COANNULAR NOZZLE WITH COLD FLOW

| M_p | M_s | V_s/V_p | T_h/A_t | \dot{m}_t/A_t | \dot{m}_s/\dot{m}_p | SPL 30° dB |
|-------|-------|-----------|---------------------------|--------------------------------|-----------------------|------------|
| .639 | .251 | .41 | 4.7 lb/in ² | 0.26 lb/sec in ² | .38 | 91.0 |
| .629 | .274 | .45 | | 0.27 | 0.42 | 90.5 |
| .618 | .295 | .49 | | 0.27 | 0.46 | 91.0 |
| .594 | .349 | .6 | | 0.28 | 0.57 | 90.0 |
| .577 | .372 | .66 | | 0.28 | 0.63 | 89.0 |
| .544 | .411 | .76 | | 0.28 | 0.75 | 88.0 |
| .481 | .485 | 1.01 | | 0.29 | 1.01 | 86.5 |
| .414 | .55 | 1.31 | | 0.29 | 1.35 | 87.5 |
| .374 | .575 | 1.51 | | 0.29 | 1.57 | 88.0 |
| .342 | .591 | 1.68 | | 0.27 | 1.78 | 89.0 |
| .298 | .615 | 2.00 | | 0.27 | 2.12 | 89.0 |
| .276 | .627 | 2.2 | | 0.27 | 2.35 | 90.0 |
| .245 | .641 | 2.52 | | 0.27 | 2.71 | 90.0 |

TABLE 3.3 (Continued)

| M_p | M_s | V_s/V_p | Th/A_t | \dot{m}_t/A_t | \dot{m}_s/\dot{m}_p | SPL 30° dB | |
|-------|-------|-----------|----------------------------|--------------------------------|--------------------------------|------------|-------|
| 0.992 | 0.366 | 0.4 | 11.1 lb/in ² | 0.42 lb/sec in ² | 0.34 | 108.5 | |
| .975 | .413 | 0.46 | | 0.43 | .39 | 108.0 | |
| .958 | .447 | 0.5 | | 0.43 | 0.44 | 107.0 | |
| .924 | .511 | 0.59 | | 0.44 | .52 | 106.5 | |
| .895 | .563 | 0.66 | | 0.45 | 0.6 | 104.5 | |
| .844 | .633 | 0.77 | | 0.46 | 0.73 | 103.5 | |
| .747 | .747 | 1.00 | | 0.46 | 1.00 | 101.5 | |
| .634 | .848 | 1.30 | | 0.47 | 1.38 | 101.5 | |
| .570 | .893 | 1.50 | | 0.46 | 1.63 | 101.5 | |
| 0.514 | 0.922 | 1.70 | | 0.44 | 1.89 | 102.0 | |
| 0.447 | 0.958 | 2.00 | | 0.43 | 2.3 | 103.5 | |
| 0.412 | 0.973 | 2.19 | | 0.43 | 2.54 | 104.0 | |
| 0.367 | 0.991 | 2.49 | | 0.43 | 2.92 | 104.0 | |
| 1.049 | 0.576 | 0.61 | | 14.3 lb/in ² | 0.51 lb/sec in ² | 0.51 | 111.0 |
| 1.017 | 0.634 | 0.67 | | | 0.52 | 0.59 | 110.0 |
| .960 | .710 | 0.77 | | | 0.53 | 0.71 | 108.5 |
| .847 | .846 | 1.00 | | | .52 | 1.00 | 107.0 |
| .716 | .967 | 1.3 | 0.53 | | 1.4 | 106.5 | |
| .642 | 1.015 | 1.48 | 0.52 | | 1.67 | 106.0 | |
| .577 | 1.051 | 1.63 | .51 | | 1.96 | 107.0 | |

TABLE 3.4

SUMMARY OF FLOW PARAMETERS AND ACOUSTIC RESULTS FOR THE CONSTANT
 MASS FLOW SERIES FOR THE FOUR-INCH COANNULAR
 NOZZLE WITH COLD FLOW

| M_p | M_s | V_s/V_p | Th/A_t | \dot{m}_t/A_t | \dot{m}_s/\dot{m}_p | SPL 30° dB |
|-------|-------|-----------|----------------------------|--------------------------------|-----------------------|---------------|
| .573 | .281 | 0.50 | 4.09 lb/in ² | 0.25 lb/sec in ² | .48 | 88.5 |
| .54 | .314 | .59 | 3.88 | | .57 | 86.5 |
| .536 | .313 | 0.6 | 3.87 | | .57 | 87.0 |
| .505 | .348 | 0.7 | 3.78 | | .68 | 87.0 |
| .479 | .381 | 0.8 | 3.72 | | .79 | 84.0 |
| .450 | .405 | .91 | 3.68 | | 0.9 | 84.5 |
| .428 | .427 | 1.00 | 3.67 | | 1.00 | 84.0 |
| .41 | .455 | 1.11 | 3.67 | | 1.11 | 85.0 |
| .388 | .465 | 1.19 | 3.67 | | 1.21 | 86.0 |
| .368 | .486 | 1.31 | 3.72 | | 1.33 | 84.5 |
| .353 | .501 | 1.4 | 3.76 | | 1.44 | 85.0 |
| .337 | .516 | 1.51 | 3.81 | | 1.55 | 85.0 |
| .327 | .536 | 1.61 | 3.86 | | 1.67 | 87.0 |
| .303 | .558 | 1.80 | 3.95 | | 1.88 | 87.0 |
| .281 | .578 | 2.01 | 4.05 | | 2.11 | 88.5 |

TABLE 3.4 (continued)

| M_p | M_s | V_s/V_p | Th/A_t | \dot{m}_t/A_t | \dot{m}_s/\dot{m}_p | SPL 30° dB |
|-------|-------|-----------|----------------------------|--------------------------------|-----------------------|---------------|
| .812 | .385 | 0.5 | 8.11 lb/in ² | 0.37 lb/sec in ² | .45 | 101.0 |
| .765 | .445 | 0.6 | 7.78 | | .56 | 100.0 |
| .721 | .491 | 0.7 | 7.58 | | .66 | 98.0 |
| .680 | .536 | 0.8 | 7.44 | | .78 | 97.0 |
| .642 | .574 | 0.9 | 7.39 | | .88 | 94.5 |
| .606 | .607 | 1.00 | 7.38 | | 1.00 | 94.5 |
| .58 | .647 | 1.11 | 7.39 | | 1.12 | 96.0 |
| .548 | .667 | 1.2 | 7.44 | | 1.24 | 95.5 |
| .521 | .691 | 1.3 | 7.49 | | 1.35 | 95.0 |
| .496 | .713 | 1.4 | 7.55 | | 1.47 | 95.5 |
| .475 | .732 | 1.5 | 7.61 | | 1.59 | 95.5 |
| .455 | .753 | 1.6 | 7.72 | | 1.72 | 96.0 |
| .418 | .785 | 1.8 | 7.88 | | 1.96 | 98.0 |
| .387 | .814 | 2.01 | 8.1 | | 2.21 | 98.5 |
| 1.079 | .605 | 0.64 | 14.54 | 0.53 | .52 | 113.0 |
| 1.014 | .678 | .71 | 14.71 | | .63 | 111.0 |
| .958 | .742 | .8 | 14.57 | | .75 | 109.5 |
| .901 | .799 | .9 | 14.45 | | .87 | 108.0 |
| .848 | .848 | 1.0 | 14.44 | | 1.00 | 107.0 |
| .81 | .905 | 1.1 | 14.44 | | 1.13 | 107.0 |
| .760 | .935 | 1.2 | 14.51 | | 1.26 | 106.5 |
| .719 | .974 | 1.3 | 14.66 | | 1.41 | 107.0 |
| .683 | 1.004 | 1.4 | 14.74 | | 1.54 | 106.5 |
| .651 | 1.034 | 1.46 | 14.65 | | 1.68 | 107.0 |

Examination of the acoustic data presented in Tables 3.3 and 3.4 shows that the minimum sound generation usually occurs near a velocity ratio of one. For the constant mass flow series, the thrust is a minimum at this condition, and for the constant thrust series the mass flow is a maximum. Once again it is of most interest to compare test points for which the total thrust and the total mass flow are the same. Figure 3.7 shows the OASPL directivities for a constant thrust series. The conventional velocity profile condition ($V_s/V_p = .50$) and the inverted velocity profile condition ($V_s/V_p = 2.00$) also have the same total mass flow. These directivities show that the conventional velocity profile is about 1 dB quieter than the inverted at large angles to the jet axis. In the high noise region, as the axis of the jet is approached, the inverted profile makes less noise than the conventional. The maximum difference measured is about 5 dB at 20° from the axis. Integration of the acoustic intensity distribution from $\theta = 20^\circ$ to $\theta = 120^\circ$ for the two velocity profiles shows that the overall sound power generated by the inverted profile jet is approximately 2 dB less than the conventional.

Similar trends are shown in Figures 3.8 for $V_s/V_p = 0.60$ and $V_s/V_p = 1.60$ from a constant mass flow series.

Figure 3.9 shows a comparison of the sound pressure spectra at 30° for the constant thrust series of Figure 3.7. The spectra show that the inverted velocity profile radiates more high frequency noise and less noise in the region of the peak frequency than the conventional profile in this direction.

Figure 3.10 shows the variation of OASPL at 30° with velocity ratio, V_p/V_s or V_s/V_p , for the constant thrust series on the four-inch nozzle. Also shown on this figure are the synthesized sound pressure level and the OASPL corresponding to a fully mixed flow. The lower portion of Figure 3.10 gives the variation of total mass flow with velocity ratio for the constant thrust series. Figure 3.11 shows the variation of OASPL and thrust for the constant mass flow series. A comparison between the standard velocity profile data (dark symbols) and the inverted profile data (open symbols) in Figure 3.10 shows that for the lowest thrust level there is very little difference between

| V_s/V_p | \dot{m}/A | PWL |
|-----------|-----------------------------|----------|
| ◇ 0.50 | 0.43 lb/sec in ² | 116.7 dB |
| ◆ 2.00 | 0.43 lb/sec in ² | 114.8 dB |

$$\frac{Th}{A} = 11.1 \text{ lb/in}^2$$

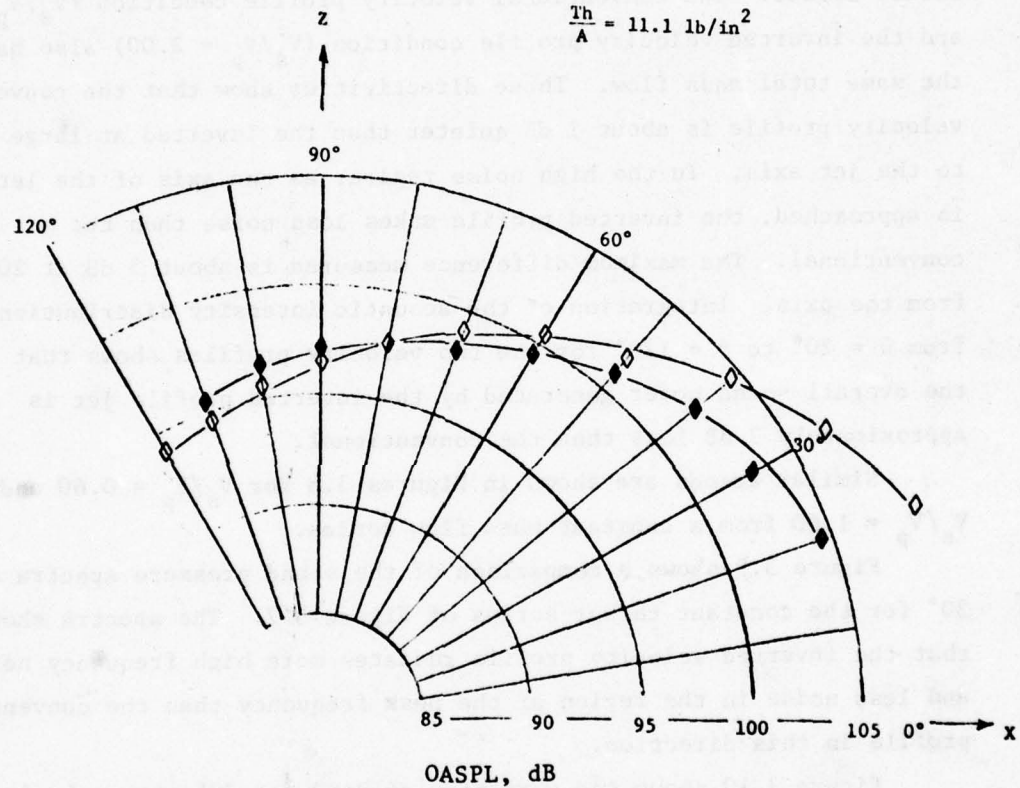


Figure 3.7. OASPL Directivities in the XZ Plane of the Four-Inch Coannular Nozzle for Two Velocity Ratios at Ambient Temperature and a Constant Thrust per Unit Area of 11.1 lb/in².

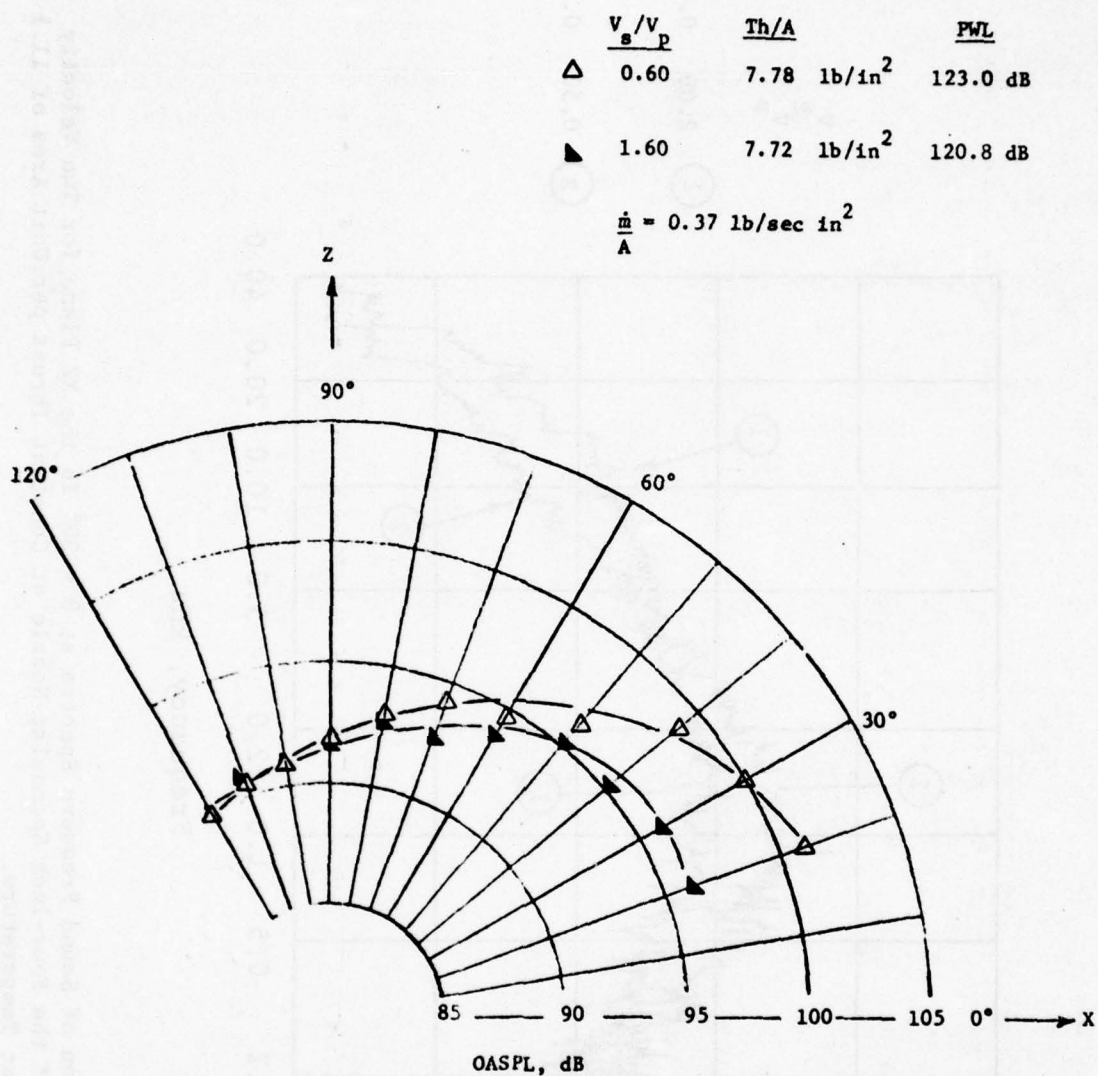


Figure 3.8. OASPL Directivities in the XZ Plane of the Four-Inch Coannular Nozzle for Two Velocity Ratios at Ambient Temperature and a Constant Mass Flow per Unit Area of 0.37 lb/sec in².

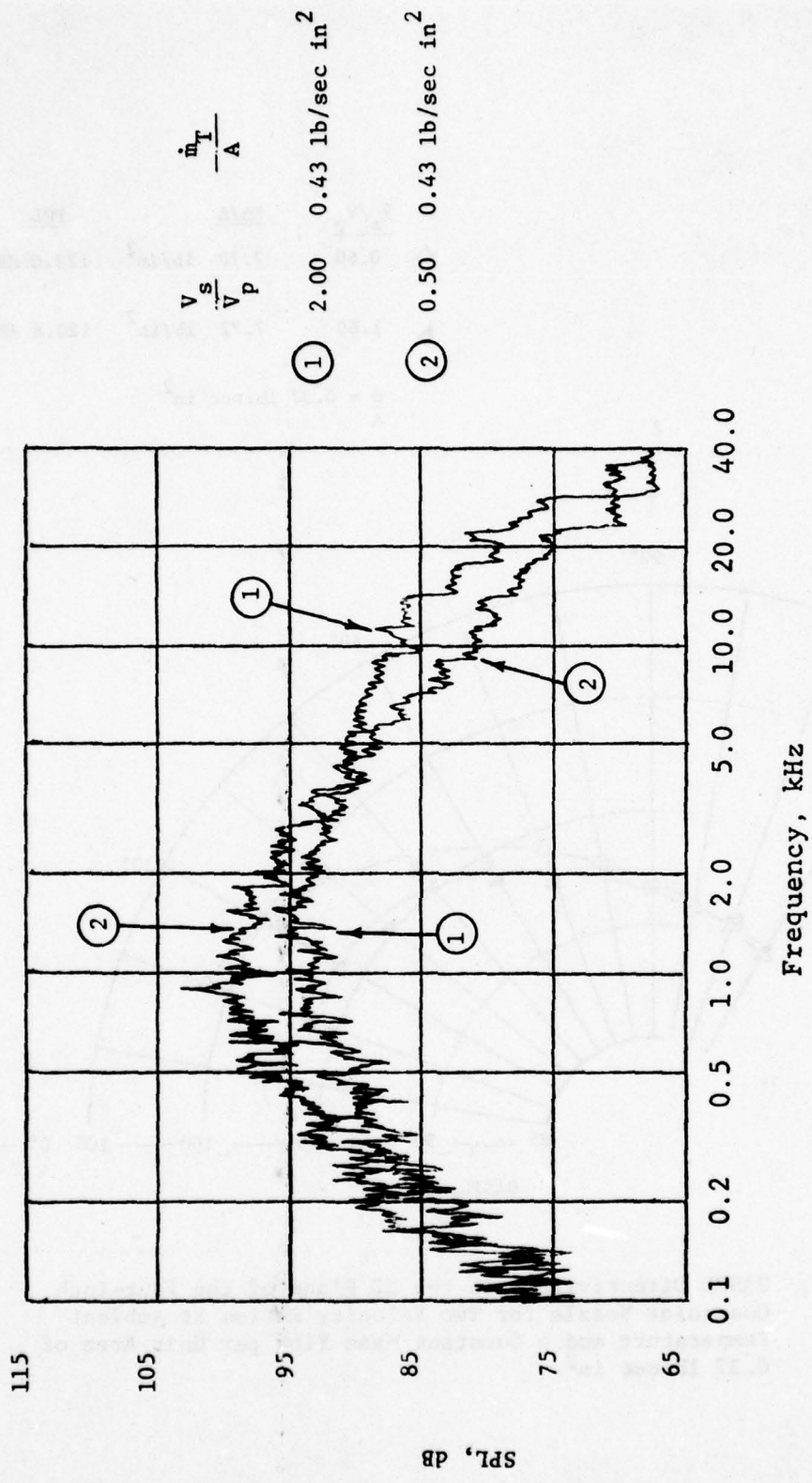


Figure 3.9. Comparison of Sound Pressure Spectra at $\theta = 30^\circ$ in the XZ Plane for Two Velocity Ratios of the Four-Inch Coannular Nozzle at Constant Thrust per Unit Area of 11.1 lb/in² at Ambient Temperature.

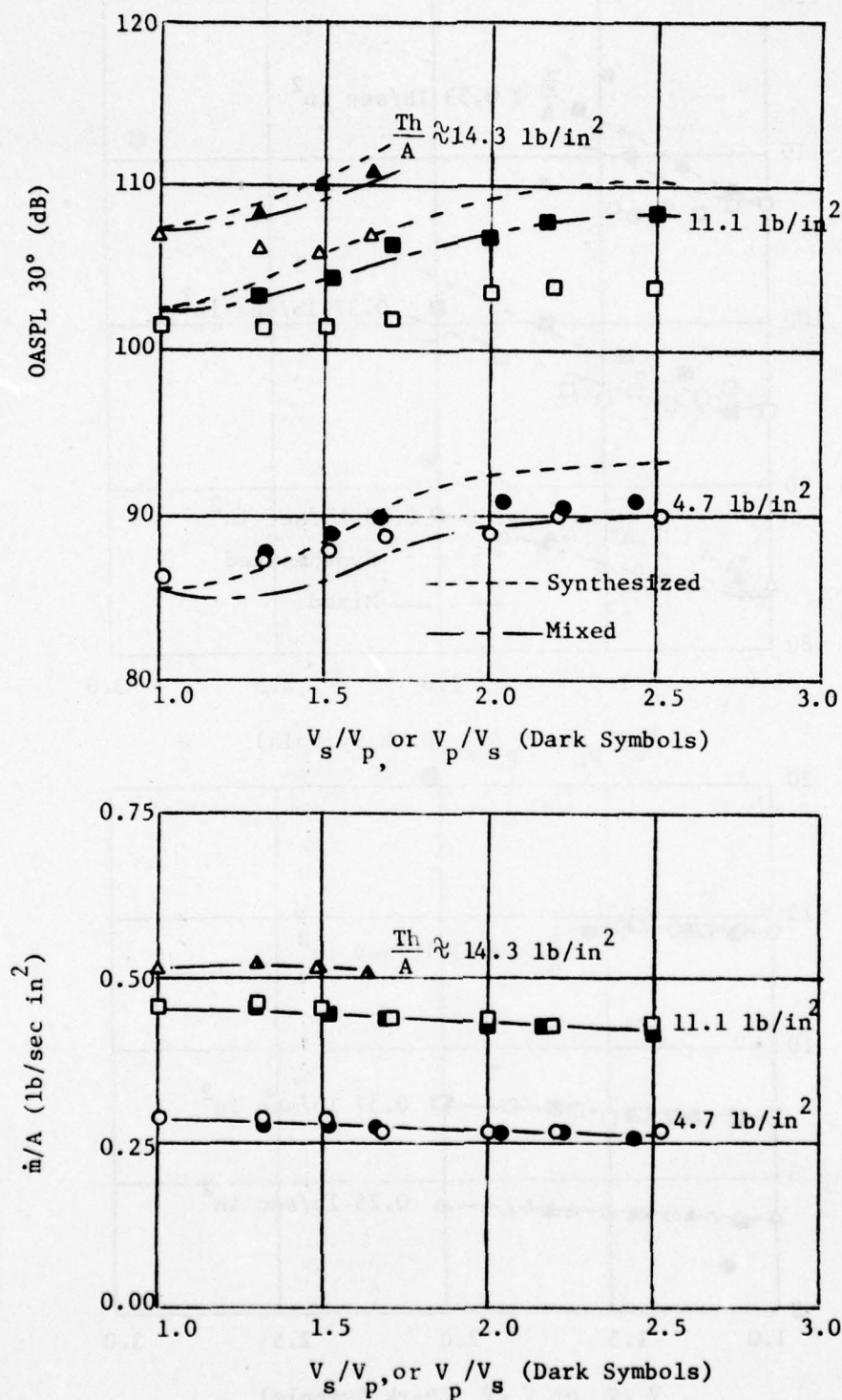


Figure 3.10 Variation of Overall Sound Pressure Level at 30° and Mass Flow per Unit Area with Velocity Ratio for Constant Thrust Series. (Four-Inch Nozzle, Ambient Temperature.)

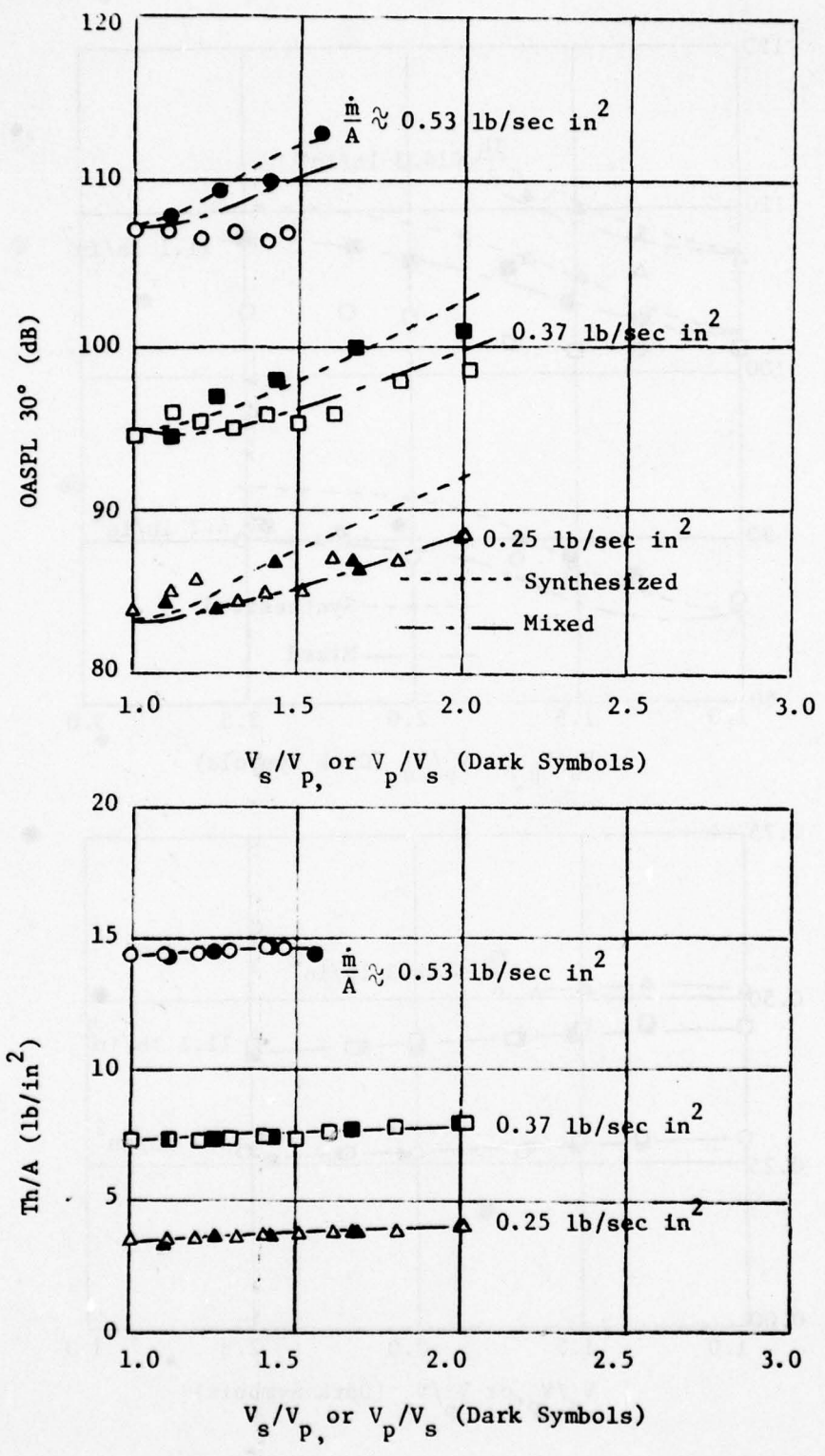


Figure 3.11. Variation of Overall Sound Pressure Level at 30° and Thrust per Unit Area with Velocity Ratio for Constant Mass Flow Series. (Four-Inch Nozzle, Ambient Temperature).

the sound radiated for these two types of flow. However, as the thrust level increases, the sound radiated by the inverted profile at 30° becomes noticeably less than that radiated by the conventional profile at the same velocity ratio. The maximum noise difference over the range of values tested is about 5 dB. Data for the constant mass flow series given in Figure 3.11 show similar trends as those for the constant thrust series.

The procedures used for computing the synthesized and fully mixed sound pressure levels is exactly the same as described earlier except that an empirical correlation for sound pressure level at 30° for circular nozzles was used. This correlation is shown in Figure 3.12 and was obtained by using the inner part of the coannular nozzle to produce the circular jet. Although the data was taken at different stagnation temperatures, a correlation in terms of velocity only was found to satisfactorily fit the data.

The results of the sound pressure calculation for a fully mixed and synthesized flows given in Figure 3.10 and 3.11 generally show that the synthesized calculation agrees fairly well with the experimental data obtained from the conventional velocity profile. The sound pressure calculated for the fully mixed flow typically falls below that for the conventional profiles.

Summarizing the results obtained for cold coannular jets, there appears to be some advantage for the inverted profile over the standard velocity profile when compared at the same thrust and the same mass flow. This advantage becomes more pronounced as the thrust level and the velocity ratio is increased but was not more than 5 dB at 30° over the range of values tested. Semi-empirical calculations estimate that a small reduction in sound would result from mixing the two cold streams of a conventional profile prior to exhausting from a nozzle. However, results reported in Section 4.0 show that mixing the hot flow prior to exhaust from the nozzles yields a larger noise reduction than mixing the cold flow as shown in Figures 3.10 and 3.11. In general, the overall results from the free field tests on the four-inch nozzle are consistent with the results obtained from the two-inch nozzle in the reverberation chamber.

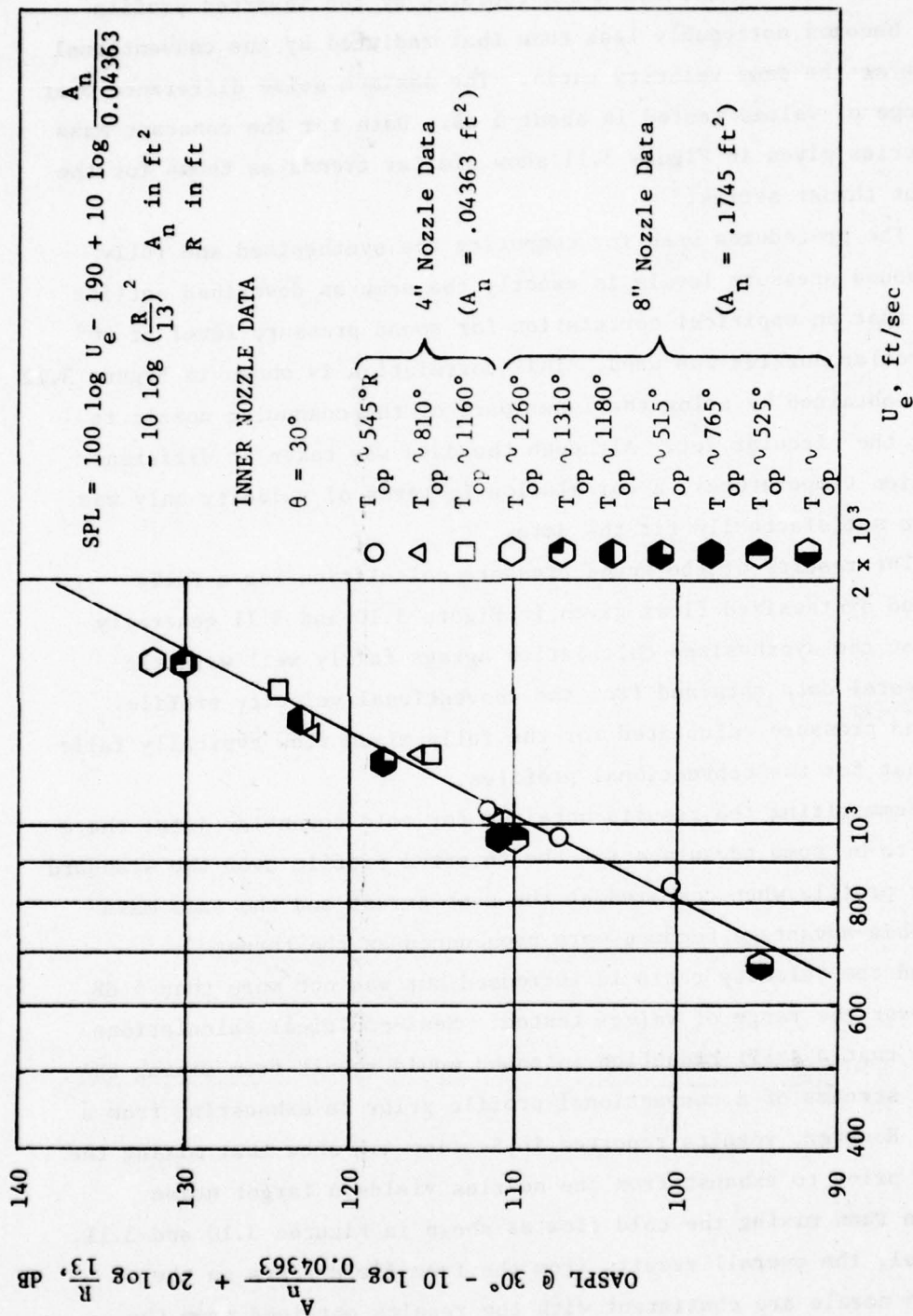


Figure 3.12. Correlation of Sound Pressure Data with Jet Exit Velocity for Inner Circular Nozzle. OASPL standardized for $D_n = 4$ inches and $R = 13$ ft.

4.0 ACOUSTIC DATA FOR HEATED FLOW.

4.1 Free Field Results for Four-Inch Nozzle.

Hot flow tests on the four-inch coannular nozzle were carried out in the free field test stand under conditions where either the primary or the secondary air flow stream was heated. As in the cold flow tests, the noise characteristics of the coannular flow were measured for different velocity ratios (V_s/V_p) while maintaining either the total thrust or the total mass flow constant. Table 4.1 summarizes the flow conditions and the acoustic results for the constant thrust per unit area series and Table 4.2 gives similar information for the constant mass flow series. For these hot flow tests only the higher thrust and higher mass flow series, which were considered to be of greatest interest, were performed.

For test series given in Table 4.1, the thrust was normally held constant by keeping the Mach numbers, that is the pressure ratios, of the primary and secondary streams constant. The different velocity ratios were obtained by varying the stagnation temperature ratio. Only for achieving extreme values of the velocity ratio were the Mach numbers occasionally changed. This is in contrast to the ambient temperature tests where the velocity ratio could be varied only by changing the pressure ratios. For the constant mass flow series both the pressure ratio and the temperature ratio changed as the velocity varied.

In the heated flow tests the piping arrangement of the free field facility was different for the conventional profile tests ($V_s/V_p < 1$) and the inverted tests ($V_s/V_p > 1$). As discussed in Section 2.0, this was necessary because only one flow stream could be heated with the test stand configuration used for these tests.

Examination of the acoustic data given in Tables 4.1 and 4.2 for heated flow show some interesting results. A comparison of the inverted velocity profile ($V_s/V_p > 1$) data for the same thrust and mass flow shows a significant advantage to the inverted profile. Not only is the sound pressure level at 30° reduced by a substantial amount but also the sound power level for the inverted profile is smaller, in some cases by more than 7 dB.

TABLE 4.1

SUMMARY OF FLOW PARAMETERS AND ACOUSTIC RESULTS FOR THE CONSTANT THRUST SERIES FOR THE FOUR-INCH COANNULAR NOZZLE WITH HEATED FLOW

| M_p | M_s | V_s/V_p | Th/A_t | \dot{m}_t/A_t | \dot{m}_s/\dot{m}_p | T_{os} °R | T_{op} °R | T_{os}/T_{op} | OASPL 30° dB | PWL dB |
|-------|-------|-----------|--------------------------|----------------------------|-----------------------|----------------|----------------|-----------------|-----------------|-----------|
| .75 | .76 | .61 | 11.20 lb/in ² | .36 lb/sec in ² | 1.69 | 541 | 1480 | .37 | 120.5 | 134.90 |
| .75 | .76 | .65 | | .37 | 1.59 | 535 | 1305 | .41 | 119.5 | 131.68 |
| .75 | .76 | .69 | | .38 | 1.52 | 532 | 1170 | .45 | 117.0 | 131.29 |
| .75 | .76 | .74 | | .39 | 1.41 | 533 | 990 | .53 | 115.0 | 129.11 |
| .75 | .76 | .85 | | .41 | 1.23 | 532 | 768 | .69 | 109.5 | 124.65 |
| .75 | .76 | 1.03 | | .45 | 1.03 | 530 | 528 | 1.00 | 104.0 | 120.30 |
| .75 | .76 | 1.22 | | .41 | .86 | 765 | 532 | 1.44 | 104.5 | 122.05 |
| .75 | .76 | 1.41 | | .39 | .74 | 1020 | 531 | 1.92 | 107.0 | 125.06 |
| .75 | .76 | 1.59 | | .37 | .66 | 1310 | 540 | 2.43 | 110.0 | 127.91 |
| .66 | .83 | 1.87 | | .35 | .84 | 1300 | 558 | 2.33 | 110.5 | 128.28 |
| .94 | .76 | .51 | 14.30 | .40 | 1.26 | 550 | 1420 | .39 | 126.0 | 140.00 |
| .85 | .82 | .63 | | .41 | 1.49 | 550 | 1300 | .42 | 123.0 | 137.16 |
| .85 | .83 | .72 | | .43 | 1.32 | 545 | 1000 | .55 | 118.5 | 132.38 |
| .85 | .83 | .84 | | .46 | 1.14 | 550 | 750 | .73 | 113.0 | 127.38 |
| .85 | .85 | 1.00 | | .51 | 1.00 | 538 | 538 | 1.00 | 107.0 | 123.81 |
| .85 | .85 | 1.21 | | .47 | .84 | 760 | 525 | 1.45 | 108.5 | 125.41 |
| .85 | .85 | 1.36 | | .44 | .73 | 1015 | 545 | 1.86 | 110.5 | 128.55 |
| .85 | .85 | 1.53 | | .41 | .65 | 1300 | 555 | 2.34 | 113.5 | 131.15 |
| .80 | .90 | 1.68 | | .40 | .75 | 1315 | 567 | 2.32 | 114.0 | 131.19 |
| .74 | .95 | 1.95 | | .39 | .85 | 1410 | 575 | 2.45 | 115.5 | 133.39 |

TABLE 4.1a
 SUMMARY OF TEST CONDITIONS AND COMPUTED MIXED FLOW CONDITIONS FOR THE
 CONSTANT THRUST SERIES $T_h/A = 14.30 \text{ lb/in}^2$ FOR THE FOUR-INCH COANNULAR NOZZLE ($A_N = .08726 \text{ ft}^2$)

| M_p | M_s | P_{op}^2 lb/ft ² abs | P_{os} lb/ft ² abs | P_{om} lb/ft ² | T_{op} °R | T_{os} °R | T_{om} °R | V_s/V_p | A_m ft ² | OASPL 30 for Mixed Flow dB |
|-------|-------|---|---------------------------------------|--------------------------------|----------------|----------------|----------------|-----------|--------------------------|-------------------------------------|
| .94 | .76 | 3599 | 2978 | 3252 | 1420 | 550 | 935 | .51 | .0902 | 120.4 |
| .85 | .82 | 3264 | 3183 | 3216 | 1300 | 545 | 848 | .63 | .0896 | 117.8 |
| .85 | .83 | 3259 | 3190 | 3220 | 1000 | 545 | 744 | .72 | .0885 | 114.8 |
| .85 | .83 | 3264 | 3197 | 3228 | 750 | 550 | 644 | .84 | .0877 | 111.8 |
| .85 | .85 | 3273 | 3282 | 3278 | 538 | 538 | 538 | 1.00 | .0875 | 108.6 |
| .85 | .85 | 3268 | 3282 | 3274 | 525 | 760 | 632 | 1.21 | .0878 | 112.1 |
| .85 | .85 | 3272 | 3260 | 3266 | 545 | 1015 | 743 | 1.36 | .0881 | 115.5 |
| .85 | .85 | 3266 | 3264 | 3265 | 555 | 1300 | 859 | 1.53 | .0894 | 118.4 |
| .80 | .90 | 3118 | 3441 | 3256 | 567 | 1315 | 886 | 1.68 | .0899 | 119.2 |
| .74 | .95 | 2937 | 3656 | 3266 | 575 | 1410 | 958 | 1.95 | .0895 | 121.1 |

TABLE 4.2

SUMMARY OF FLOW PARAMETERS AND ACOUSTIC RESULTS FOR THE CONSTANT MASS FLOW SERIES FOR THE FOUR-INCH COANNULAR NOZZLE WITH HEATED FLOW

| M_p | M_s | V_s/V_p | Th/A_t | \dot{m}_t/A_t | \dot{m}_s/\dot{m}_p | T_{os} °R | T_{op} °R | T_{os}/T_{op} | OASPL 30° dB | PWL dB |
|-------|-------|-----------|--------------------------|----------------------------|-----------------------|----------------|----------------|-----------------|-----------------|-----------|
| .84 | .73 | .57 | 12.34 lb/in ² | .36 lb/sec in ² | 1.32 | 551 | 1310 | .42 | 121.5 | 135.52 |
| .77 | .77 | .65 | 11.70 | | 1.55 | 550 | 1310 | .42 | 119.5 | 133.25 |
| .72 | .72 | .75 | 10.29 | | 1.37 | 549 | 1000 | .55 | 112.0 | 125.92 |
| .69 | .69 | .84 | 9.38 | | 1.20 | 550 | 790 | .70 | 105.0 | 120.39 |
| .61 | .63 | 1.02 | 7.69 | | 1.03 | 548 | 548 | 1.00 | 96.0 | 114.18 |
| .66 | .68 | 1.21 | 8.88 | | .88 | 760 | 548 | 1.39 | 101.0 | 118.03 |
| .70 | .72 | 1.39 | 10.04 | | .76 | 1000 | 548 | 1.82 | 105.5 | 123.62 |
| .75 | .77 | 1.58 | 11.42 | | .67 | 1300 | 552 | 2.36 | 110.5 | 128.71 |
| .72 | .81 | 1.70 | 11.69 | | .75 | 1300 | 561 | 2.32 | 112.0 | 129.92 |
| .61 | .95 | 2.22 | 12.71 | | 1.09 | 1280 | 572 | 2.24 | 115.5 | 133.88 |
| 1.05 | 1.06 | .65 | 21.34 | .52 | 1.56 | 550 | 1305 | .42 | 131.0 | 144.28 |
| .98 | .99 | .75 | 19.54 | | 1.36 | 550 | 995 | .55 | 124.0 | 137.91 |
| .92 | .94 | .87 | 17.17 | | 1.20 | 551 | 760 | .74 | 117.0 | 131.65 |
| .84 | .87 | 1.02 | 14.55 | | 1.03 | 520 | 520 | 1.00 | 107.5 | 124.49 |
| .89 | .93 | 1.22 | 16.64 | | .90 | 760 | 550 | 1.38 | 111.0 | 127.81 |
| .95 | 1.00 | 1.41 | 19.00 | | .78 | 1005 | 545 | 1.84 | 115.0 | 131.87 |
| 1.00 | 1.05 | 1.52 | 20.65 | | .70 | 1260 | 545 | 2.31 | 119.0 | 135.65 |

It can also be seen from these tables that, for both the constant thrust and the constant mass flow series, the sound pressure level increases fairly rapidly as the velocity ratio departs from one. This should not be interpreted as indicating that $V_s/V_p = 1$ is an optimum value. Since the velocity ratio in these tests was varied primarily by changing the stagnation temperature of the primary or secondary stream, the energy input for $V_s/V_p = 1$ is a minimum. The only comparisons that may be fairly made in Table 4.1 and 4.2 are between standard and inverted velocity profiles with the same thrust and same mass flow. Comparisons of acoustic data on this basis are further displayed in Figures 4.1 through 4.6.

Figure 4.1 shows two OASPL directivities from a constant thrust series ($Th/A = 11.20 \text{ lb/in}^2$). The comparison of the directivities in this figure shows that the inverted profile with hot outer flow is quieter in the region of maximum noise, that is up to about sixty degrees from the jet axis, but is slightly louder for larger angles. The maximum difference occurs at about 30° and is approximately 9 dB.

Figure 4.2 shows a comparison of the sound pressure spectra at 30° for the conventional and inverted profiles. This figure reveals that the primary noise reduction occurs in the medium to low frequency range where the spectrum for the conventional profile peaks. The spectrum for the inverted profile is relatively flat and contains a greater amount of high frequency noise.

Figures 4.3 and 4.4 show similar acoustic data for the higher thrust series ($Th/A = 14.30$). It is of interest to note that the spectrum at 30° for the inverted profile case shows a double peaked character that has been observed by other investigators (Ref. 6). Figures 4.5 and 4.6 show directivity and spectral data for the higher mass flow series, at the extreme velocity ratios. Under these conditions both the primary and secondary streams are choked with supercritical pressure ratios (cf. Table 4.2). At 30° , the OASPL of the inverted profile is approximately 12 dB lower than for the conventional profile, although the conventional profile has about a 3% thrust advantage.

A semi-empirical calculation has been carried out for the four-inch coannular nozzle data to obtain the sound pressure level at 30° for a synthesized flow and a fully mixed flow. The procedure for computing

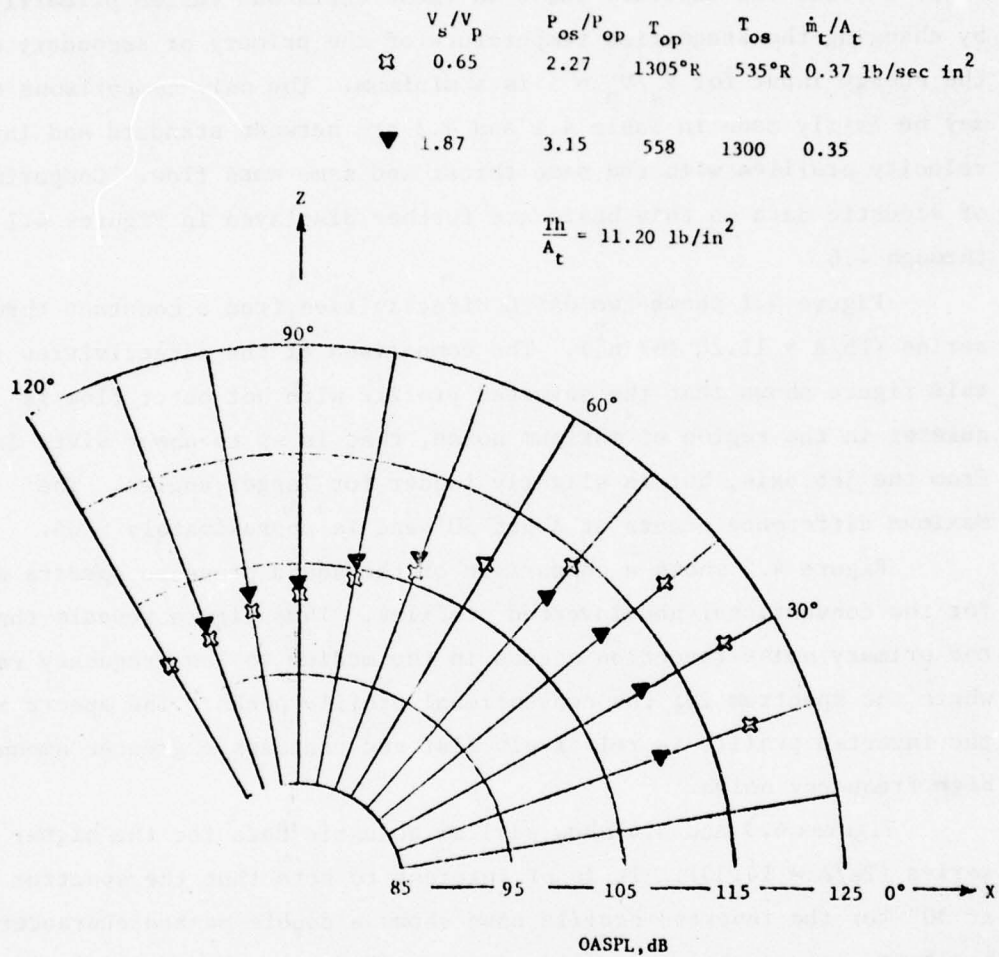


Figure 4.1. OASPL Directivities in the XZ Plane of the Four-Inch Coannular Nozzle at Elevated Temperatures and Constant Thrust.

| | | | |
|---|-------------------|---------------------------|-------------------------|
| | $\frac{V_s}{V_p}$ | $\frac{\dot{m}_t}{A_t}$ | $\frac{T_{os}}{T_{op}}$ |
| 1 | 0.65 | .37 lb/secin ² | 0.41 |
| 2 | 1.87 | .35 | 2.33 |

$\frac{T_h}{A_t} = 11.20 \text{ lb/in}^2$

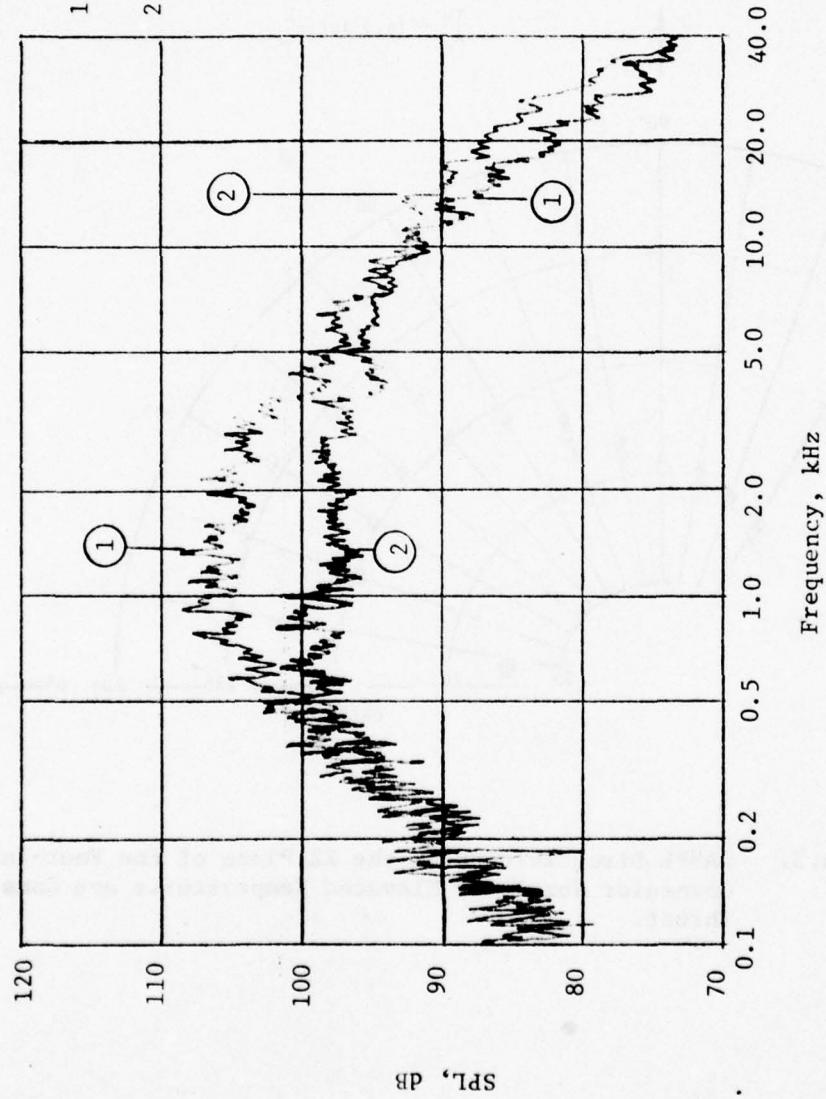


Figure 4.2 Comparison of Sound Pressure Spectra at $\theta = 30^\circ$ in the XZ Plane of the 4-Inch Coannular Nozzle at Constant Thrust and Elevated Temperature.

| | v_s/v_p | P_{os}/P_{op} | T_{op} | T_{os} | \dot{m}_t/A_t |
|---|-----------|-----------------|----------|----------|-----------------------------|
| ◇ | .51 | 1.38 | 1420°R | 550°R | 0.40 lb/sec in ² |
| ◆ | 1.95 | 2.96 | 575 | 1410 | 0.39 |

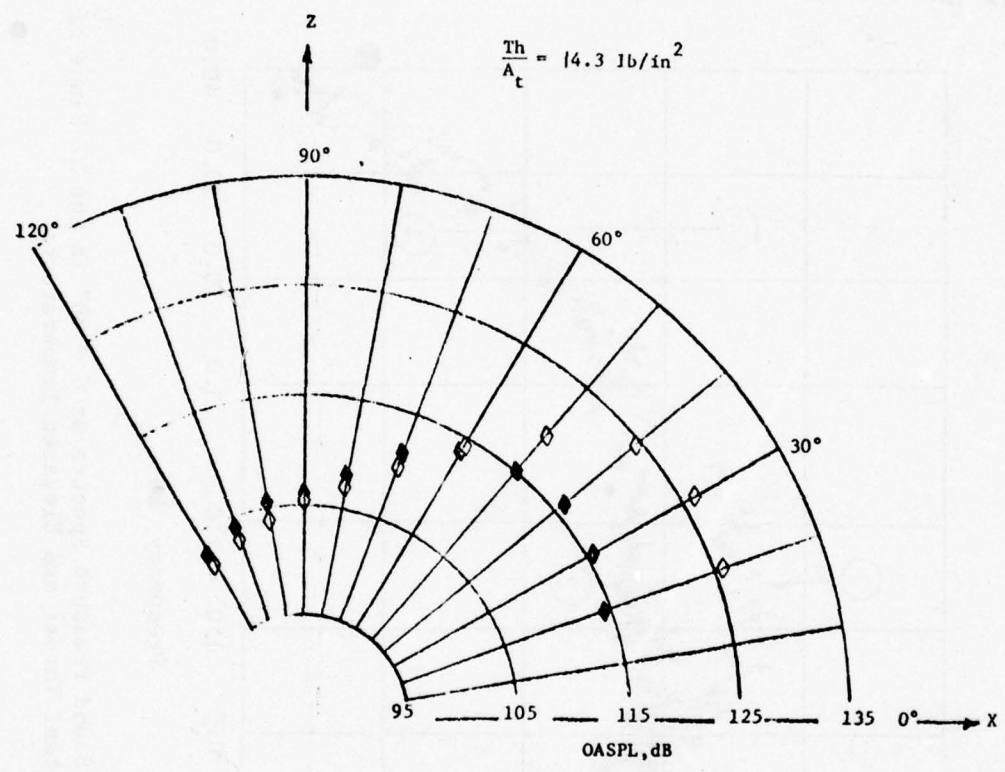


Figure 4.3. OASPL Directivities in the XZ Plane of the Four-Inch Coannular Nozzle at Elevated Temperatures and Constant Thrust.

| | | |
|-------------------|-----------------------------|-------------------------|
| $\frac{V_s}{V_p}$ | $\frac{\dot{m}_t}{A_t}$ | $\frac{T_{os}}{T_{op}}$ |
| 1 0.51 | .40 lbs/sec in ² | 0.39 |
| 2 1.95 | .39 | 2.45 |

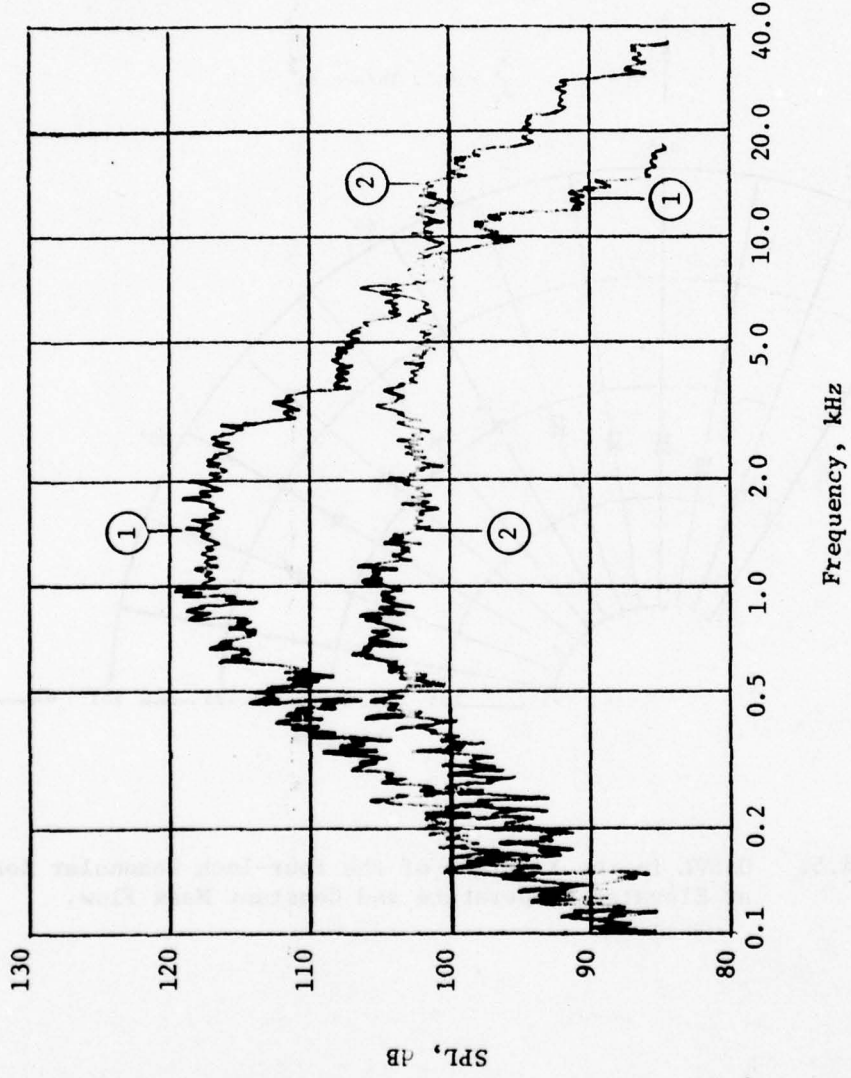
 $\frac{T_h}{A_t} = 14.3 \text{ lb/in}^2$


Figure 4.4 Comparison of Sound Pressure Spectra at $\theta = 30^\circ$ in the XZ Plane of the 4-Inch Coannular Nozzle at Constant Thrust and Elevated Temperature.

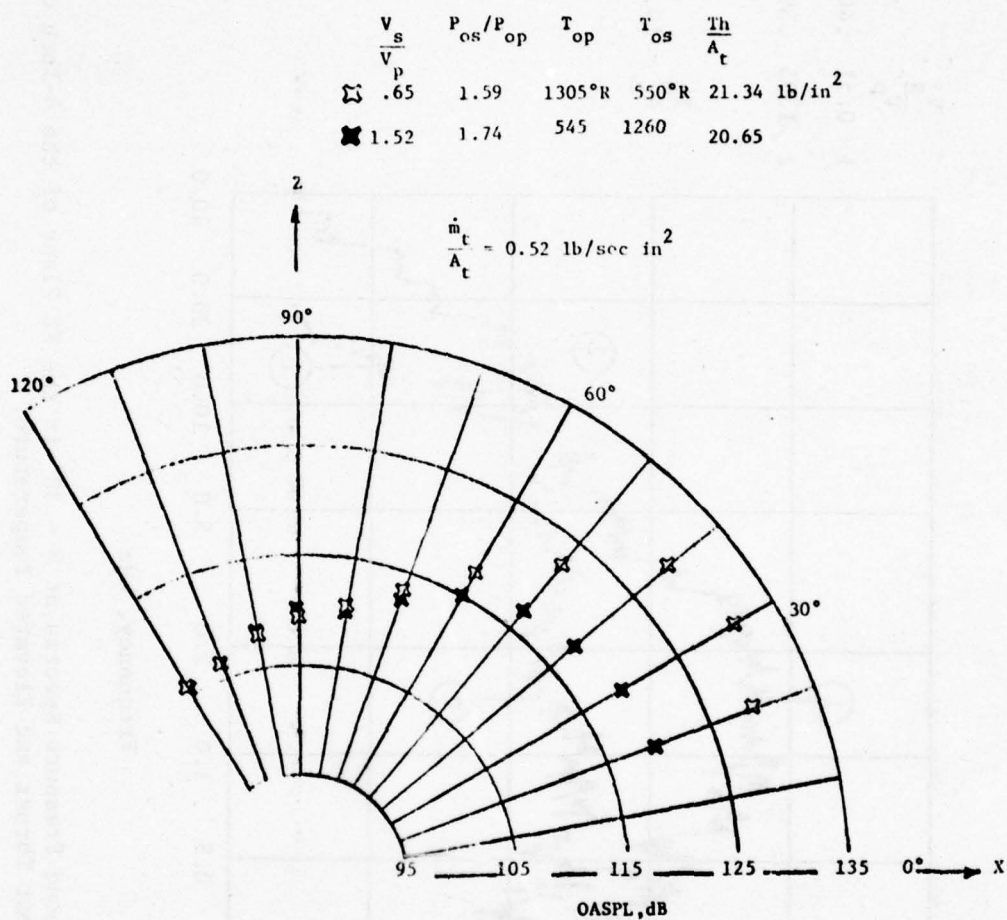


Figure 4.5. OASPL in the XZ Plane of the Four-Inch Conical Nozzle at Elevated Temperature and Constant Mass Flow.

| | $\frac{V_s}{V_p}$ | $\frac{T_h}{A_t}$ | $\frac{T_{OS}}{T_{op}}$ |
|---|-------------------|---------------------------|-------------------------|
| 1 | 0.65 | 21.34 lbs/in ² | 0.42 |
| 2 | 1.52 | 20.65 | 2.31 |

$$\frac{\dot{m}_t}{A_t} = 0.52 \text{ lb/sec in}^2$$

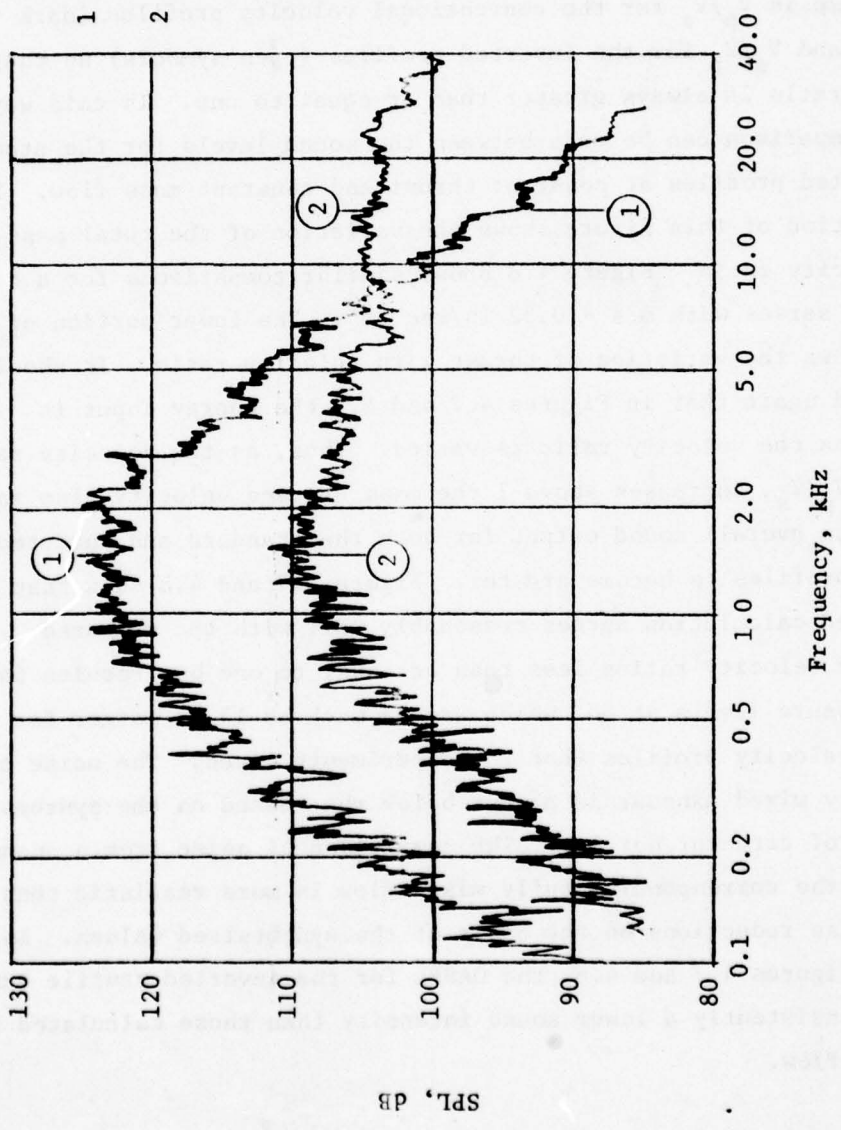


Figure 4.6. Comparison of Sound Pressure Spectra at $\theta = 30^\circ$ in the XZ Plane of the 4-Inch Coannular Nozzle at Constant Mass Flow and Elevated Temperature.

the synthesized and fully mixed sound pressure levels is the same as described in Section 3.0 where the empirical curve fit was used for the single nozzle sound pressure level at 30° . Table 4.1a gives a summary of the test conditions for the constant thrust series of $Th/A = 14.30 \text{ lb/in}^2$ along with computed mixed flow conditions. Figure 4.7 shows a comparison between measured sound pressure data from this series and the computed synthesized and mixed values. The abscissa in this figure is V_p/V_s for the conventional velocity profiles (dark symbols) and V_s/V_p for the inverted profiles (open symbols) so that the velocity ratio is always greater than or equal to one. In this way a direct comparison can be made between the sound levels for the standard and inverted profiles at constant thrust and constant mass flow. The lower portion of this figure shows the variation of the total mass flow with velocity ratio. Figure 4.8 shows similar comparisons for a constant mass flow series with $\dot{m}/A = 0.52 \text{ lb/sec in}^2$. The lower portion of this figure shows the variation of thrust with velocity ratio. It should be emphasized again that in Figures 4.7 and 4.8 the energy input is changing as the velocity ratio is varied. Thus, as the velocity ratio, V_s/V_p or V_p/V_s , increases above 1 the mass average velocity also increases causing the overall sound output for both the standard and inverted velocity profiles to become greater. Figure 4.7 and 4.8 show that the synthesized calculation agrees reasonably well with the measured values for velocity ratios less than or equal to one but results in sound pressure levels at 30° which are as much as 15 dB larger for the inverted velocity profiles than the experiments given. The noise calculated for a fully mixed exhaust is always below that based on the synthesis of the noise of circular nozzles. The comparison of noise from a coannular flow with the corresponding fully mixed flow is more realistic than citing noise reductions on the basis of the synthesized values. As shown in Figures 4.7 and 4.8, the OASPL for the inverted profile experiments display consistently a lower sound intensity than those calculated for the mixed flow.

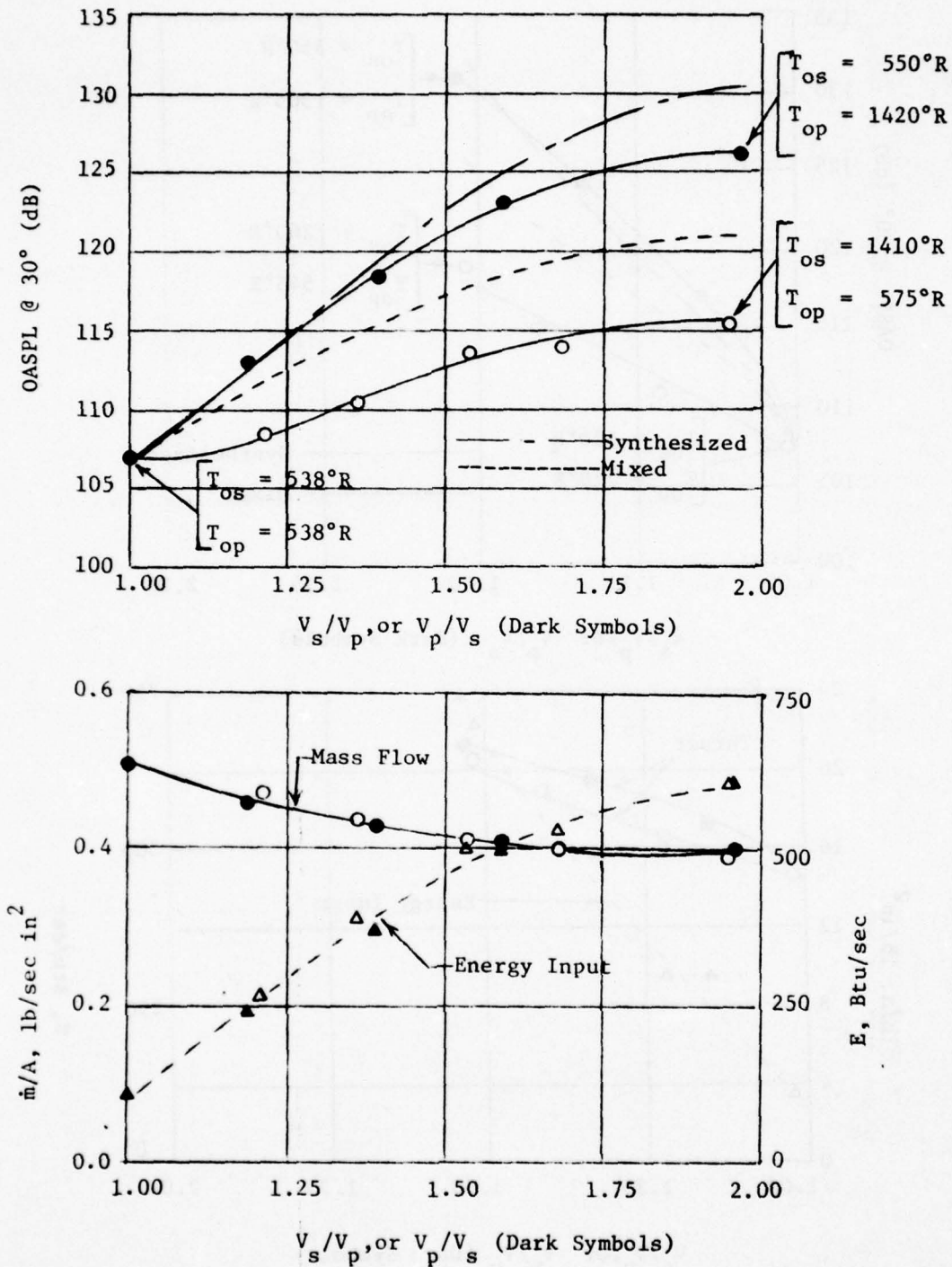


Figure 4.7. Sound Pressure Level, Mass Flow, and Energy Input versus Velocity Ratio for Constant Thrust/Area = 14.30 lb/in² (Four-Inch Nozzle, Hot Flow).

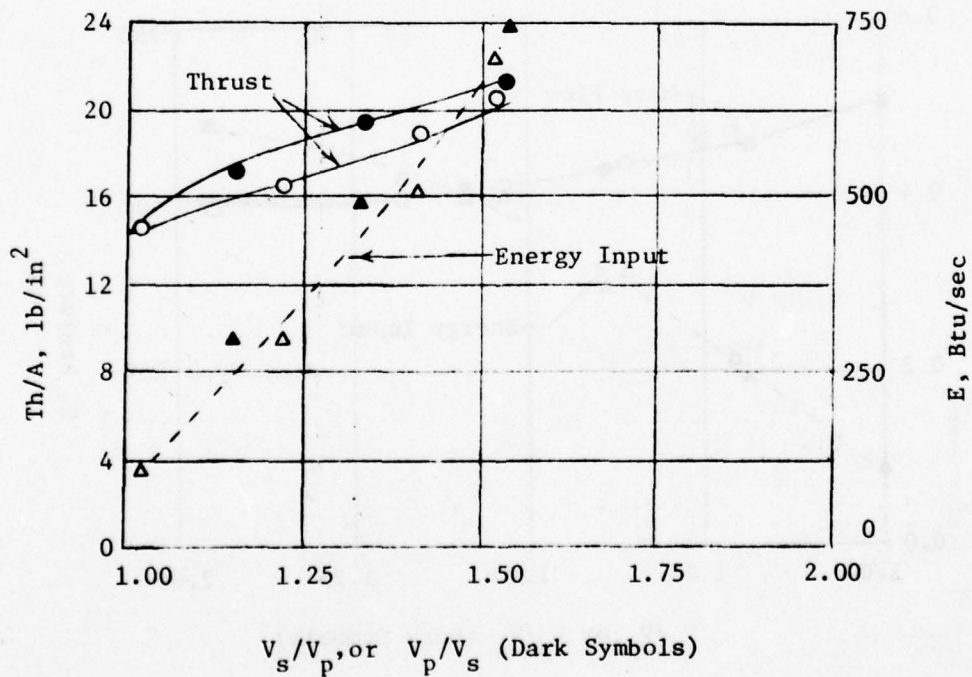
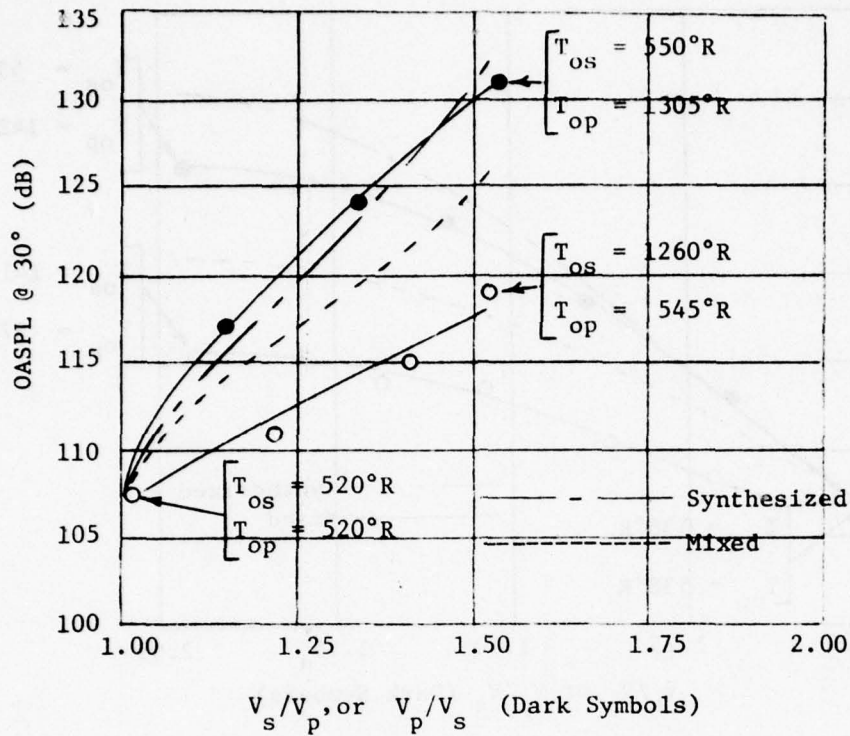


Figure 4.8. Sound Pressure Level, Thrust, and Energy Input versus Velocity Ratio for Constant Mass Flow/Area = 0.52 lb/sec in². (Four-Inch Nozzle, Hot Flow).

Comparing the sound pressure levels for the standard and inverted profiles in these figures shows that the reduction in noise associated with the inverted velocity profile increases initially with increasing velocity ratio. For the constant thrust series shown in Figure 4.7 the difference appears to be leveling off as a velocity ratio of two is approached. For the constant mass flow series the difference is still increasing at the highest velocity ratio measured.

4.1.1 JT8D Test Series.

In addition to the constant thrust and constant mass flow series for the four-inch coannular nozzle, a separate test program was performed to simulate operating conditions for the JT8D engine and to determine the effect of profile inversion on the noise characteristics of this engine. Primary and secondary flow parameters were set to simulate the core jet and fan stream conditions for typical takeoff, cutback, and approach power settings. In the comparable tests for the inverted profiles the primary and secondary flow conditions were simply reversed.

Table 4.3 summarizes the flow conditions and the acoustic results for the JT8D conditions. The sound pressure levels cited in this table are values measured at 30° to the jet axis or calculated for a synthesized or fully mixed flow using an empirical correlation as explained before. For the conventional profiles, A through C, the measured OASPL values generally lie between the synthesized and mixed values, although they are closer to the synthesized values. For the inverted profiles the experimental data is as much as 12 dB below the synthesized values and 7 dB below the fully mixed. Since the exit areas for the primary and secondary streams are the same, the differences between the calculated noise levels for the conventional and inverted flow are due only to slight differences in run conditions. Table 4.3a gives a summary of the test conditions and the computed mixed flow conditions for the JT8D series.

Figure 4.9 and 4.10 shows a direct comparison between the acoustic data obtained for the conventional takeoff condition and its inverse. These data show trends similar to other "constant thrust-constant mass flow" comparisons presented in preceding parts of this section. The directivity comparison in Figure 4.9 shows about a 10 dB reduction in the region of maximum sound pressure (convective lobe) for the inverted flow but only a slight difference at the larger angles with their low sound pressure.

TABLE 4.3
 SUMMARY OF FLOW PARAMETERS AND ACOUSTIC RESULTS
 FOR JT8D TEST SERIES FOR THE FOUR-INCH COANNULAR NOZZLE WITH HEATED FLOW

30°

| Designation | M_p | M_s | V_s/V_p | Th/A_t lb/in ² | \dot{m}/A_t lb/in ² sec | \dot{m}_s/\dot{m}_p | T_{cs}/T_{cp} | Measured OASPL (30°) dB | OASPL SNY dB | OASPL MIXED dB | JT8D CONDITION |
|-------------|-------|-------|-----------|--------------------------------|---|-----------------------|-----------------|-------------------------------|--------------------|----------------------|-------------------|
| A | 1.11 | 1.06 | .65 | 21.96 | .557 | 1.43 | .43 | 131.0 | 133.9 | 127.1 | TAKE OFF |
| B | .96 | .93 | .66 | 17.82 | .478 | 1.43 | .46 | 126.0 | 127.5 | 121.5 | CUT BACK |
| C | .79 | .78 | .68 | 12.02 | .386 | 1.44 | .47 | 119.0 | 119.1 | 113.8 | APPROACH |
| D | 1.05 | 1.10 | 1.50 | 21.80 | .548 | .71 | 2.25 | 121.0 | 133.7 | 127.3 | INVERSE OF A |
| E | .93 | .96 | 1.50 | 17.74 | .476 | .71 | 2.14 | 115.0 | 127.5 | 122.6 | INVERSE OF B |
| F | .79 | .79 | 1.45 | 12.17 | .287 | .69 | 2.09 | 108.7 | 119.2 | 114.1 | INVERSE OF C |

TABLE 4. 3a
 SUMMARY OF TEST CONDITIONS AND COMPUTED MIXED FLOW CONDITIONS FOR JT8D TEST
 SERIES WITH FOUR-INCH NOZZLE ($A_N = .08726 \text{ ft}^2$)

| Designation | P_{op} lb/ft ² abs | P_{os} lb/ft ² abs | P_{om} lb/ft ² abs | T_{op} °R | T_{os} °R | T_{om} °R | V_s/V_p | A_m ft ² | OASPL @ 30° FOR MIXED FLOW dB |
|-------------|---------------------------------------|---------------------------------------|---------------------------------------|----------------|----------------|----------------|-----------|--------------------------|-------------------------------------|
| A | 4422 | 4130 | 4250 | 1265 | 542 | 840 | .65 | .0902 | 127.1 |
| B | 3692 | 3579 | 3625 | 1195 | 545 | 812 | .66 | .0692 | 121.5 |
| C | 3054 | 3038 | 3045 | 1162 | 550 | 800 | .68 | .0899 | 113.8 |
| D | 4100 | 4392 | 4222 | 560 | 1262 | 852 | 1.50 | .0900 | 127.2 |
| E | 3570 | 3685 | 3618 | 555 | 1190 | 818 | 1.50 | .0891 | 121.5 |
| F | 3054 | 3063 | 3063 | 551 | 1160 | 800 | 1.45 | .0887 | 114.0 |

| | Designation | $\frac{V_S}{V_P}$ | T_{OS} | T_{OP} |
|---|-------------|-------------------|----------|----------|
| ⊞ | A | 0.65 | 542° R | 1265° R |
| ✕ | D | 1.50 | 1262° R | 560° R |

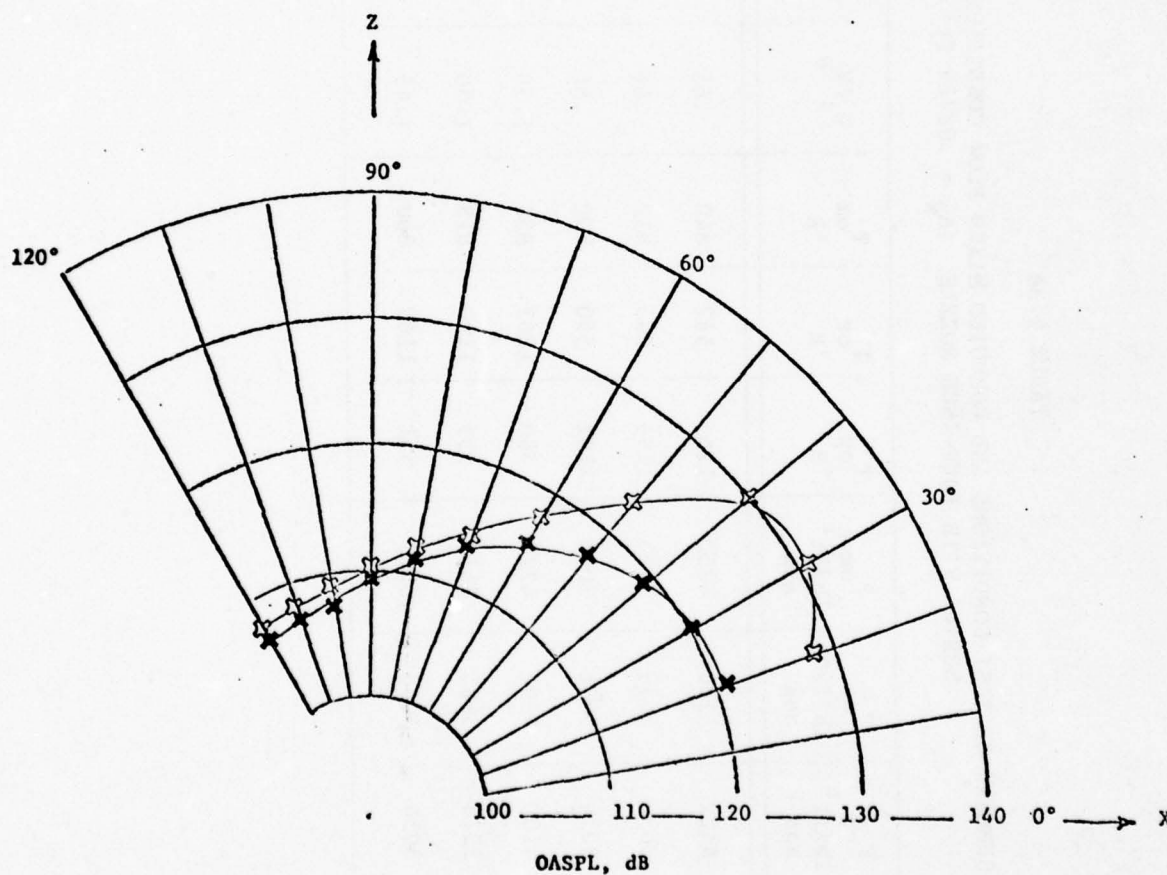


Figure 4.9. Comparative Directivities for Simulated Takeoff Conditions A and D for the JT8D Series with Four-Inch Nozzle at Mean Thrust Per Unit Area of 21.88 lb/in^2 and Mean Mass Flow Per Unit Area of $0.553 \text{ lb/sec in}^2$.

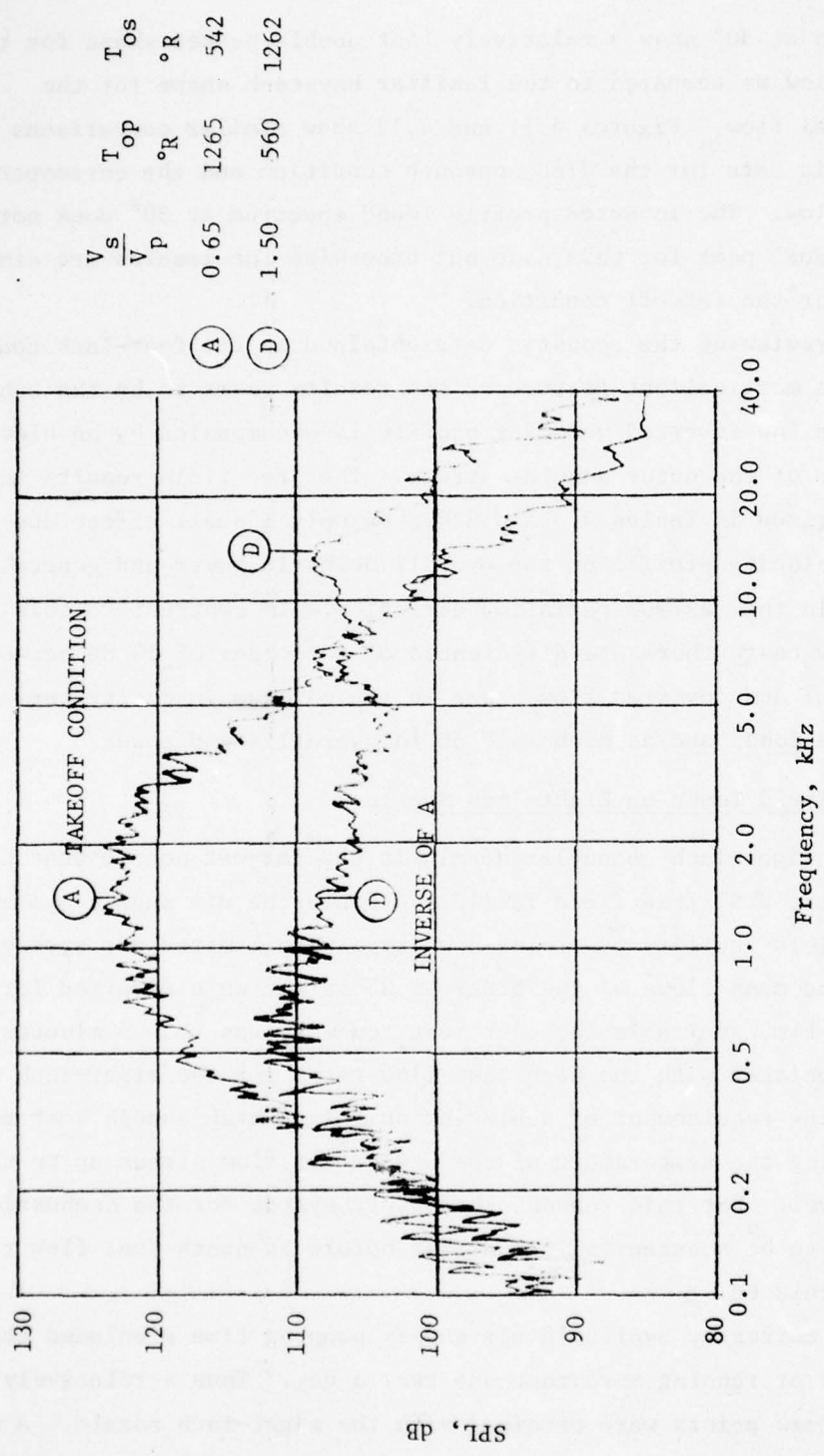


Figure 4.10. Comparative Spectra at 30° for Simulated Takeoff Conditions A and D for the JT8D Series with 4" Nozzle at Mean Thrust per Unit Area of 21.88 lb/in² and Mean Mass Flow per Unit Area of 0.553 lb/sec in².

The spectra at 30° show a relatively flat double peaked shape for the inverted flow as compared to the familiar haystack shape for the conventional flow. Figures 4.11 and 4.12 show similar comparisons between the acoustic data for the JT8D approach condition and the corresponding inverted flow. The inverted profile sound spectrum at 30° does not exhibit a dual peak for this case but otherwise the results are similar to those for the takeoff condition.

In reviewing the acoustic data obtained on the four-inch coannular nozzle, the most salient feature of the results seems to be the enhanced effect when the inverted velocity profile is accompanied by an elevated temperature of the outer annular stream. The free field results for cold flow summarized in Tables 3.3 and 3.4 show only a small effect due to the inverted velocity profile on the overall acoustic power and generally only 3 to 5 dB in the maximum radiation direction. In contrast to this for the heated flow tests there are differences of the order of 10 dB between the conventional and inverted flow cases in the maximum intensity region (convective lobe) and as much as 8 dB in overall sound power.

4.2 Free Field Tests on Eight-Inch Nozzle.

The eight-inch coannular nozzle is the largest nozzle that has been tested in the UTSI free field facility. Since the air supply system for the free field facility is a blow down type with limited air storage capacity and mass flows of the order of 25 lb/sec were required for these tests, the time available for each test run was less than 5 minutes.

Associated with the high mass flow rates for the eight-inch nozzle tests was the requirement of achieving quickly a high enough heat release rate to bring the temperature of the heated air flow stream up to the desired level. For this reason, the supply system for the combustion heater had to be substantially modified before adequate fuel flow rates could be achieved.

The currently available air supply pump-up time precluded the possibility of running more than one test a day. Thus a relatively small number of data points were obtained with the eight-inch nozzle. A major objective of the experiments for different nozzle sizes was to determine how well data from the four-inch tests could be scaled up to the eight-inch

| Designation | $\frac{V_s}{V_p}$ | T_{os} | T_{op} |
|-------------|-------------------|----------|----------|
| ◇ C | 0.68 | 550° R | 1162° R |
| ● F | 1.45 | 1160° R | 555° R |

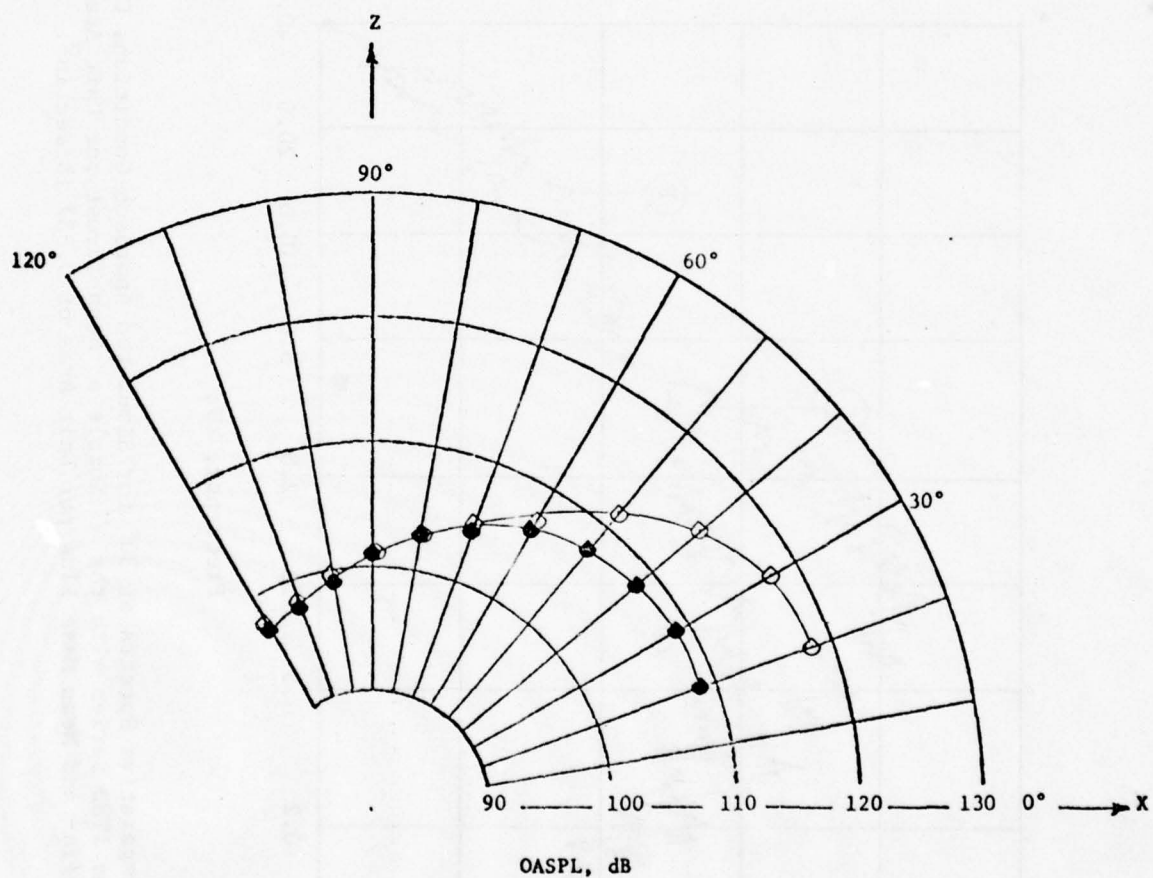
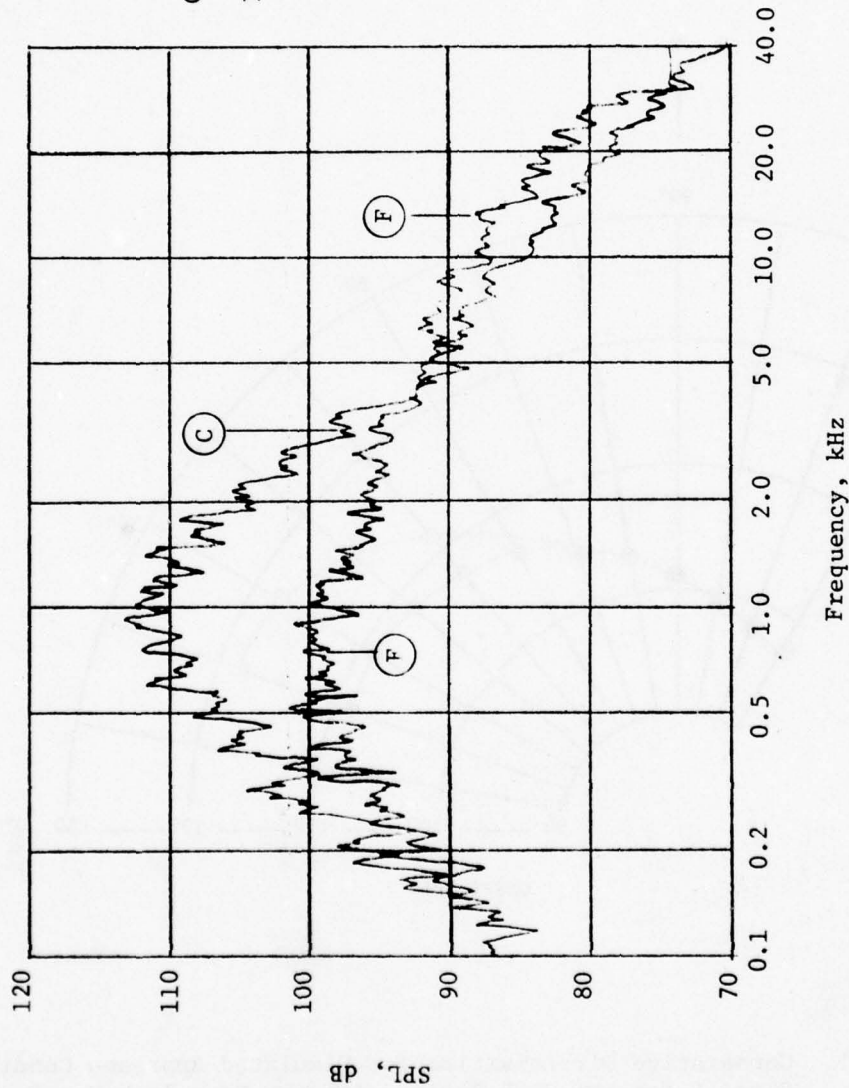


Figure 4.11. Comparative Directivities for Simulated Approach Conditions C and F for the JT8D Series with the Four-Inch Nozzle at Mean Thrust Per Unit Area of 12.10 lb/in² and Mean Mass Flow Per Unit Area of 0.337 lb/sec in².



| | $\frac{V_s}{V_p}$ | T_{op} °R | T_{os} °R |
|---|-------------------|----------------|----------------|
| C | 0.68 | 1162 | 550 |
| F | 1.45 | 557 | 1160 |

Figure 4.12. Comparative Spectra at 30° for Simulated Approach Conditions C and F for the JT8D Series with the 4" Nozzle at Mean Thrust per Unit Area of 12.10 lb/in² and Mean Mass Flow per Unit Area of 0.337 lb/sec in².

nozzle size. Thus, much of the eight-inch nozzle data presented in this section is displayed along with the corresponding four-inch data scaled up, and in the case of spectra, frequency shifted, to account for the difference in diameter.

The relatively short run times for the eight-inch nozzle dictated a change in data acquisition procedure. Two data channels were used for the eight-inch nozzle tests with one microphone being set at 30° from the jet axis and the second at 90° . Spectra from these two microphones were taken for each test condition. For runs where the mass flow rate was low or where test conditions stabilized fairly quickly, a sweep was then made with the 30° microphone. However, there were a number of runs where a sweep could not be obtained before the supply air pressure dropped below the operational level.

The eight-inch nozzle test program included a series of simulated JT8D conditions, a constant thrust series, and a constant mass flow series.

4.2.1 JT8D Test Series.

Table 4.4 summarizes the flow parameters and the acoustic results for the eight-inch test program. The first three conditions in the table designated A through C simulate operating conditions for the JT8D engine and are essentially the same as like designated conditions in Table 4.3 for the four-inch nozzle. The test conditions designated D through F were obtained by interchanging the primary and secondary stagnation conditions. Since the primary and secondary nozzle exit areas are the same, this interchange preserves total thrust and total mass flow. Included in this table are measured OASPL values at $\theta = 30^\circ$ and $\theta = 90^\circ$ as well as synthesized values at 30° and the computed values of sound pressure level for a fully mixed flow. Table 4.4a gives the test conditions for the JT8D series and the computed mixed flow conditions.

Figures 4.13 through 4.17 show a comparison of the acoustic results for the JT8D takeoff condition (A) and condition (D), its inverse, along with corresponding data from the four-inch test series scaled up to the eight-inch nozzle by adding 6 dB to the measured sound pressure level. Figure 4.13 shows the OASPL at 30° and 90° for the eight-inch nozzle tests along with a sweep from the four-inch nozzle tests. The agreement

TABLE 4.4
 SUMMARY OF FLOW PARAMETERS AND ACOUSTIC RESULTS FOR THE JT8D SERIES
 FOR THE EIGHT-INCH COANNULAR NOZZLE WITH HEATED FLOW

| Designation | M_p | M_s | T_{os}/T_{op} | V_s/V_p | \dot{m}_s/\dot{m}_p | Th/A lb/in ² | \dot{m}/A lb/in ² sec | 30° | | | COMMENTS | |
|-------------|-------|-------|-----------------|-----------|-----------------------|------------------------------|---------------------------------------|---------------|---------------|---------------|----------|---------------|
| | | | | | | | | SPL 30° dB | SPL SYN dB | SPL MIX dB | | |
| A | 1.11 | 1.06 | .41 | .62 | 1.47 | 23.20 | .552 | 138.0 | 140.50 | 133.10 | 116.0 | JT8D TAKEOFF |
| B | .96 | .94 | .46 | .66 | 1.44 | 17.81 | .489 | 133.0 | 132.58 | 126.73 | 111.0 | JT8D CUTBACK |
| C | .78 | .76 | .46 | .66 | 1.44 | 11.67 | .383 | 125.0 | 124.78 | 118.87 | 106.5 | JT8D APPROACH |
| D | 1.05 | 1.11 | 2.37 | 1.61 | .69 | 23.20 | .550 | 129.0 | 140.29 | 133.27 | 116.5 | INVERSE OF A |
| E | .94 | .96 | 2.07 | 1.47 | .72 | 17.90 | .487 | 122.0 | 132.38 | 127.03 | 112.5 | INVERSE OF B |
| F | .76 | .78 | 2.16 | 1.52 | .71 | 11.73 | .377 | 116.0 | 125.61 | 119.67 | 108.5 | INVERSE OF C |

TABLE 4.4a

SUMMARY OF TEST CONDITIONS AND COMPUTED MIXED FLOW CONDITIONS FOR JT8D
 SERIES WITH EIGHT-INCH NOZZLE ($A_N = .349 \text{ ft}^2$)

| Designation | P_{op} lb/ft ² abs | P_{os} lb/ft ² abs | P_{om} lb/ft ² abs | T_{op} °R | T_{os} °R | T_{om} °R | V_s/V_p | A_m ft ² | OASPL @ 30° FOR MIXED FLOW dB |
|-------------|---------------------------------------|---------------------------------------|---------------------------------------|----------------|----------------|----------------|-----------|--------------------------|--|
| A | 4392 | 4123 | 4232 | 1300 | 535 | 844 | .62 | .360 | 133.10 |
| B | 3682 | 3533 | 3629 | 1150 | 525 | 781 | .66 | .357 | 126.73 |
| C | 3030 | 2985 | 3007 | 1160 | 530 | 788 | .66 | .357 | 118.87 |
| D | 4110 | 4406 | 4231 | 545 | 1290 | 849 | 1.61 | .360 | 133.27 |
| E | 3594 | 3699 | 3638 | 545 | 1130 | 789 | 1.47 | .356 | 127.03 |
| F | 2981 | 3055 | 3012 | 550 | 1190 | 814 | 1.52 | .357 | 119.67 |

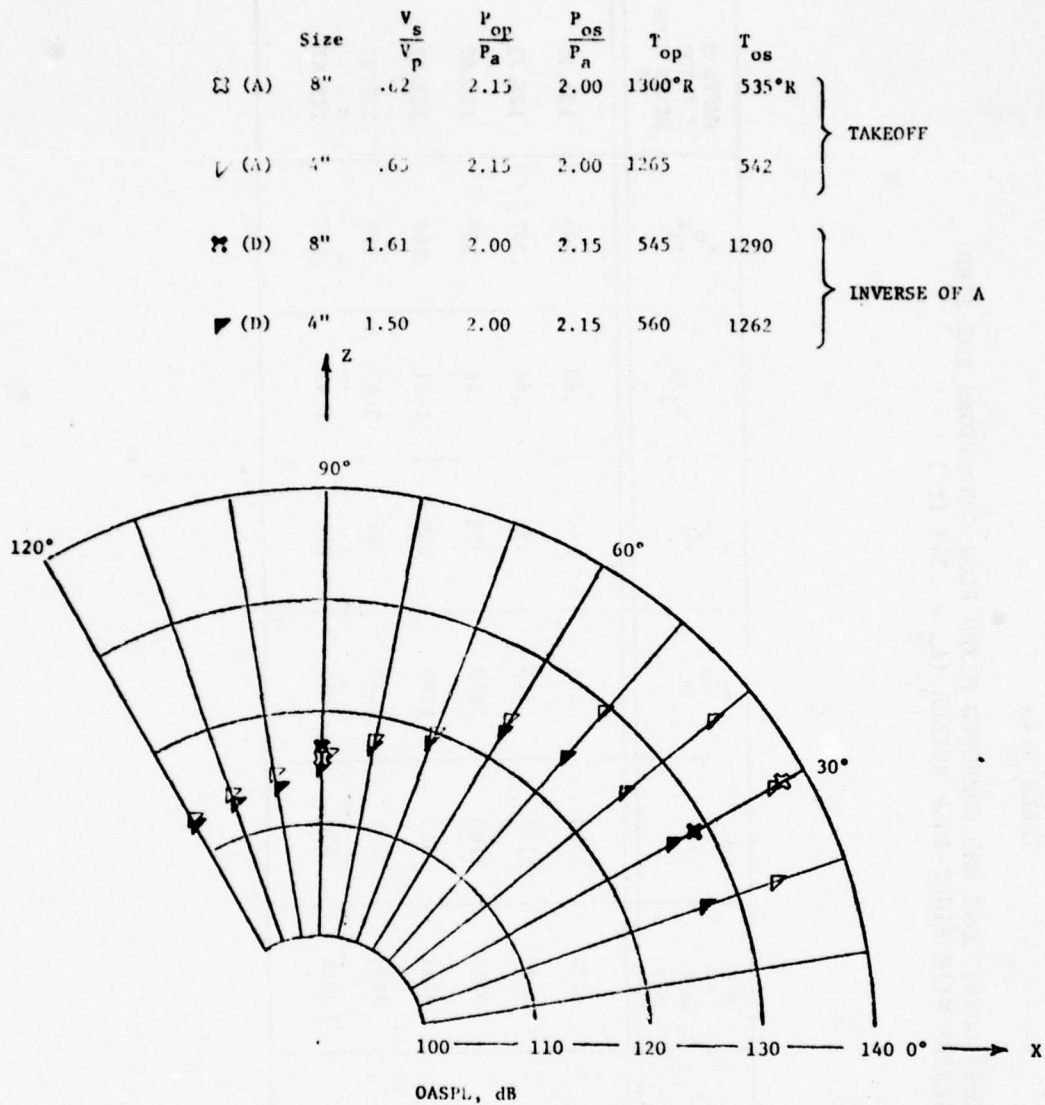


Figure 4.13. Directivities for Simulated JT8D Takeoff Conditions A and D Comparing 8-Inch Nozzle Data with Scaled 4-Inch Nozzle Data at Mean Thrust Per Unit Area of 22.54 lb/in² and Mean Mass Flow Per Unit Area of 0.552 lb/sec in².

| | $\frac{V_s}{V_p}$ | $\frac{P_{op}}{P_a}$ | $\frac{P_{os}}{P_a}$ | T_{op} | T_{os} |
|-----|-------------------|----------------------|----------------------|----------|----------|
| (A) | .62 | 2.15 | 2.00 | 1300°R | 535°R |
| (D) | 1.61 | 2.00 | 2.15 | 545 | 1290 |

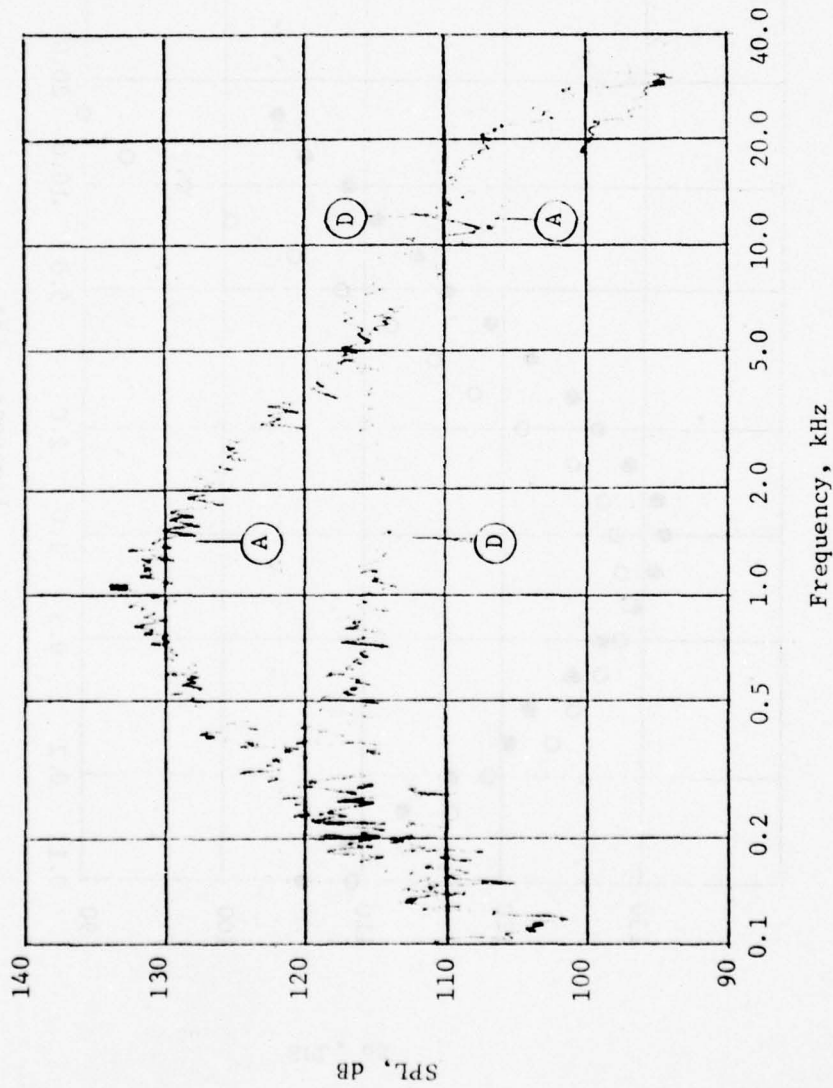


Figure 4.14. Comparative Spectra of the 8-Inch Nozzle at 30° for Simulated JT8D Takeoff Conditions A and D at Mean Thrust per Unit Area of 23.20 lb/in² and Mean Mass Flow per Unit Area of 0.551 lb/sec in².

JT8D TAKEOFF CONDITION

| Size | $\frac{V_s}{V_p}$ | T_{op} | T_{os} |
|------|-------------------|----------|----------|
| ● 8" | .62 | 1300°R | 535°R |
| ○ 4" | .65 | 1265 | 542 |

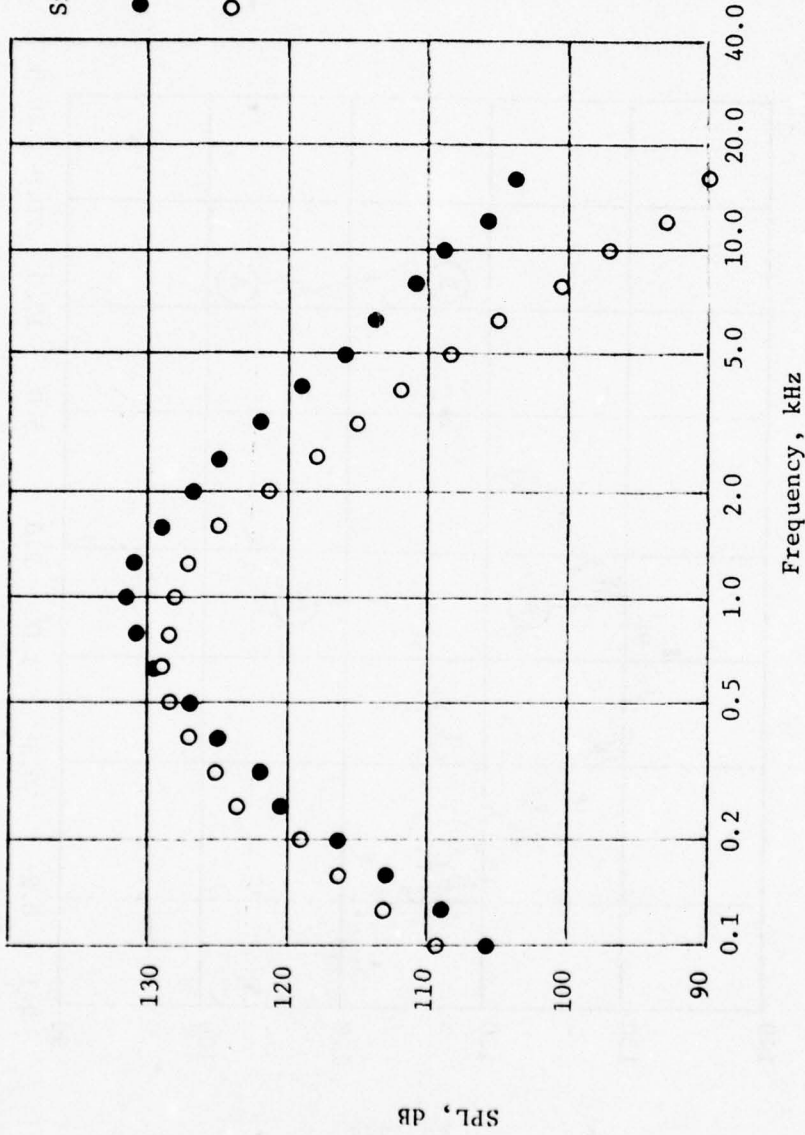


Figure 4.15. Comparison of 8-Inch Nozzle Spectra with Scaled 4-Inch Nozzle Spectra at 30° for Simulated JT8D Takeoff Condition A at Mean Thrust per Unit Area of 22.58 lb/in² and Mean Mass Flow per Unit Area of 0.555 lb/sec in².

INVERSE OF TAKEOFF

| | $\frac{V_s}{V_p}$ | T_{op} | T_{os} |
|-------|-------------------|----------|----------|
| ● 8" | 1.61 | 545°R | 1290°R |
| ○ 04" | 1.50 | 560 | 1262 |

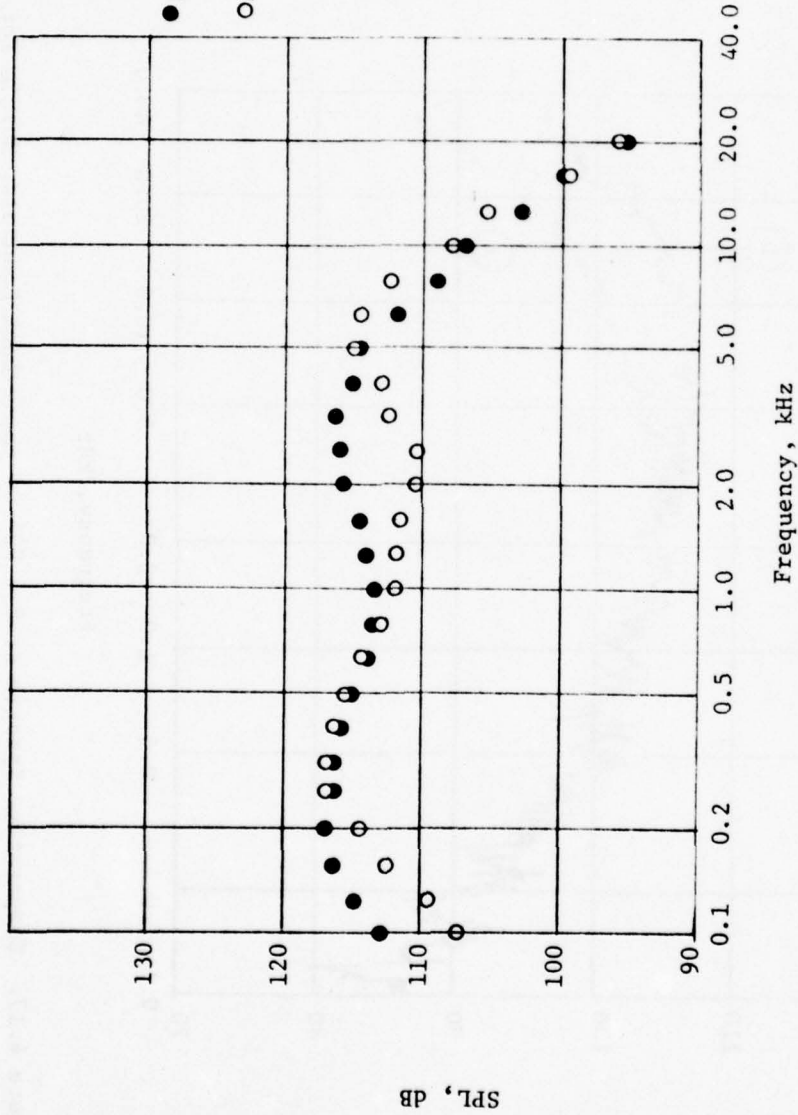


Figure 4.16. Comparison of 8-Inch Nozzle Spectra with Scaled 4-Inch Nozzle Spectra at 30° for Simulated JT8D Takeoff Condition D at Mean Thrust per Unit Area of 22.50 lb/in² and Mean Mass Flow per Unit Area of 0.549 lb/sec in².

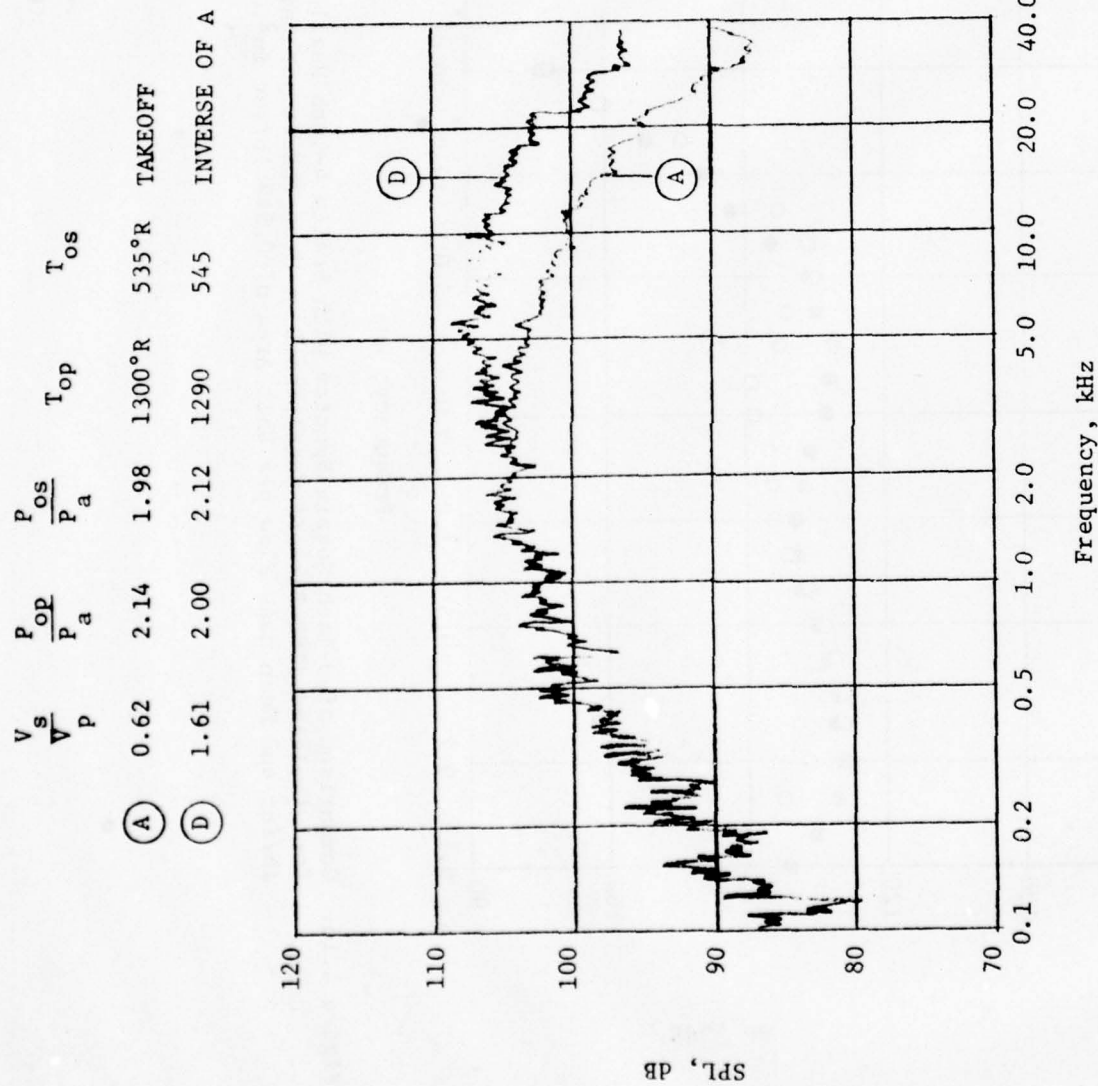


Figure 4.17. Comparative Spectra at $\theta = 90^\circ$ of the 8-Inch Coannular Nozzle for Simulated JT8D Takeoff Conditions A and D at Mean Thrust per Unit Area of 23.20 lb/in² and Mean Mass Flow per Unit Area of 0.551 lb/sec in².

between the two is quite good - the inverted profile of the eight-inch nozzle test is quieter at 30° by approximately 9 dB and about 0.5 dB louder at 90° . Comparison of the spectra at 30° for the eight-inch nozzle in Figure 4.14 shows that the maximum noise reduction occurs in the mid-frequency range where the peak intensity is being radiated by the conventional profile.

Figures 4.15 and 4.16 show comparisons of the spectra at 30° from the eight-inch nozzle and the four-inch nozzle for conditions A and D respectively. The standard profile curves (condition A) of Figure 4.15 show that the eight-inch spectra peaks around 1000 Hz and the Strouhal scaled four-inch spectra peaks around 700 Hz. The data agree within 1 to 2 dB in the vicinity of the peaks but gradually deviate as the frequency increases. The inverted profile curves (condition D) in Figure 4.16 show better agreement in the high frequency region although there is some discrepancy in the location of the second peak. In general, the agreement of the spectral data is considered to be quite good.

Figure 4.17 shows a comparison of the sound pressure level spectra at 90° for the conventional and inverted profile conditions for the eight-inch nozzle. There is no discernable difference between the two spectra up to 2000 Hz. However, for higher frequencies the inverted profile becomes increasingly noisy as compared to the conventional profile. The noise spectra at 90° to the jet axis are thought to give the most direct information about the characteristics of the sound sources themselves. This is because the sensor at 90° sees the radiation from the source region without that sound being significantly altered due to oblique propagation through the turbulent shear layer or by the effects of convective amplification and Doppler frequency shifts. The comparative spectra in Figure 4.17 seems to indicate that the inverted velocity profile causes an increase in the gross strength of the high frequency sound sources while not appreciably changing the strength of the low frequency sources. Then if the sound sources themselves are randomly oriented so that there is no inherent preferred orientation to the source radiation, the noise reduction at lower angles associated with the inverted velocity profile must be primarily due to effects other than source modification. It should be

noted that the directional characteristics of the sound radiated from a conventional jet are currently attributed to convection and refraction effects rather than a preferred orientation of the sound sources.

Figures 4.18 and 4.22 present comparisons similar to those discussed above for the JT8D cutback condition (B) and the corresponding inverted profile condition (E). Figures 4.23 through 4.27 show analogous data for the approach condition and its inverse. Virtually all of the statements made about the takeoff conditions apply to the comparisons for cutback and approach. The inverted profile is quieter by approximately 10 dB at 30° and slightly louder at 90°. The scaled up data from the four-inch test agree quite well with the eight-inch data both with regard to overall level and frequency content. At the lower power settings the double peaked character of the sound spectrum at 30° for the inverted profile disappears and is replaced by a flattened broadband noise spectrum. The maximum noise reduction is shifted to lower frequencies as the velocity level decreases. Figures 4.22 and 4.27 compare the conventional and inverted sound spectra at 90° for the cutback and approach conditions respectively. Both of these exhibit the same trends as shown in Figure 4.17, that is, no appreciable change in the low frequency noise but the inverted velocity profile radiating more high frequency noise in the 90° direction.

Figure 4.28 gives a summarizing graph for the JT8D test conditions showing both the four-inch data and eight-inch data plotted versus thrust. OASPL data for both standard profiles and inverted profiles are given along with computed values for the synthesized noise and the noise from a fully mixed flow. The synthesized estimate agrees reasonably well with the measured data for the conventional profile although overpredicting the noise by about 3 dB at high thrust. The OASPL for the inverted velocity profile is consistently about 10 dB below the standard profile over the whole thrust range. The sound pressure level for the fully mixed flow lies about mid-way between that for the standard and inverted profiles indicating that the inverted flow has about a 5 dB advantage over the fully mixed flow.

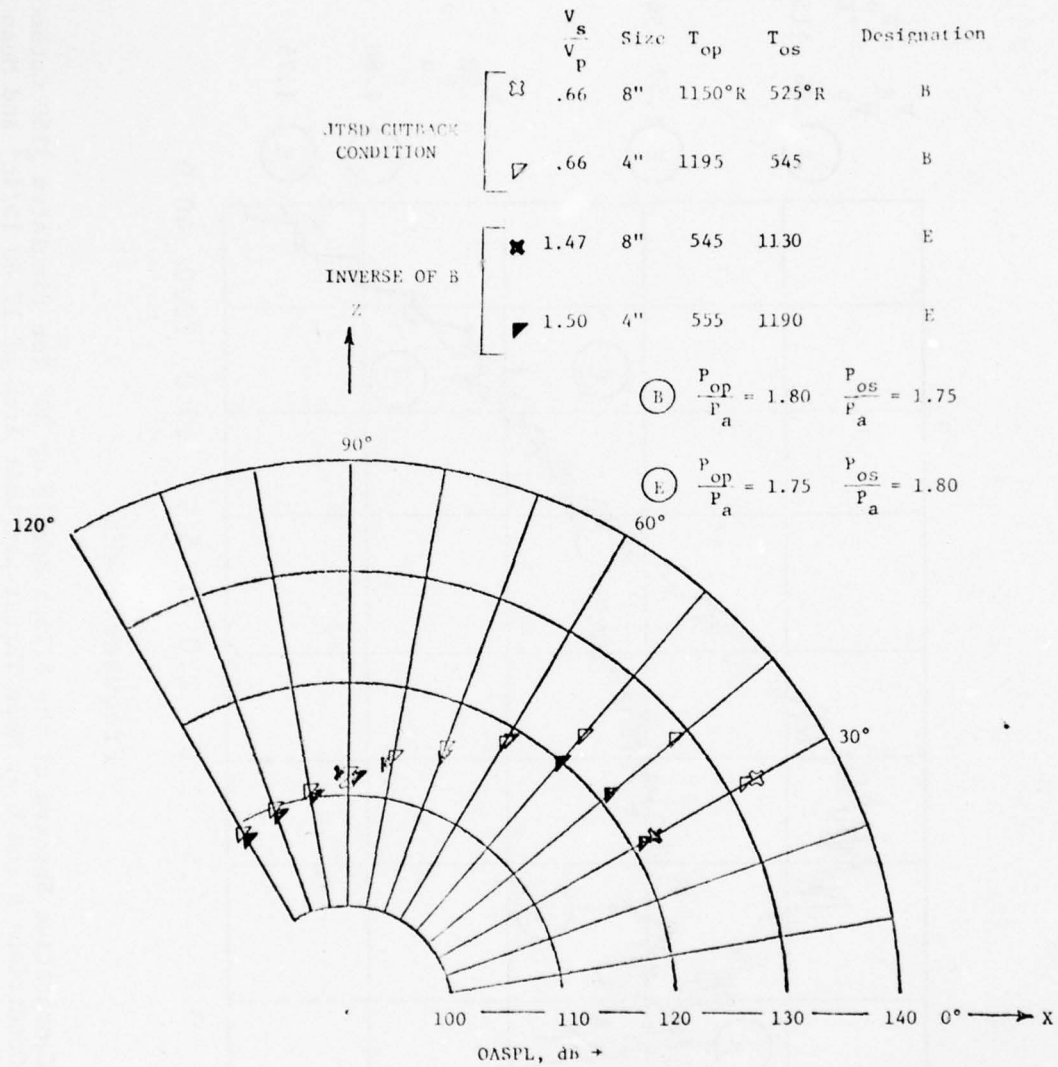


Figure 4.18. Directivities for Simulated JT8D Cutback Conditions B and E Comparing 8-Inch Nozzle Data with Scaled 4-Inch Nozzle Data at Mean Thrust Per Unit Area of 17.82 lb/in² and Mean Mass Flow Per Unit Area of 0.483 lb/sec in².

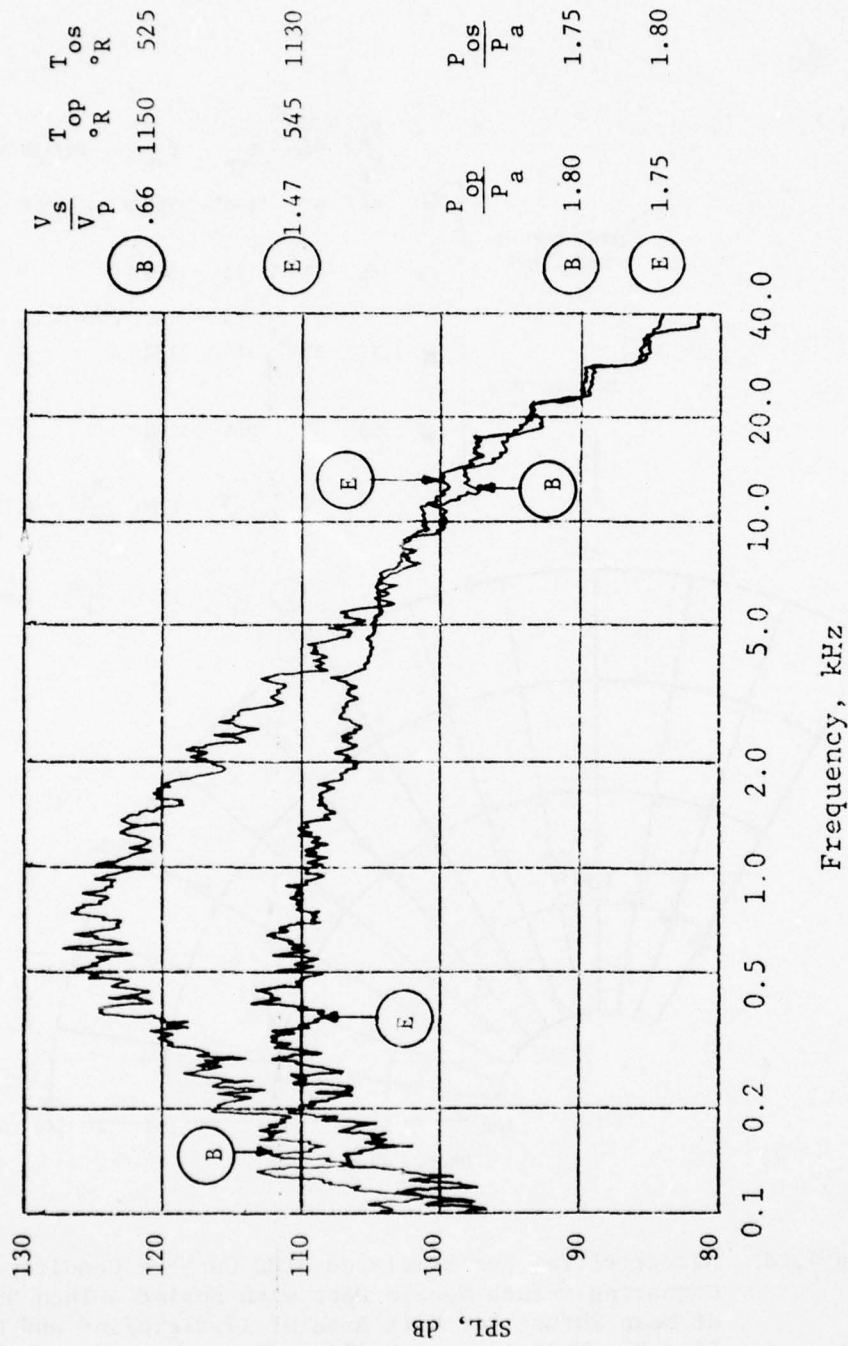


Figure 4.19. Comparative Spectra of the 8 Inch Nozzle at 30° for Simulated JT8D Cutback Conditions B and E at Mean Thrust per Unit Area of 17.86 lb/in² and Mean Mass Flow per Unit Area of 0.488 lb/sec in².

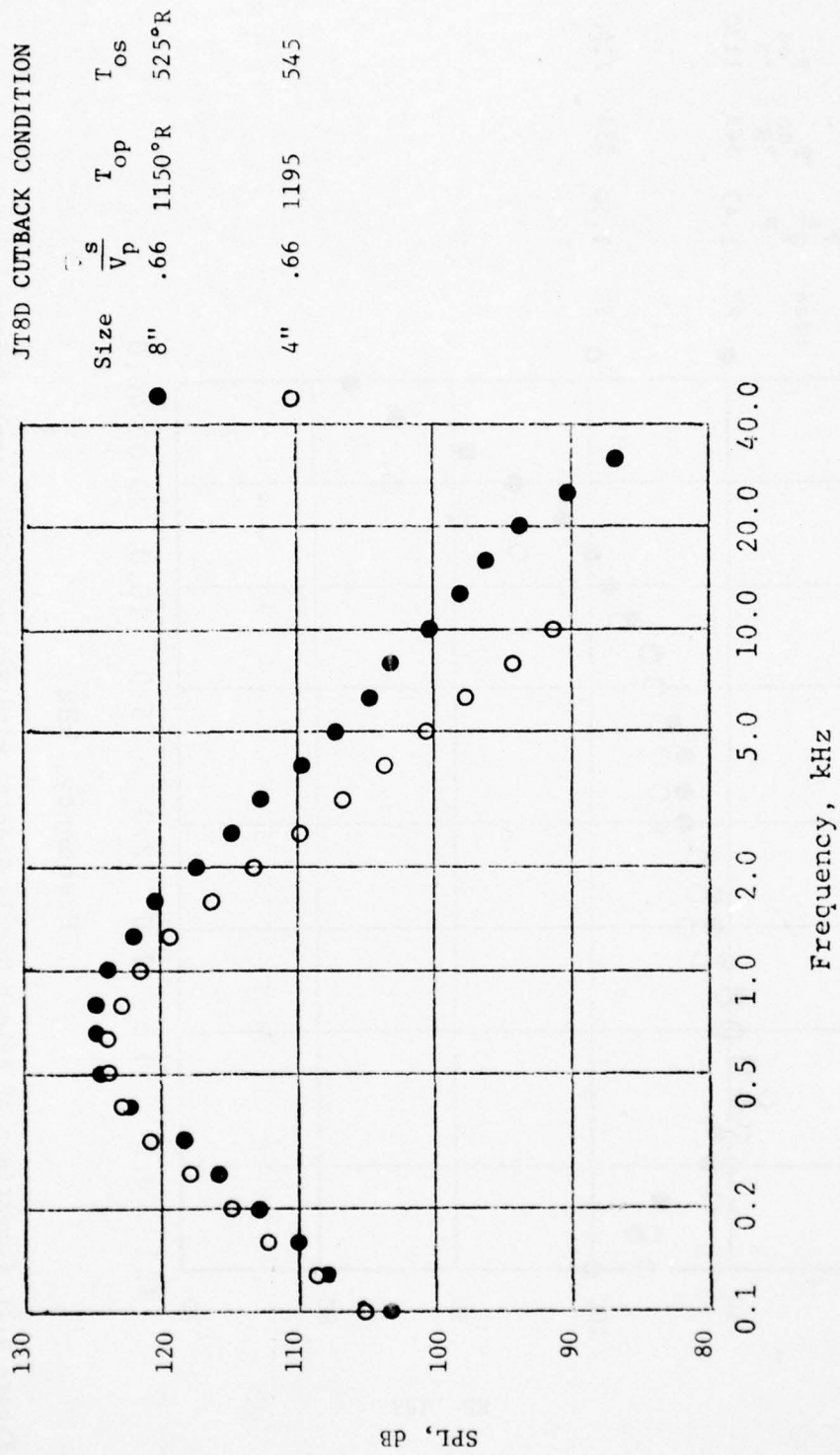


Figure 4.20. Comparison of 8-Inch Nozzle Spectra with Scaled 4-Inch Nozzle Spectra at 30° for Simulated JT8D Cutback Condition B at Mean Thrust per Unit Area of 17.82 lb/in² and Mean Mass Flow per Unit Area of 0.484 lb/sec in².

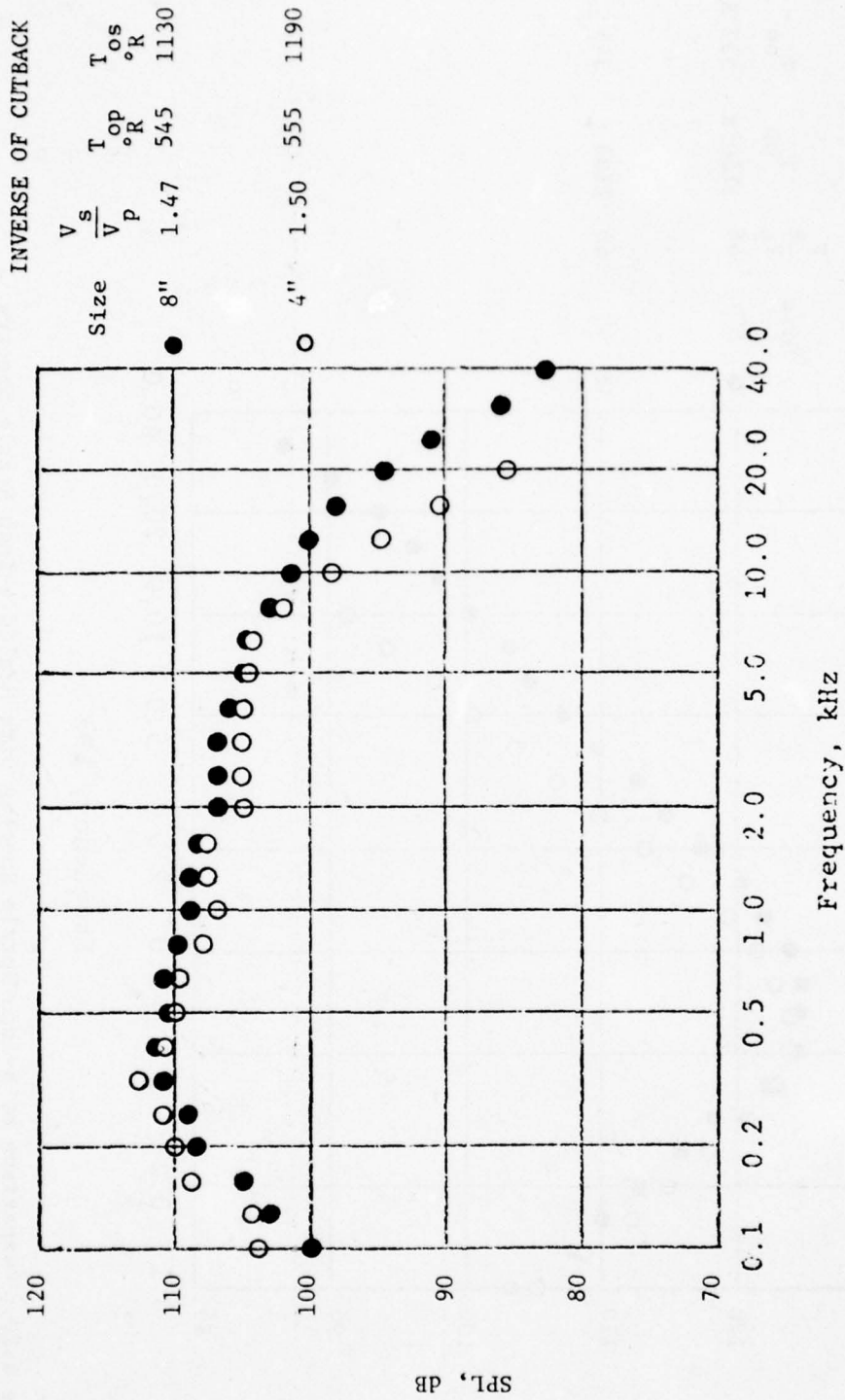


Figure 4.21. Comparison of 8-Inch Nozzle Spectra with Scaled 4-Inch Nozzle Spectra at 30° for Simulated JT8D Cutback Condition E at Mean Thrust per Unit Area of 17.82 lb/in² and Mean Mass Flow per Unit Area of 0.482 lb/sec in.²

| | $\frac{V_s}{V_p}$ | $\frac{P_{op}}{P_a}$ | $\frac{P_{os}}{P_a}$ | T_{op} | T_{os} | CUTBACK CONDITION |
|-----|-------------------|----------------------|----------------------|----------|----------|-------------------|
| (B) | .66 | 1.79 | 1.73 | 1150°R | 525°R | |
| (E) | 1.47 | 1.75 | 1.78 | 545 | 1130 | INVERSE OF B |

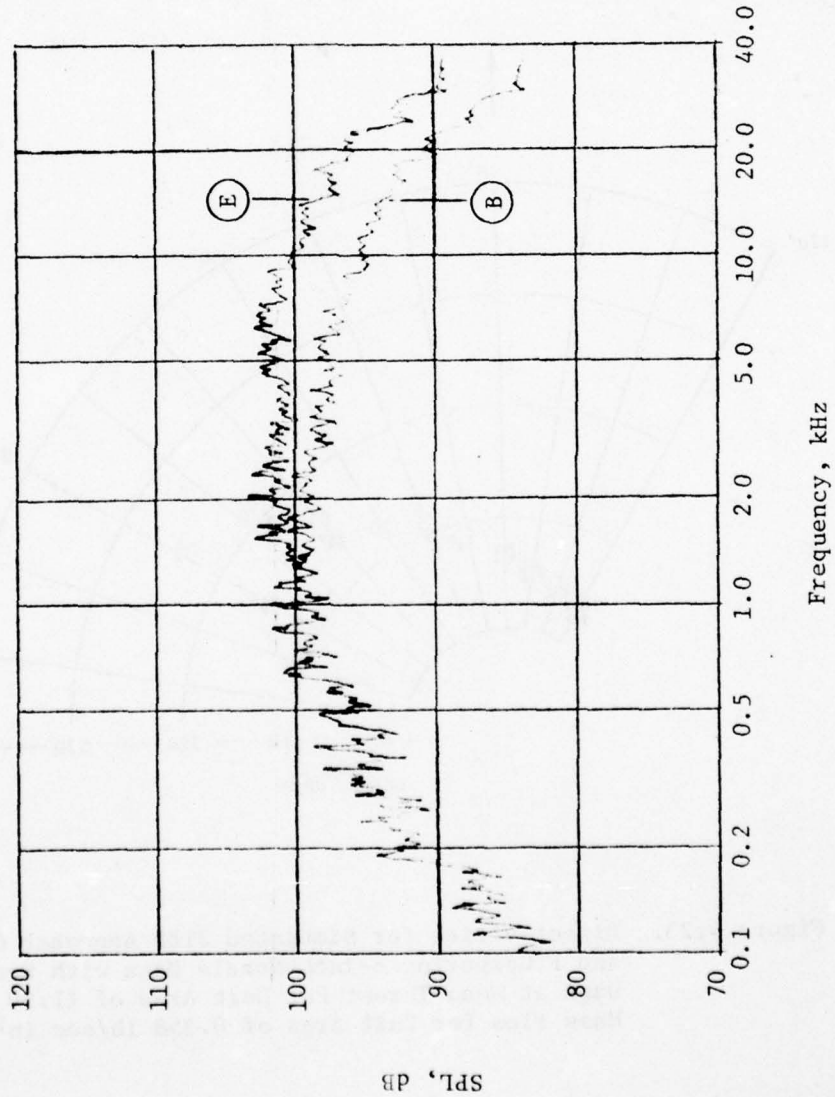


Figure 4.22. Comparative Spectra at $\theta = 90^\circ$ of the 8-Inch Coannular Nozzle for Simulated JT8D Cutback Conditions B and E at Mean Thrust per Unit Area of 17.86 lb/in² and Mass Flow per Unit Area of 0.488 lb/sec in².

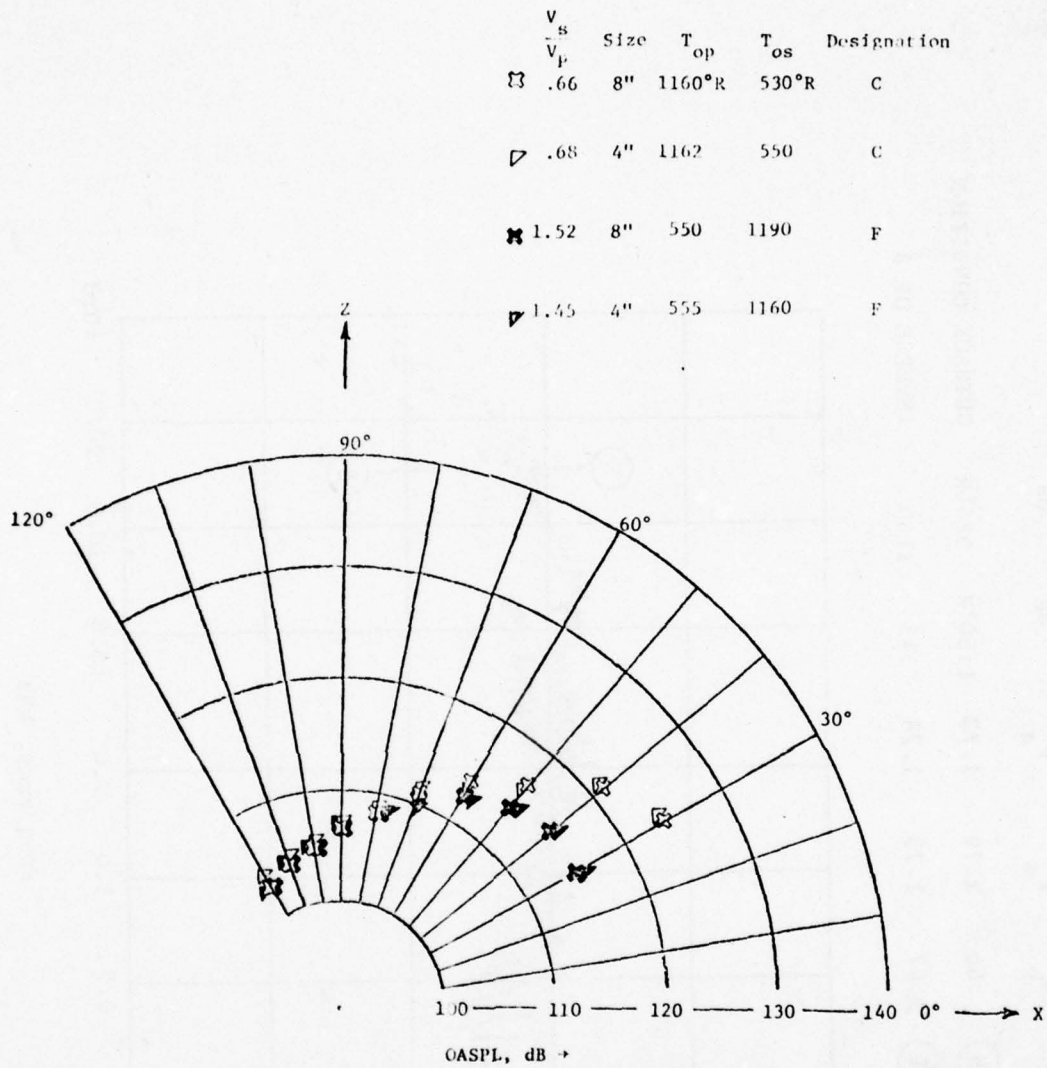


Figure 4.23. Directivities for Simulated JT8D Approach Conditions C and F Comparing 8-Inch Nozzle Data with Scaled 4-Inch Nozzle Data at Mean Thrust Per Unit Area of 11.90 lb/in^2 and Mean Mass Flow Per Unit Area of $0.358 \text{ lb/sec in}^2$.

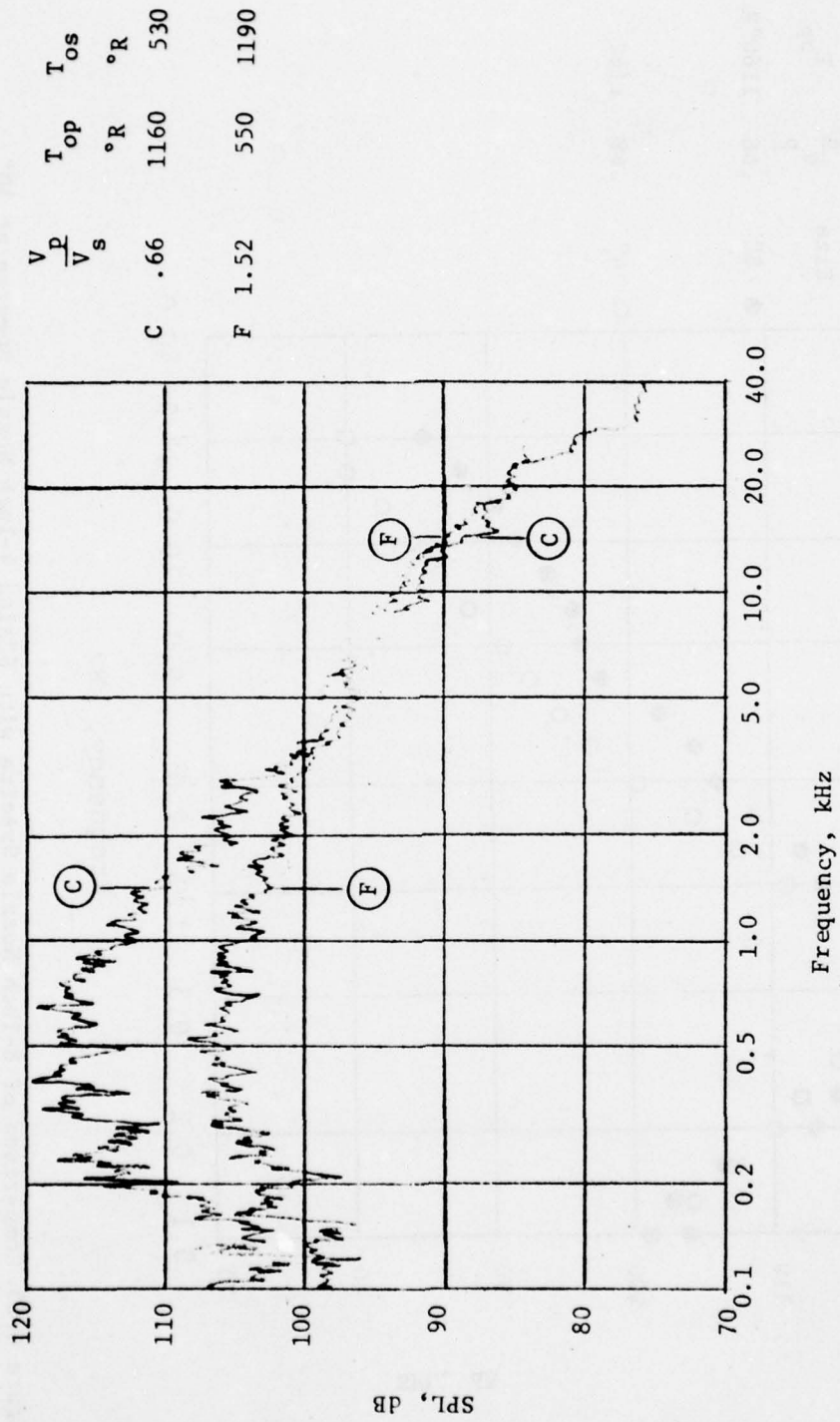


Figure 4.24. Comparative Spectra of the 8-Inch Nozzle at 30° for Simulated JT8D Approach Conditions C and F at Mean Thrust per Unit Area of 11.70 lb/in² and Mean Mass Flow per Unit Area of 0.380 lb/sec in².

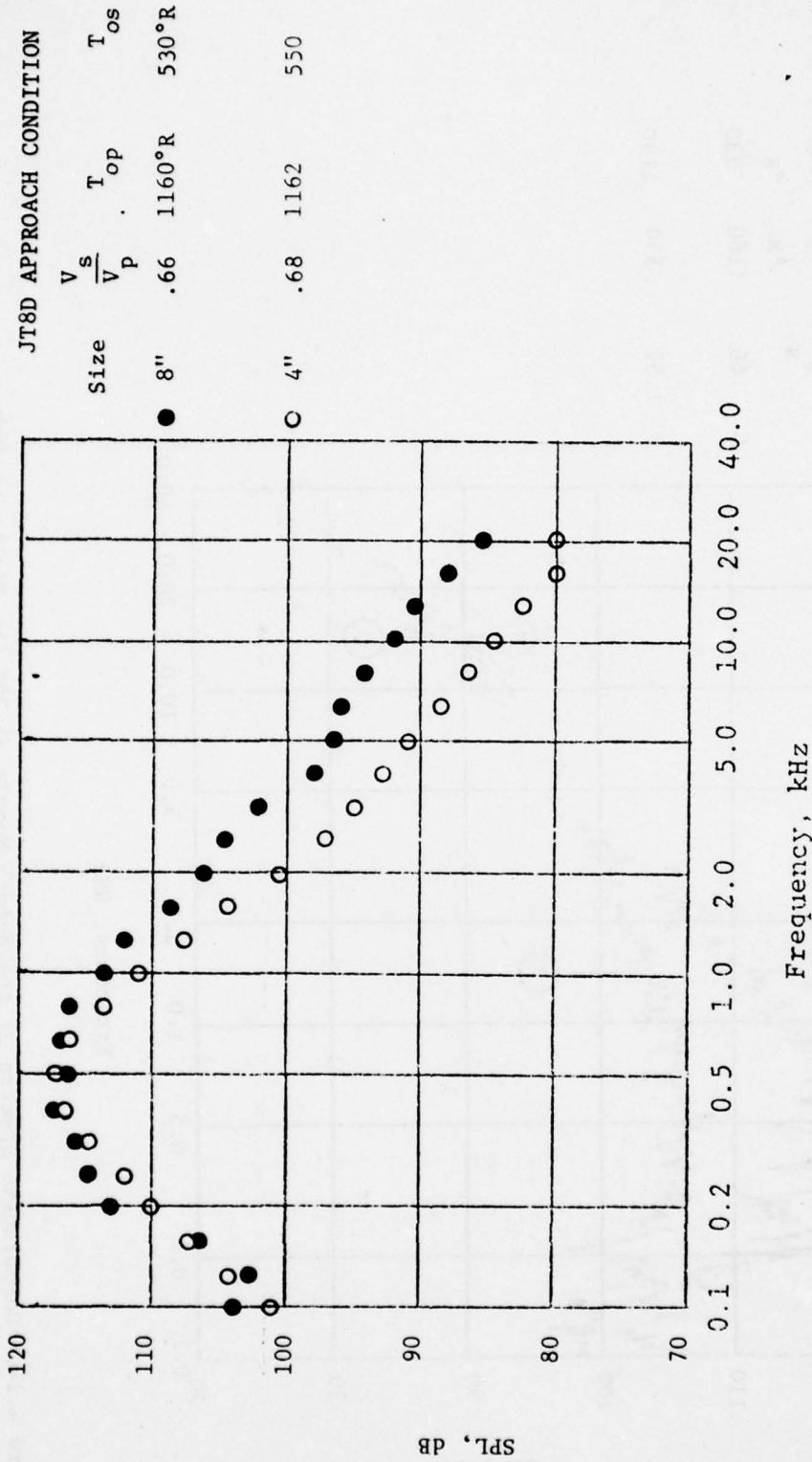


Figure 4.25. Comparison of 8-Inch Nozzle Spectra with Scaled 4-Inch Nozzle Spectra at 30° for Simulated JT8D Approach Condition C at Mean Thrust per Unit Area of 11.85 lb/in² and Mean Mass Flow per Unit Area of 0.385 lb/sec in².

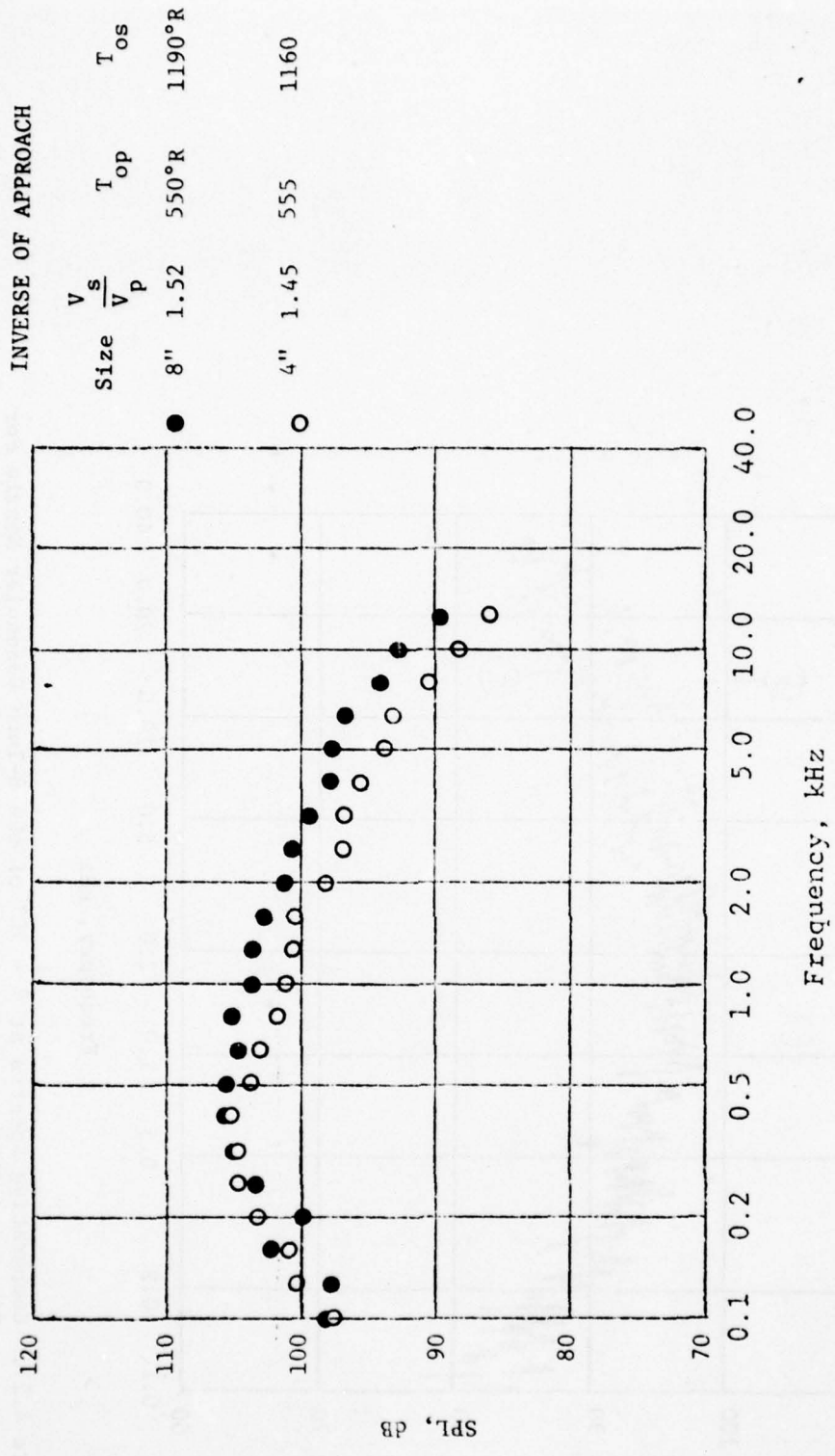


Figure 4.26. Comparison of 8-Inch Nozzle Spectra with Scaled 4-Inch Nozzle Spectra at 30° for Simulated JT8D Approach Condition F at Mean Thrust per Unit Area of 11.95 lb/in² and Mean Mass Flow per Unit Area of 0.332 lb/sec in².

| | $\frac{V_s}{V_p}$ | $\frac{P_{OP}}{P_a}$ | $\frac{P_{OS}}{P_a}$ | T_{OP} | T_{OS} | APPROACH CONDITION |
|-----|-------------------|----------------------|----------------------|----------|----------|--------------------|
| (C) | 0.66 | 1.48 | 1.45 | 1160°R | 530°R | |
| (F) | 1.52 | 1.45 | 1.48 | 1190 | 550 | INVERSE OF C |

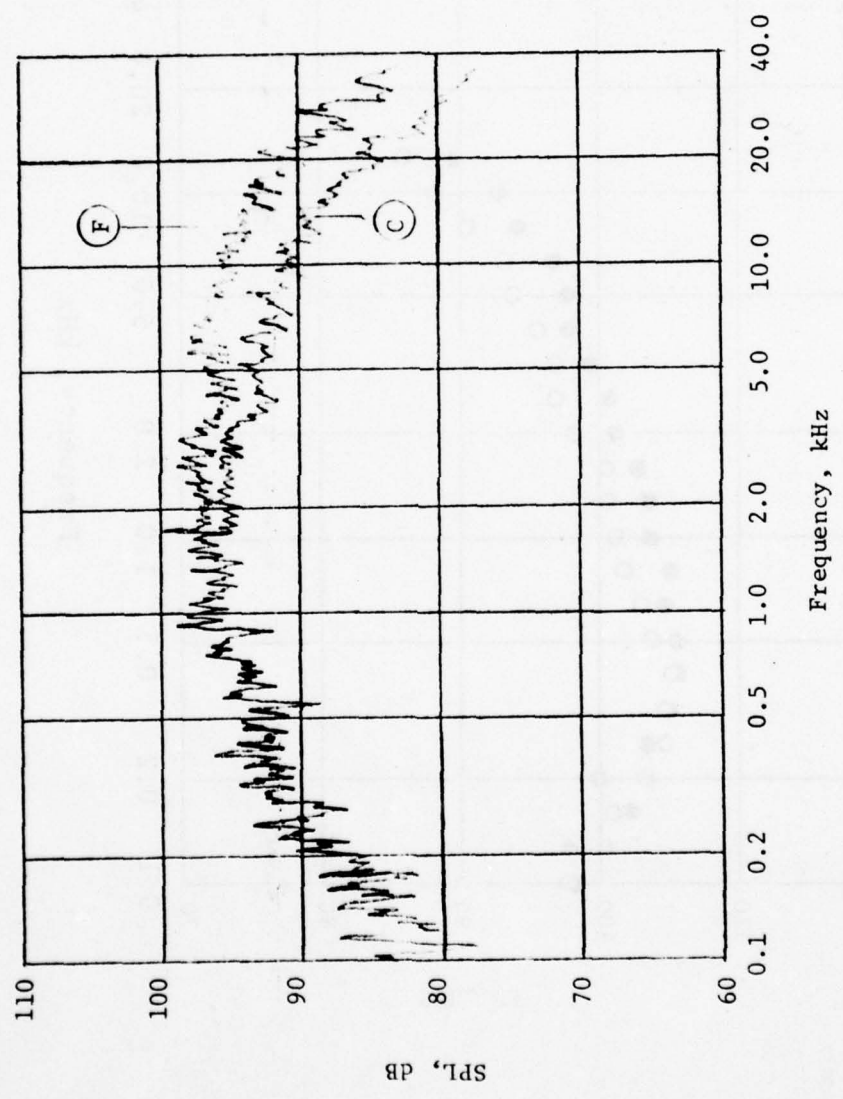


Figure 4.27. Comparative Spectra at $\theta = 90^\circ$ of the 8-Inch Coannular Nozzle for Simulated JT8D Approach Conditions C and F at Mean Thrust per Unit Area of 11.70 lb/in² and Mean Mass Flow per Unit Area of 0.380 lb/sec in².

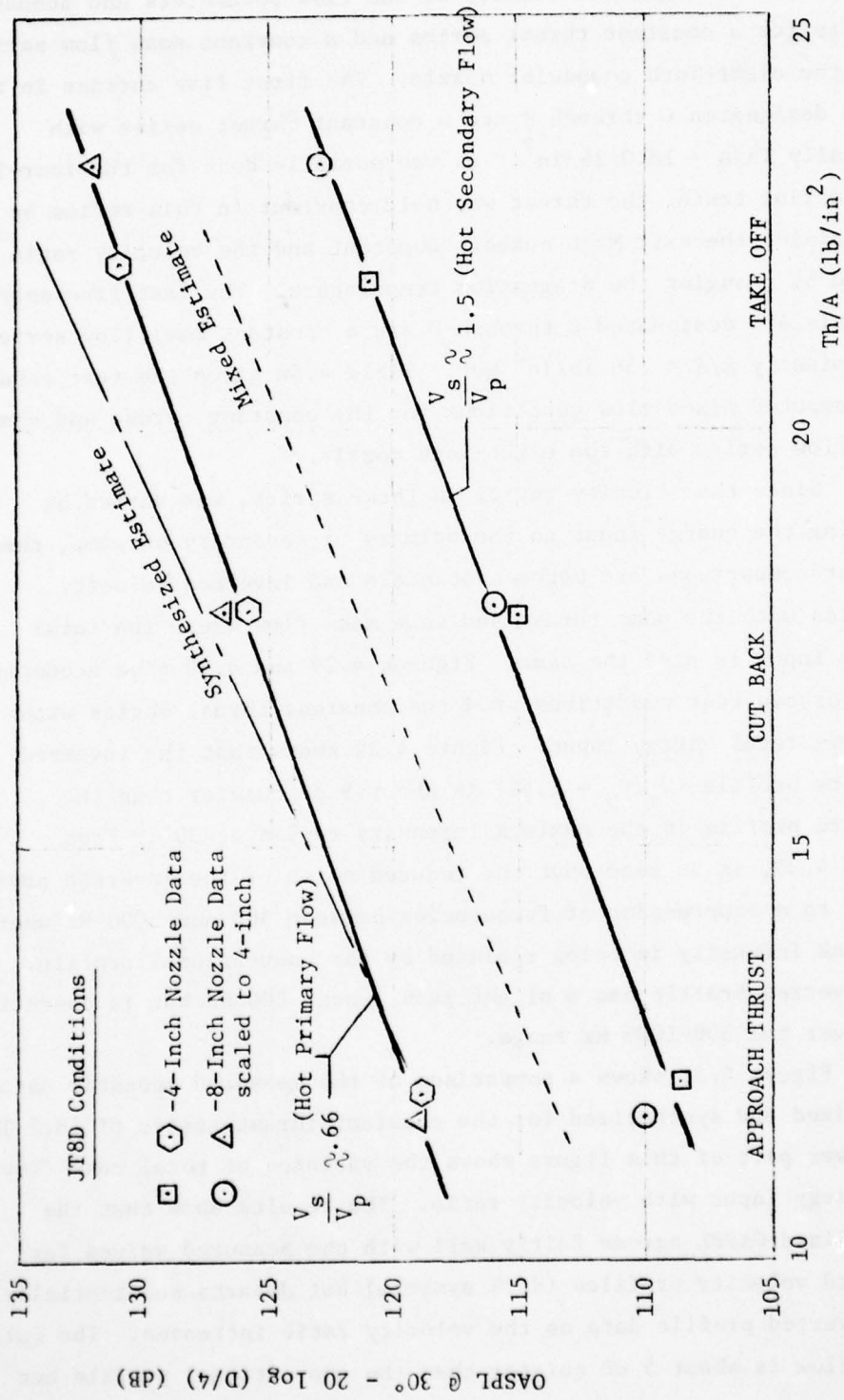


Figure 4.28. Comparison of Noise from Conventional and Inverted Profiles for 4-Inch and 8-Inch Nozzles for the JT8D Test Series.

4.2.2 Constant Thrust and Constant Mass Flow Series.

Table 4.5 gives a summary of the flow parameters and acoustic results for a constant thrust series and a constant mass flow series with the eight-inch coannular nozzle. The first five entries in the table designated G through K are a constant thrust series with nominally $Th/A = 18.0 \text{ lb/in}^2$. As was normally done for the four-inch heated flow tests, the thrust was held constant in this series by maintaining the exit Mach numbers constant and the velocity ratio varied by changing the stagnation temperature. The last five entries in Table 4.5 designated L through P are a constant mass flow series of nominally $\dot{m}/A = .36 \text{ lb/in}^2 \text{ sec}$. Table 4.5a gives the test conditions and computed mixed flow conditions for the constant thrust and constant mass flow series with the eight-inch nozzle.

Since the velocity ratio, in these series, was varied by changing the energy input to the primary or secondary streams, the fairest comparisons are between standard and inverted velocity profiles with the same thrust and same mass flow where the total energy input is also the same. Figures 4.29 and 4.30 give acoustic data for two test conditions from the constant thrust series with the same total energy input. Figure 4.29 shows that the inverted velocity profile ($V_s/V_p = 1.54$) is about 9 dB quieter than the standard profile in the maximum intensity region at 30° . From Figure 4.30, it is seen that the reduced noise of the inverted profile is due to a suppression of frequencies between 300 and 5000 Hz where the peak intensity is being radiated by the conventional profile. The inverted profile has a slight peak around 500 Hz but is essentially flat over the 300-1000 Hz range.

Figure 4.31 shows a comparison of the measured acoustic data with mixed and synthesized for the constant thrust series of 18.1 lbs/in^2 . The lower part of this figure shows the variation of total mass flow and energy input with velocity ratio. The results show that the synthesized OASPL agrees fairly well with the measured values for standard velocity profiles (dark symbols) but departs substantially from the inverted profile data as the velocity ratio increases. The fully mixed flow is about 5 dB quieter than the conventional profile but

TABLE 4.5
 SUMMARY OF FLOW PARAMETERS AND ACOUSTIC RESULTS FOR THE CONSTANT THRUST AND CONSTANT MASS
 FLOW SERIES FOR THE EIGHT-INCH COANNULAR NOZZLE WITH HEATED FLOW

| Designation | M_p | M_s | T_{os}/T_{op} | V_s/V_p | \dot{m}_s/\dot{m}_p | Th/A_t lb/in ² | 30° | | | SPL MIX dB | SPL 90° dB | COMMENTS |
|-------------|-------|-------|-----------------|-----------|-----------------------|--------------------------------|---------------|----------------|---------------|---------------|------------------|----------|
| | | | | | | | SPL 30° dB | SPL SYN. dB | SPL 90° dB | | | |
| G | .95 | .94 | .40 | .63 | 1.56 | 17.75 | 133.5 | 135.00 | 128.03 | 111.5 | CONST. THRUST | |
| H | .95 | .97 | .50 | .72 | 1.44 | 18.22 | 130.5 | 129.92 | 125.75 | 110.5 | CONST. THRUST | |
| I | .95 | .96 | 1.00 | 1.01 | 1.01 | 18.16 | 118.0 | 118.99 | 118.89 | 107.0 | CONST. THRUST | |
| J | .96 | .95 | 2.00 | 1.41 | .70 | 17.98 | 122.0 | 130.51 | 126.03 | 112.0 | CONST. THRUST | |
| K | .95 | .96 | 2.35 | 1.54 | .66 | 18.15 | 123.0 | 135.09 | 128.80 | 113.0 | CONST. THRUST | |
| L | 1.00 | .58 | .41 | .39 | .85 | 13.18 | 134.5 | 136.94 | 126.71 | 111.5 | CONST. MASS FLOW | |
| M | .91 | .55 | .52 | .46 | .79 | 11.24 | 125.0 | 128.29 | 120.11 | 106.5 | CONST. MASS FLOW | |
| N | .62 | .61 | 1.00 | .98 | .98 | 7.53 | 102.0 | 101.54 | 101.55 | 96.0 | CONST. MASS FLOW | |
| O | .51 | .92 | 1.76 | 2.28 | 1.44 | 10.92 | 118.0 | 127.54 | 120.15 | 109.0 | CONST. MASS FLOW | |
| P | .53 | .97 | 2.25 | 2.57 | 1.29 | 12.05 | 122.0 | 135.21 | 125.69 | 113.0 | CONST. MASS FLOW | |

TABLE 4.5a

SUMMARY OF TEST CONDITIONS AND COMPUTED MIXED FLOW CONDITIONS FOR CONSTANT THRUST AND CONSTANT MASS FLOW SERIES FOR THE EIGHT-INCH COANNULAR NOZZLE ($A_N = .349 \text{ ft}^2$)

| Designation | P_{op} lb/ft ² abs | P_{os} lb/ft ² abs | P_{om}^2 lb/ft ² abs | T_{op} °K | T_{os} °R | T_{om} °R | V_s/V_p | A_m ft ² | OASPL @ 30° FOR MIXED FLOW db |
|-------------|---------------------------------------|---------------------------------------|---|----------------|----------------|----------------|-----------|--------------------------|--|
| G | 3623 | 3593 | 3605 | 1320 | 530 | 838 | .63 | .358 | 128.0 |
| H | 3643 | 3720 | 3688 | 1030 | 520 | 729 | .72 | .354 | 125.7 |
| I | 3672 | 3840 | 3756 | 520 | 520 | 520 | 1.01 | .343 | 118.9 |
| J | 3667 | 3642 | 3657 | 530 | 1060 | 748 | 1.41 | .353 | 126.0 |
| K | 3662 | 3685 | 3671 | 550 | 1290 | 843 | 1.54 | .357 | 128.8 |
| L | 3857 | 2553 | 3260 | 1315 | 540 | 960 | .39 | .332 | 126.7 |
| M | 3497 | 2504 | 3058 | 1030 | 540 | 813 | .46 | .331 | 120.1 |
| N | 2650 | 2624 | 2638 | 530 | 530 | 530 | .98 | .350 | 101.5 |
| O | 2434 | 3522 | 3077 | 560 | 983 | 809 | 2.28 | .318 | 120.1 |
| P | 2375 | 3713 | 3171 | 572 | 1285 | 970 | 2.57 | .325 | 125.7 |

AD-A061 719

TENNESSEE UNIV SPACE INST TULLAHOMA
INVESTIGATION OF COANNULAR NOZZLES WITH CONVENTIONAL AND INVERT--ETC(U)
APR 78 B H GOETHERT, J R MAUS, W A DUNNILL DOT-FA72WA-3053

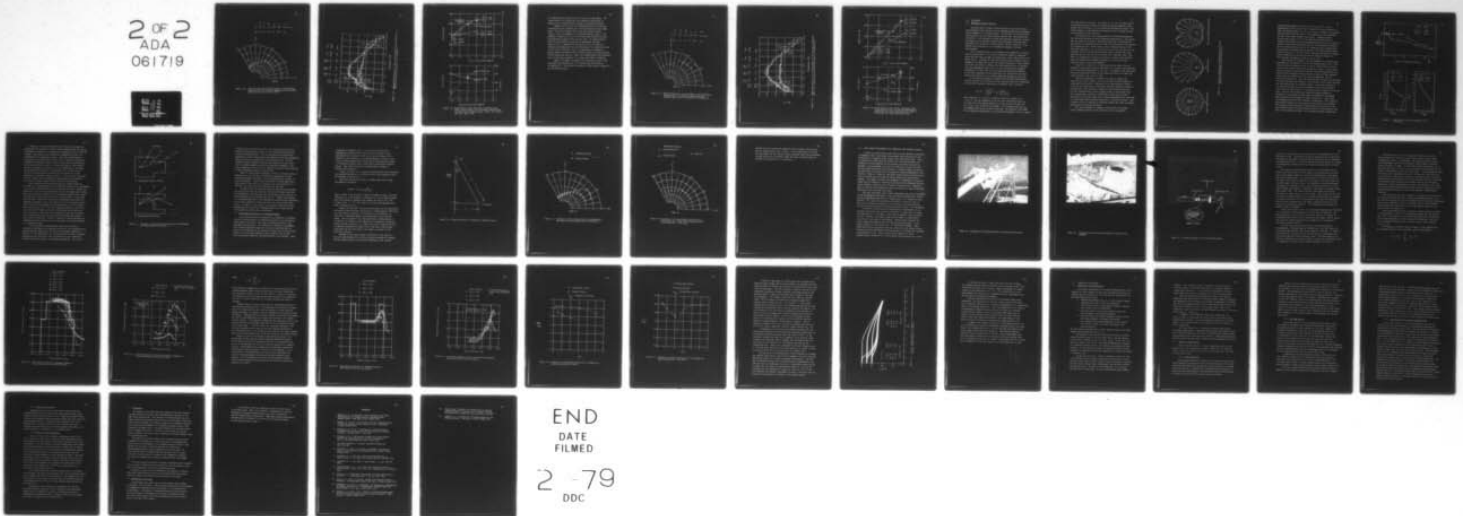
F/G 20/1

UNCLASSIFIED

FAARD-78-32

NL

2 OF 2
ADA
061719



END
DATE
FILMED

2 -79
DDC

| | $\frac{V_s}{V_p}$ | $\frac{P_{op}}{P_a}$ | $\frac{P_{os}}{P_a}$ | T_{op} | T_{os} | \dot{m}/Λ |
|---|-------------------|----------------------|----------------------|----------|----------|----------------------------|
| ☒ | .63 | 1.78 | 1.76 | 1320°R | 530°R | .47 lb/sec in ² |
| ☒ | 1.54 | 1.79 | 1.80 | 550 | 1290 | .48 |

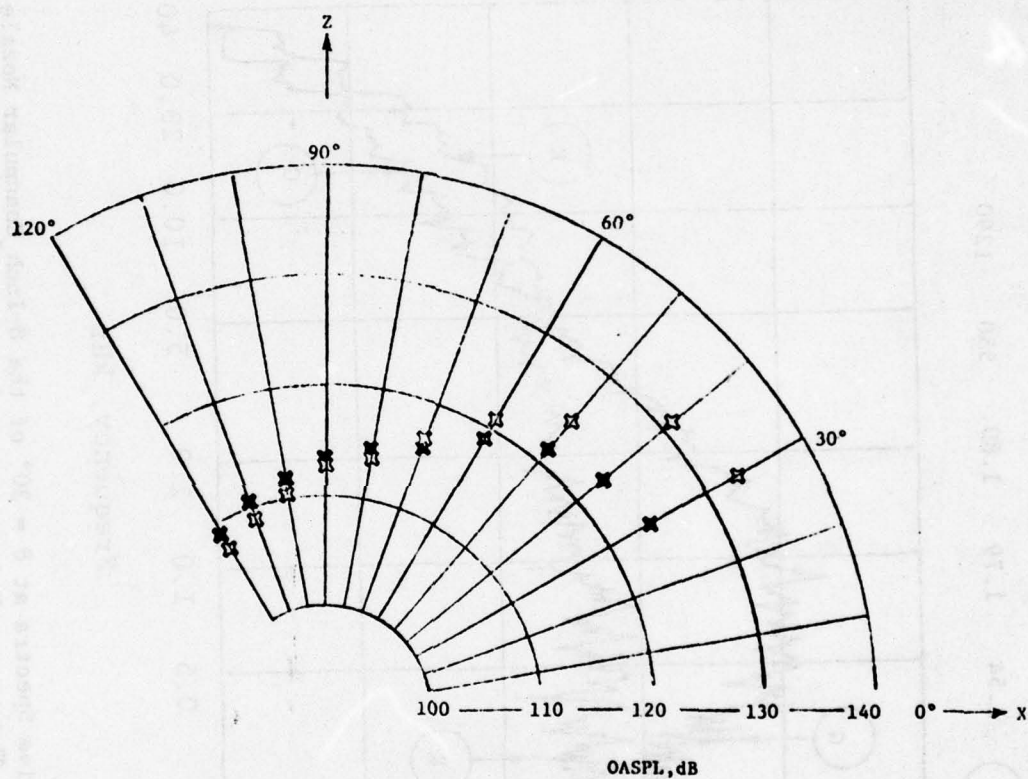


Figure 4.29. OASPL Directivities in the XZ Plane of the Eight-Inch Coannular Nozzle at Elevated Temperature and a Constant Thrust Per Unit Area of 18.1 lb/in².

| | $\frac{V_a}{V_p}$ | $\frac{P_{op}}{P_a}$ | $\frac{P_{os}}{P_a}$ | T_{op} | T_{os} |
|-----|-------------------|----------------------|----------------------|----------|----------|
| (G) | .63 | 1.78 | 1.76 | 1320°R | 530°R |
| (K) | 1.54 | 1.79 | 1.80 | 550 | 1290 |

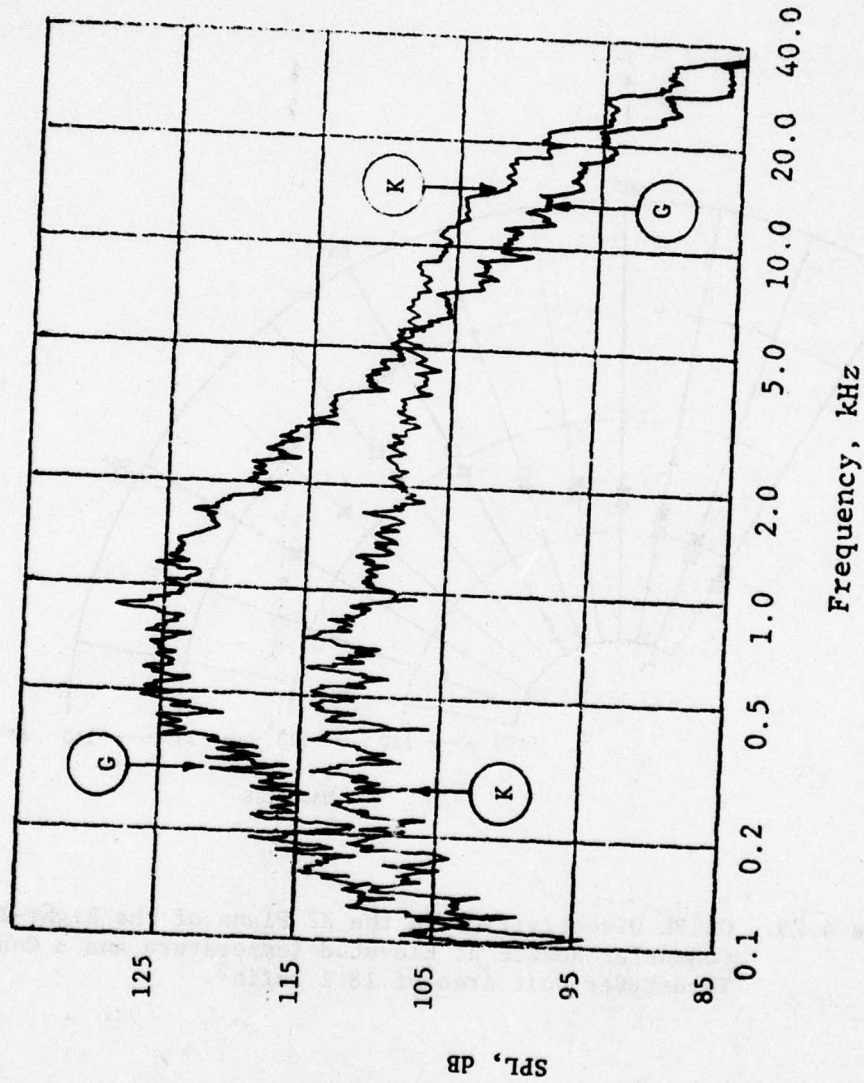


Figure 4.30. Comparative Spectra at $\theta = 30^\circ$ of the 8-Inch Coaxial Nozzle at a Constant Thrust per Unit Area of 18.1 lbs/in².

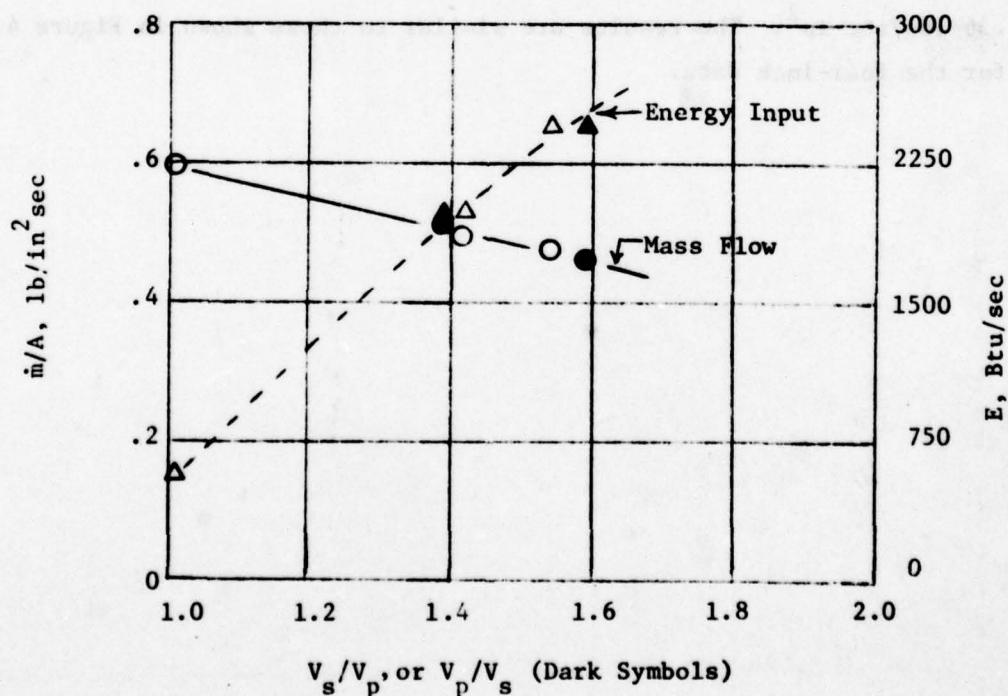
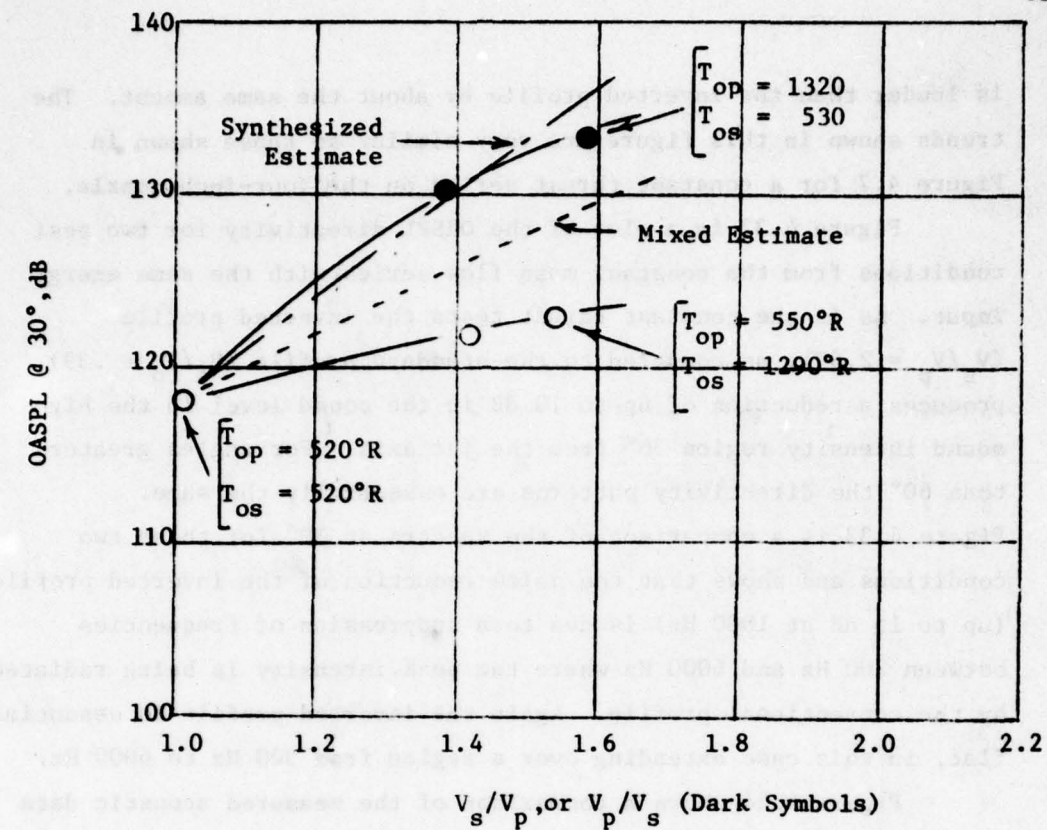


Figure 4.31. Sound Pressure Level, Mass Flow, and Energy Input Versus Velocity Ratio for the Constant Thrust Series, with the 8-Inch Coannular Nozzle. $Th/A = 18.1$ lb/in², (Hot Flow, Table 4.5a).

is louder than the inverted profile by about the same amount. The trends shown in this figure are very similar to those shown in Figure 4.7 for a constant thrust series on the four-inch nozzle.

Figure 4.32 is a plot of the OASPL directivity for two test conditions from the constant mass flow series with the same energy input. As in the constant thrust tests the inverted profile ($V_s/V_p = 2.57$), as compared to the standard profile ($V_s/V_p = .39$), produces a reduction of up to 10 dB in the sound level in the high sound intensity region 30° from the jet axis. For angles greater than 60° the directivity patterns are essentially the same.

Figure 4.33 is a comparison of the spectra at 30° for these two conditions and shows that the noise reduction of the inverted profile (up to 15 dB at 1000 Hz) is due to a suppression of frequencies between 200 Hz and 6000 Hz where the peak intensity is being radiated by the conventional profile. Again the inverted profile is essentially flat, in this case extending over a region from 300 Hz to 6000 Hz.

Figure 4.34 shows a comparison of the measured acoustic data with mixed and synthesized for the constant mass flow series of $.36 \text{ lbs/sec in}^2$. The results are similar to those shown in Figure 4.8 for the four-inch data.

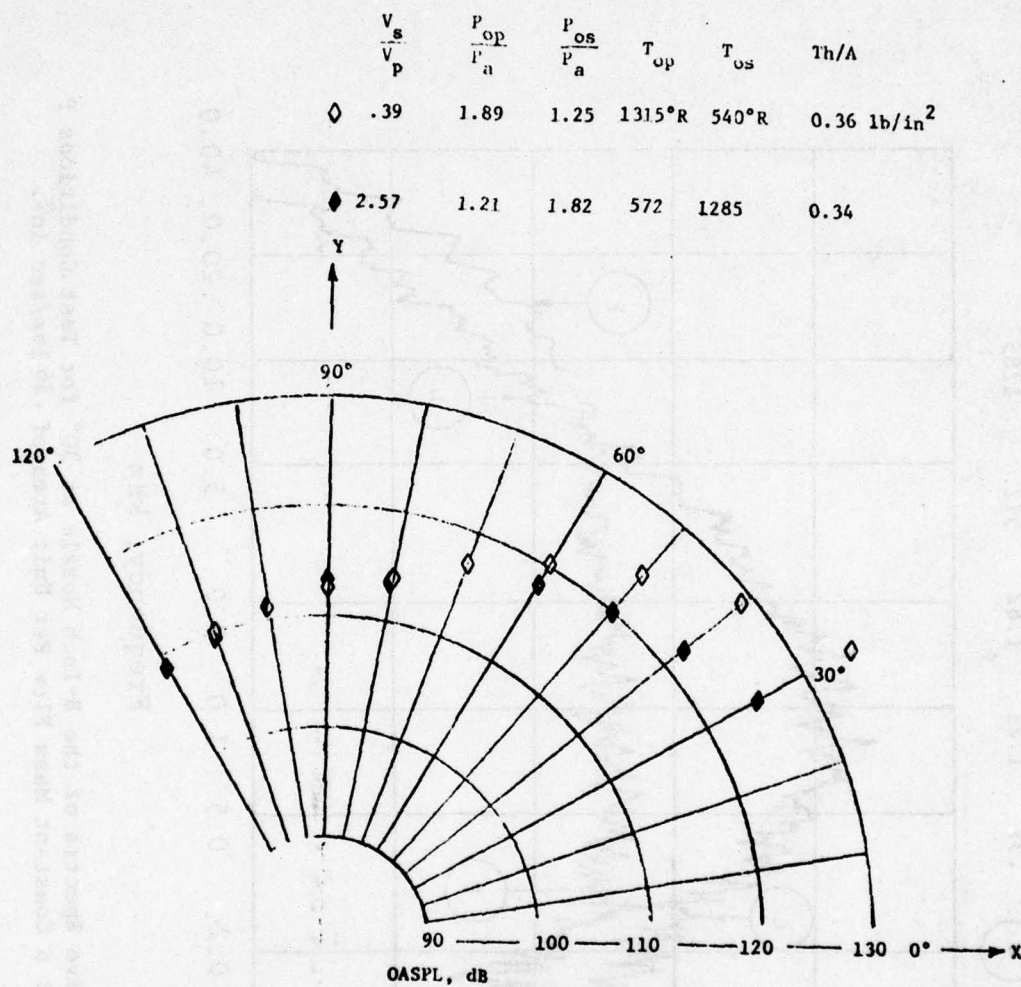


Figure 4.32. OASPL Directivities in the XZ Plane of the Eight-Inch Coannular Nozzle at Elevated Temperatures and a Constant Mass Flow per Unit Area of .36 lbs/sec in².

| | | | | |
|-------------------|----------------------|----------------------|----------|----------|
| $\frac{V_s}{V_p}$ | $\frac{P_{OP}}{P_a}$ | $\frac{P_{OS}}{P_a}$ | T_{Op} | T_{Os} |
| 2.57 | 1.89 | 1.25 | 1315°R | 540°R |

(P)

(L)

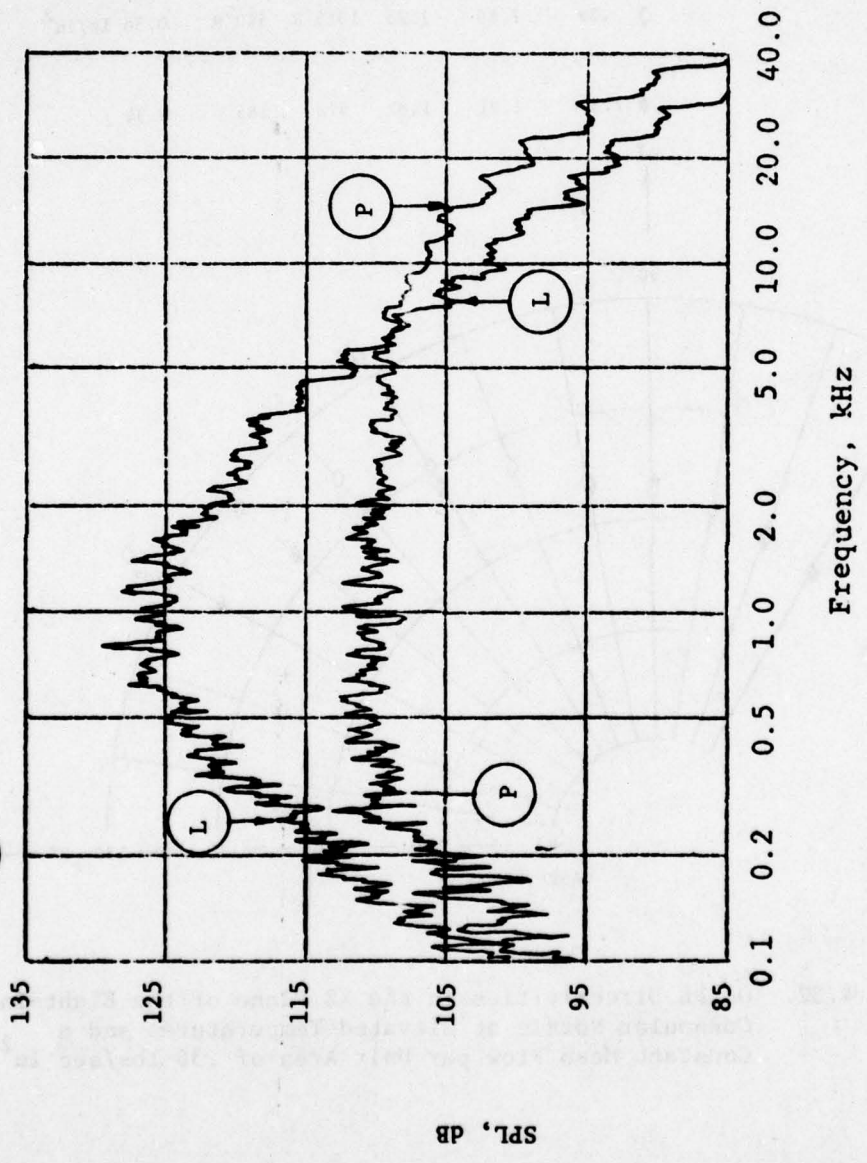


Figure 4.33. Comparative Spectra of the 8-Inch Nozzle at 30° for Test Conditions P and L at a Constant Mass Flow Per Unit Area of .36 lbs/sec in².

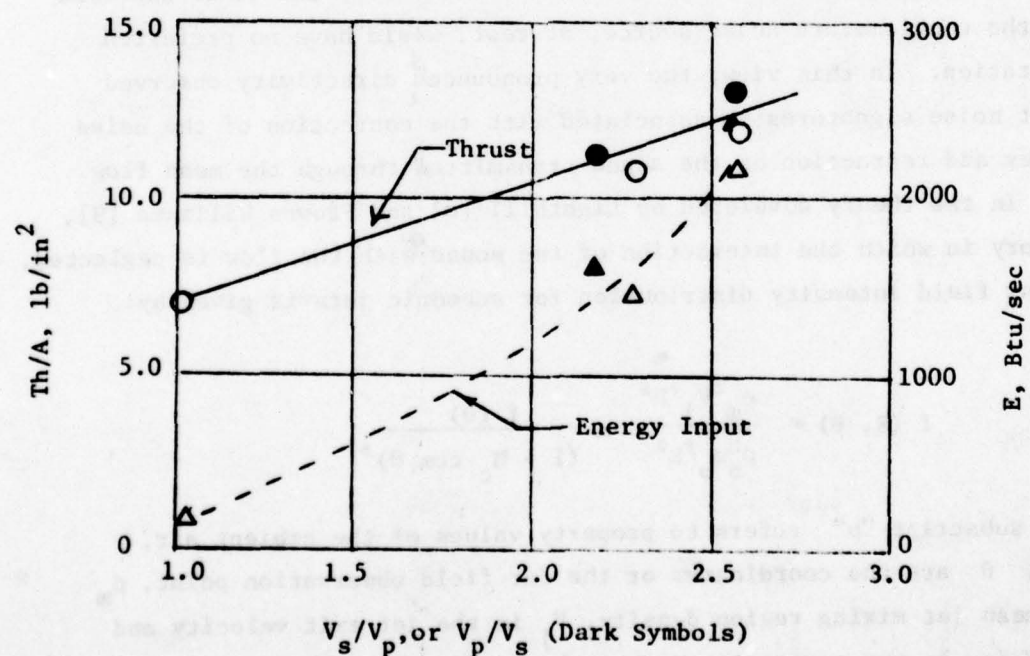
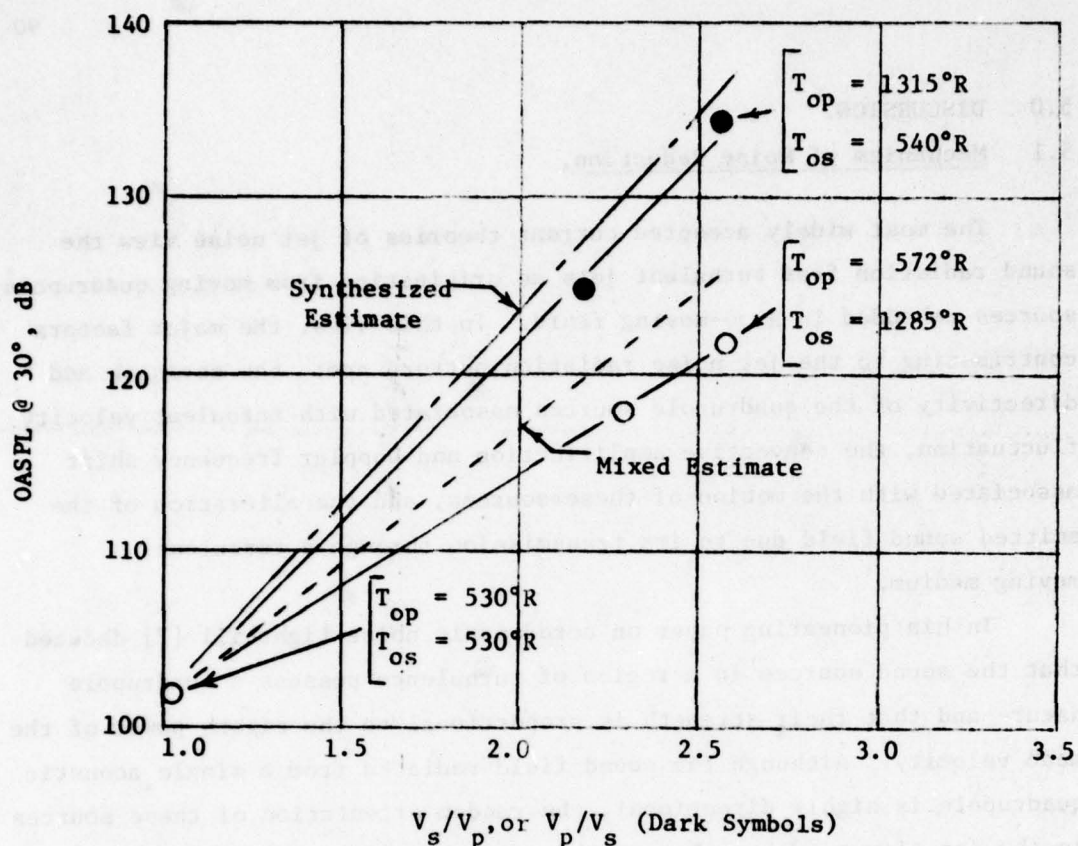


Figure 4.34. Sound Pressure Level, Thrust, and Energy Input Versus Velocity Ratio for the Constant Mass Flow Series with the 8-Inch Coannular Nozzle, $\dot{m}/A = 0.36 \text{ lb/sec in}^2$, (Hot Flow, Table 4.5a).

5.0 DISCUSSION.

5.1 Mechanism of Noise Reduction.

The most widely accepted current theories of jet noise view the sound radiation from turbulent jets as originating from moving quadrupole sources embedded in a co-moving fluid. In this view, the major factors contributing to the jet noise radiation pattern are: the strength and directivity of the quadrupole sources associated with turbulent velocity fluctuation, the convective amplification and Doppler frequency shift associated with the motion of these sources, and the alteration of the emitted sound field due to its transmission through a turbulent moving medium.

In his pioneering paper on aerodynamic noise Lighthill [7] deduced that the sound sources in a region of turbulence possess a quadrupole nature and that their strength is proportional to the eighth power of the mean velocity. Although the sound field radiated from a single acoustic quadrupole is highly directional, the random orientation of these sources in the jet flow tends to obscure this directionality and it is expected that the conglomerate noise source, at rest, would have no preferred orientation. In this view, the very pronounced directivity observed in jet noise signatures is associated with the convection of the noise sources and refraction of the sound transmitted through the mean flow.

In the theory developed by Lighthill [8] and Ffowcs Williams [9], a theory in which the interaction of the sound with the flow is neglected, the far field intensity distribution for subsonic jets is given by:

$$I(R, \theta) \propto \frac{\rho_m^2 V_j^8 D^2}{\rho_o a_o^5 R^2} \times \frac{f(\theta)}{(1 - M_c \cos \theta)^5}$$

where subscript "o" refers to property values of the ambient air, R and θ are the coordinates of the far field observation point, ρ_m is a mean jet mixing region density, V_j is the jet exit velocity and $M_c = V_c/a_o$ is the convection Mach number. The convection velocity, V_c , is normally taken as .65 of the jet velocity. The function $f(\theta)$ allows for the inherent directionality of the source distribution and it is argued

that this should be constant. The factor $(1 - M_c \cos \theta)^{-5}$ that appears in the above equation accounts for the motion of the quadrupole sound sources and is referred to as the convective amplification factor. This factor produces a sound intensity distribution that is focused forward, in the direction of the jet flow.

The interaction of the sound generated by the moving quadrupoles with the mean flow cannot be simply expressed quantitatively. One can say that the sound field should be governed by some kind of convected wave equation in the moving medium rather than the usual acoustic wave equation for a medium at rest. Qualitatively, one of the major effects of the sound-flow interaction is a refraction effect which for circular jets and coannular jets with conventional profiles tends to refract the sound away from the jet axis and creates a quiet zone along that axis. This effect is accentuated for heated jets and for coannular flows with the inner flow heated where temperature gradients as well as velocity gradients affect the sound transmission.

Figure 5.1 is similar to a figure presented by Ribner [10] and attempts to pictorially represent the effects of convection and refraction on the sound field generated by a jet flow. It should be noted that both the source convection effects and the refraction effects are small for sound radiated at 90° to the jet axis.

With this background, an attempt can be made to explain the reduced noise of the coannular flow with inverted profiles compared to conventional profile flow. Comparison of the sound pressure spectra at 90° for the inverted and conventional profiles presented in Chapter 4 revealed very little difference between the low and mid frequencies with the inverted profiles being slightly louder at high frequencies. The conclusion was, therefore, tentatively reached that the sound reduction at 30° was not mainly due to source modification but rather had to be also associated with either convective or refractive effects. Each of these will now be examined to determine whether they offer a possible explanation for the noise reduction.

The forward beaming of sound due to the motion of the sound sources depends primarily on the mean flow velocity through the

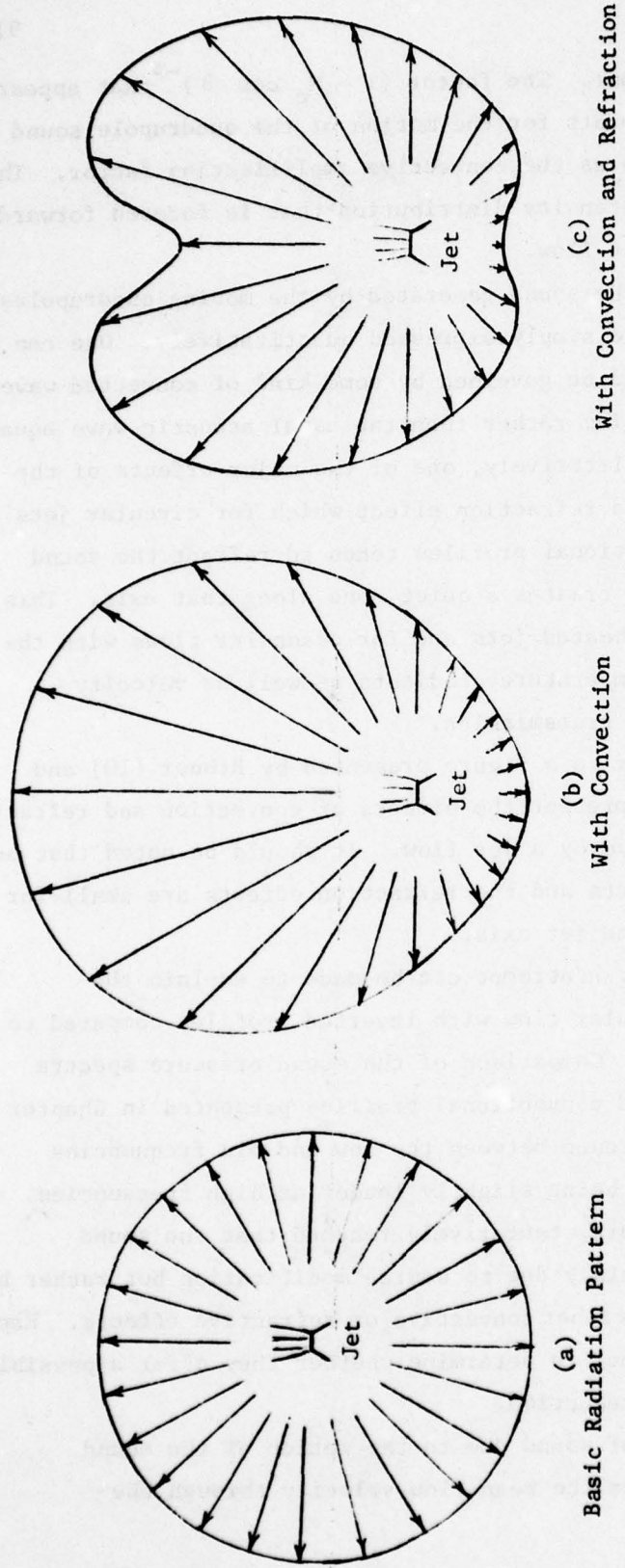


Figure 5.1. Effects of Convection and Refraction on the Sound Radiated from Randomly Oriented Quadrupoles.

convective Mach number in the factor $(1 - M_c \cos \theta)^{-5}$. If the maximum mean velocity of the flow is reduced, the sound intensity at small and moderate angles to the jet axis will be reduced in accordance with the above convection factor. This reduction is over and above any due to the source strength modification. Comparative mean velocity data (Figure 5.2) for the conventional profile and the inverted profiles show that the maximum mean velocity for the inverted profiles decays much more quickly than for the conventional profiles. This is because the high velocity jet exhausting from a comparatively thin annulus is slowed relatively quickly by the high turbulent shear forces acting on it. Thus the overall convective amplification effects should be smaller for the inverted profile causing a reduction of noise at small and moderate angles to the jet axis.

This qualitative argument can be strengthened by considering the differences in the spectra at 30° (See, for example, Figure 4.14). High frequency sound is generated close to the exit plane where the shear layer is thin and the mean velocity gradient is large. In this region both the acoustic source strength and the convective amplification are larger for the inverted velocity profiles so that more high frequency noise should be radiated to 30° for this configuration. This is observed in Figure 4.14. Very low frequency noise is generated relatively far downstream where the influence of the details of the initial profiles has been destroyed by the turbulent mixing. The velocity profile in fully developed region is governed primarily by the total momentum efflux from the nozzle which for the spectra shown in Figure 4.14 was the same. Sound in the mid-frequency ranges are probably generated primarily in the transition region where differences in the maximum mean velocity are the greatest as shown in Figure 5.2. Thus, these mid-frequencies would be most affected by differences in the convective amplification between the conventional and inverted velocity profiles. The inverted profile, having the lower maximum mean velocity in this region should radiate less mid-frequency sound to the microphone at 30° . This is also observed in Figure 4.14 and similar spectral comparisons.

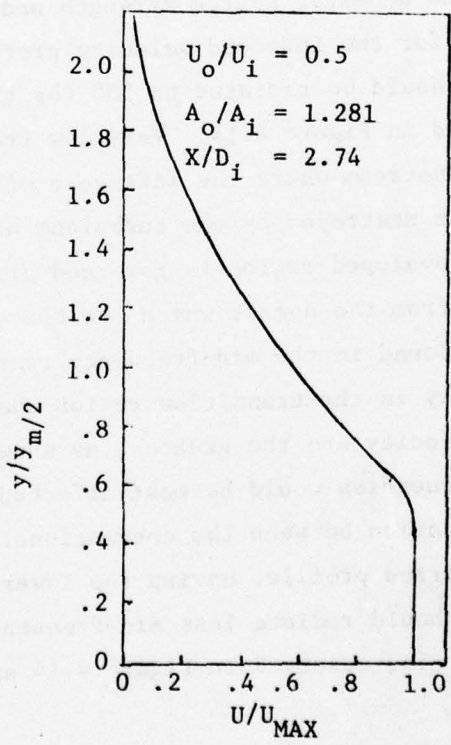
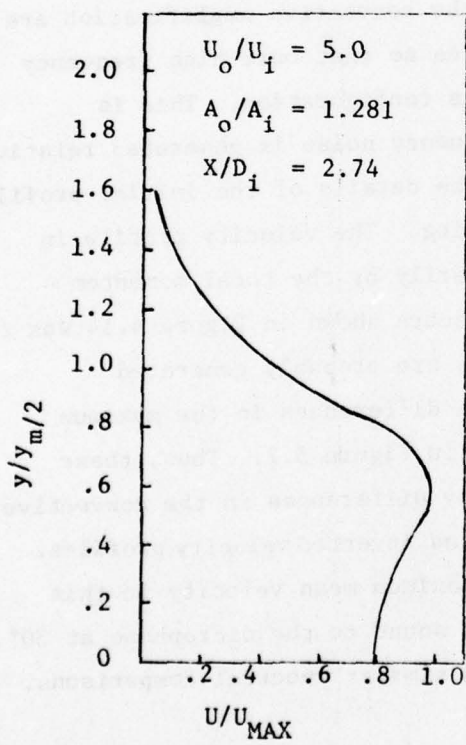
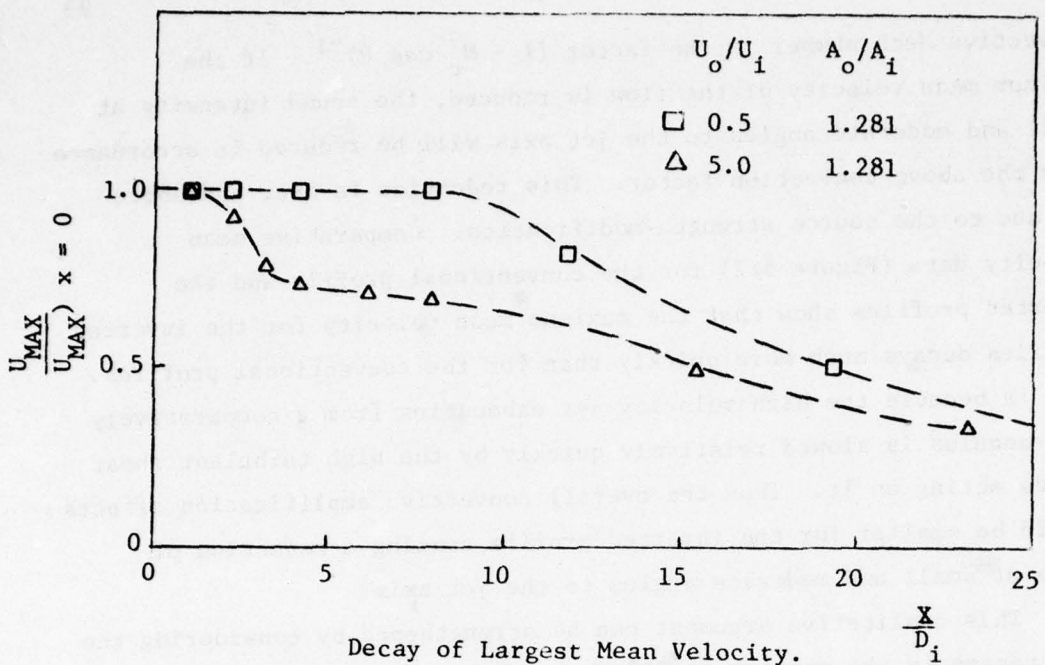


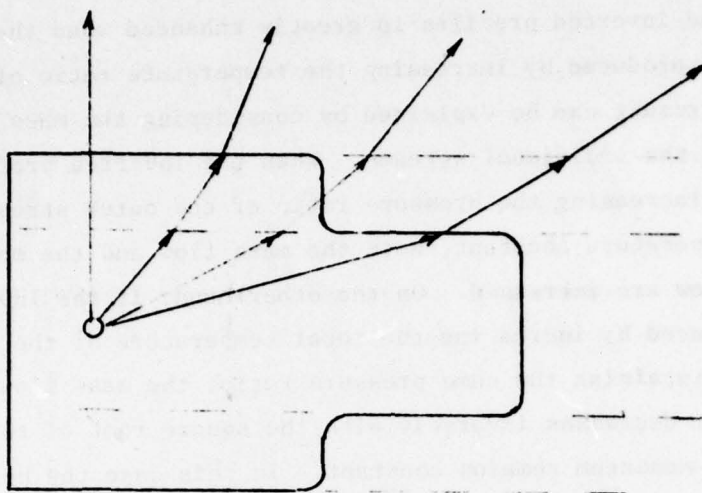
Figure 5.2. Mean Velocity Data from Reference [12], Cold Flow.

Finally, it has been observed that the differences between the conventional and inverted profiles is greatly enhanced when the velocity differences are produced by increasing the temperature ratio of the two streams. This result can be explained by considering the mass flow and momentum of the individual streams. When the inverted profile is produced by increasing the pressure ratio of the outer stream while holding the temperature constant, both the mass flow and the momentum of the outer flow are increased. On the other hand, if the inverted profile is produced by increasing the total temperature of the bypass stream while maintaining the same pressure ratio, the mass flow of the outer stream decreases inversely with the square root of the temperature and momentum remains constant. In this case the hot bypass air will rapidly lose its momentum by mixing with the cold ambient air and the convective amplification effect will be decreased.

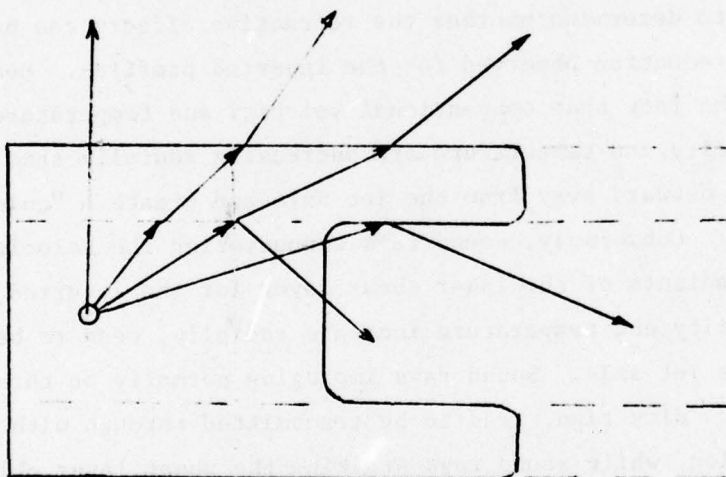
Next, consider the interaction between the radiated sound and the mean flow to determine whether the refractive effects can be responsible for the noise reduction observed for the inverted profiles. Mention has been made of the fact that conventional velocity and temperature profiles, where the velocity and temperature are decreasing radially tend to bend the sound rays outward away from the jet axis and create a "quiet zone" along the axis. Conversely, sound rays encountering the velocity and temperature gradients of the inner shear layer for the inverted profile, where the velocity and temperature increase radially, tend to be bent back toward the jet axis. Sound rays impinging normally on this shear layer in the 90° direction, tend to be transmitted through with very little alteration, while sound rays striking the shear layer obliquely tend to be partially reflected back into the flow and thus partially ducted down the flow tube. Figure 5.3 attempts to show pictorially the transmission effects produced by the conventional and inverted profiles for a coannular nozzle.

It can be argued the mid-frequency sound will be primarily affected by differences in transmission effects for the conventional and inverted profiles resulting in the spectral differences exhibited in Figure 4.14. As discussed before, the high frequency sound is primarily generated by the outer shear layer and therefore is not transmitted through the inverse velocity and temperature gradients. The very low

Sound Ray



a) Conventional Velocity Profile



b) Inverted Velocity Profile

Figure 5.3. Schematic of Flow-Acoustic Interaction for Conventional and Inverted Velocity Profiles.

frequency noise is probably generated far enough downstream that the velocity and temperature profiles for the conventional and inverted flows are becoming similar. The low frequency noise would then be generated by similar sound sources and subjected to the same transmission effects for both the conventional and inverted profiles. The mid-frequency sound is probably generated near enough to the exit plane that the inverse gradients would offer substantial impedance to the sound transmission and thus cause a reduction in the far field intensity at small and moderate angles to the jet axis.

Since the characteristic impedance of air is a strong function of temperature, it is clear that increasing the temperature of outer stream would enhance the effect of the inverted velocity profile on sound transmission. Indeed, Ahuja and Dosanjh [11] have shown that a heated annular flow can act as a shield to the noise generated by a cold inner jet even if the flow velocities are the same.

It appears then that both the convective amplification phenomena and the interaction of the transmitted sound with the mean flow could be contributing to the advantage that the inverted profile exhibits in sound radiation over the conventional profile. Cargill and Duponchel [2] have mentioned both of these phenomena as possibly being responsible for the noise reduction although they favor the acoustic-flow interaction. It appears to the authors of the present report that further experimentation is required to determine which one of these effects is dominating the noise reduction mechanism.

5.2 Noise Reduction Potential of Inverted Profiles.

It has been shown that the maximum noise radiated by a coannular jet with inverted velocity and temperature profiles is on the order of 10 dB quieter than that of a jet with conventional profiles at the same mass flow and thrust. This reduction is confined to the maximum noise radiation direction (about 30° to the jet axis) and there is little if any reduction in the sideline direction (90° to the jet axis). However, it is the noise radiated at small angles to the jet axis that is primarily reduced by the forward motion of the aircraft. Also,

an observer is generally twice as far from the aircraft when experiencing the noise radiated at 30° to the jet axis as when experiencing noise radiated at 90° to the axis (See Figure 5.4). Therefore it is pertinent to ask how much quieter a flying aircraft using a turbofan engine with inverted velocity profiles would appear to a stationary observer than a plane with a conventional turbofan engine. Some rough calculations have been made to attempt to estimate this difference.

Figure 5.5 shows the comparative directivities of the conventional and inverted JT8D take-off conditions for the 4-inch coannular nozzle as presented in Section 4.0.

This data has been corrected for forward speed effect using the empirical correction

$$\Delta \text{OASPL} = 10 \log_{10} \left(\frac{v_j}{v_j - v_\infty} \right)^n$$

where ΔOASPL is the difference between the OASPL at static and flight conditions, v_j is the maximum jet velocity, v_∞ is the flight velocity and n is an empirical exponent that ranges from about 3 at $\theta = 90^\circ$ to about 10 at $\theta = 30^\circ$. The values of n used in this estimate were taken from Reference [13].

Figure 5.6 shows the comparative directivities of the conventional and inverted JT8D conditions corrected for a forward speed of 300 ft/sec. From this figure an estimate can be made as to the difference in noise that a stationary observer would experience as the aircraft passes. When the aircraft with the conventional turbofan engine is at position P of Figure 5.4 the observer at O experiences say 106 dB (OASPL) as read from Figure 5.6. When the aircraft reaches position Q, the observer experiences an OASPL of 114.5 dB, where 6 dB has been subtracted from the value shown in the figure to account for the doubling of distance.

Although the preceding example calculation is very crude it does give some insight into the noise reduction potential of inverted profile engines showing the significant advantage of the inverted

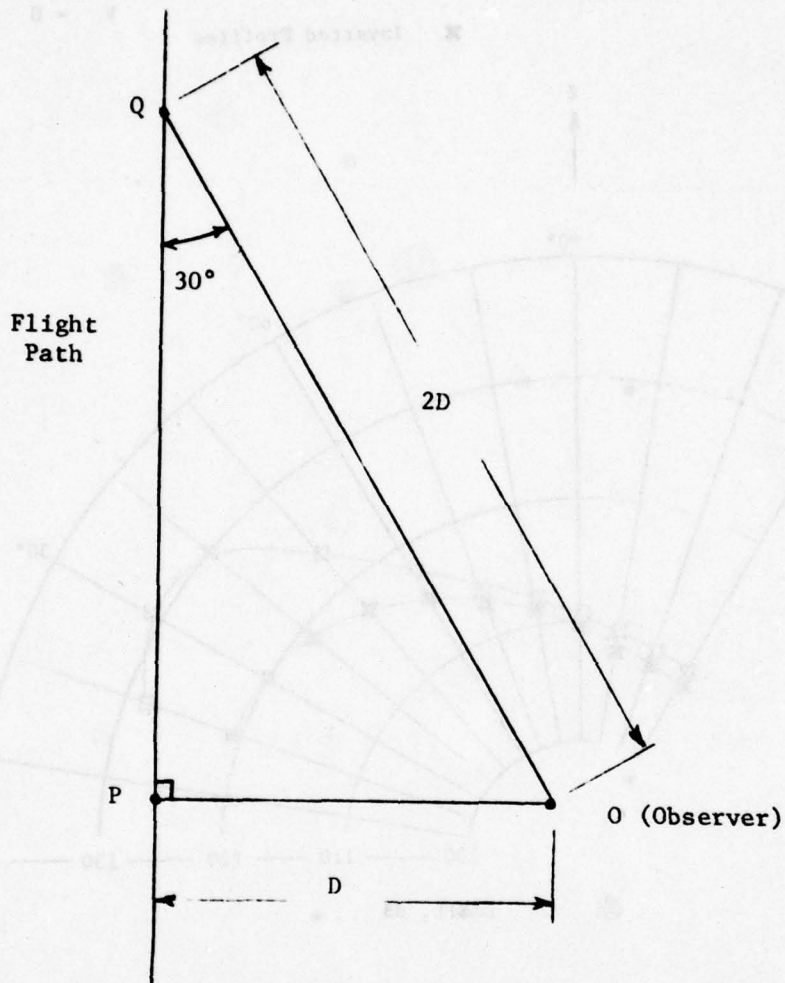


Figure 5.4. Relative Position of a Observer to Moving Aircraft.

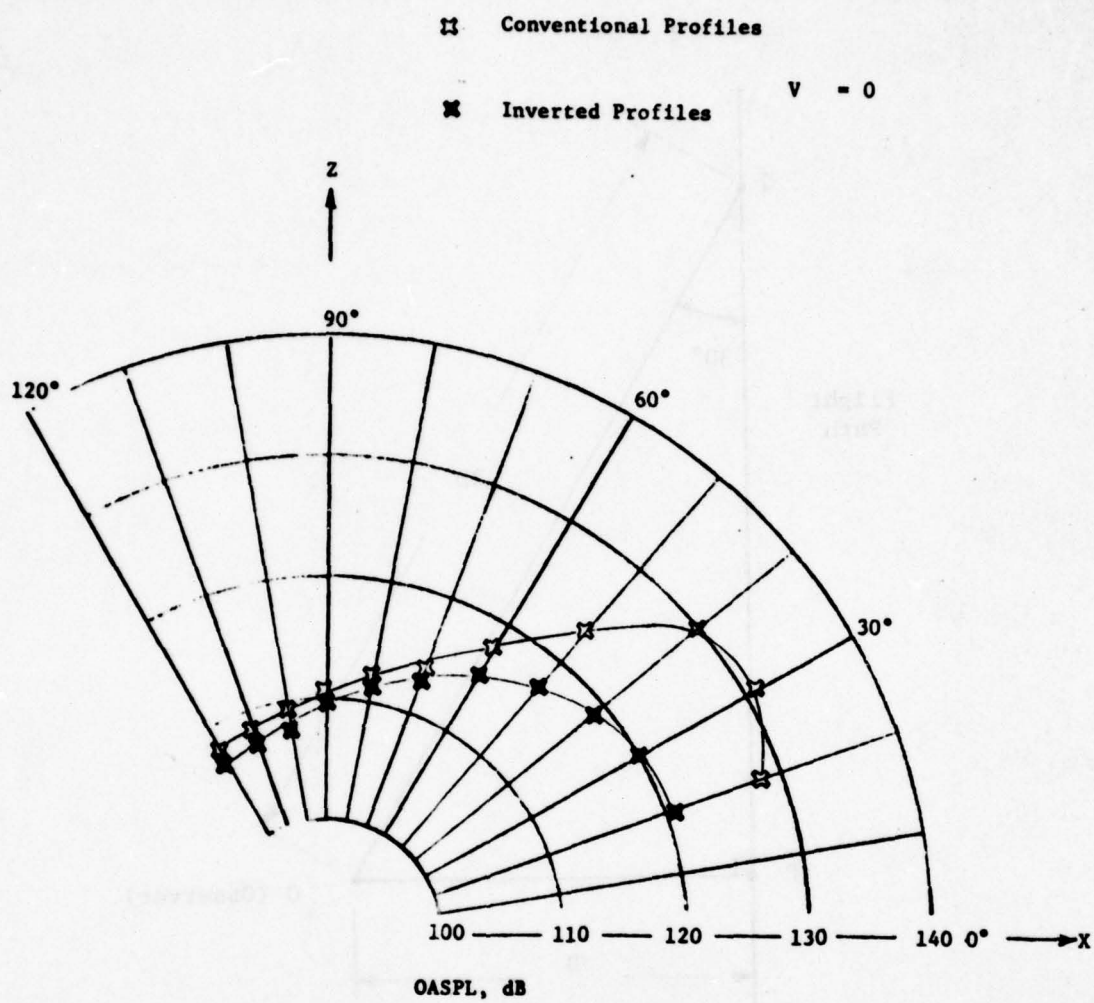


Figure 5.5. Comparison of Static Directivities for Conventional and Inverted JT8D Conditions with 4-Inch Nozzle.

JT8D Takeoff Conditions

△ - Conventional Profile

▲ - Inverted Profile

$V_{\infty} = 300 \text{ ft/sec}$

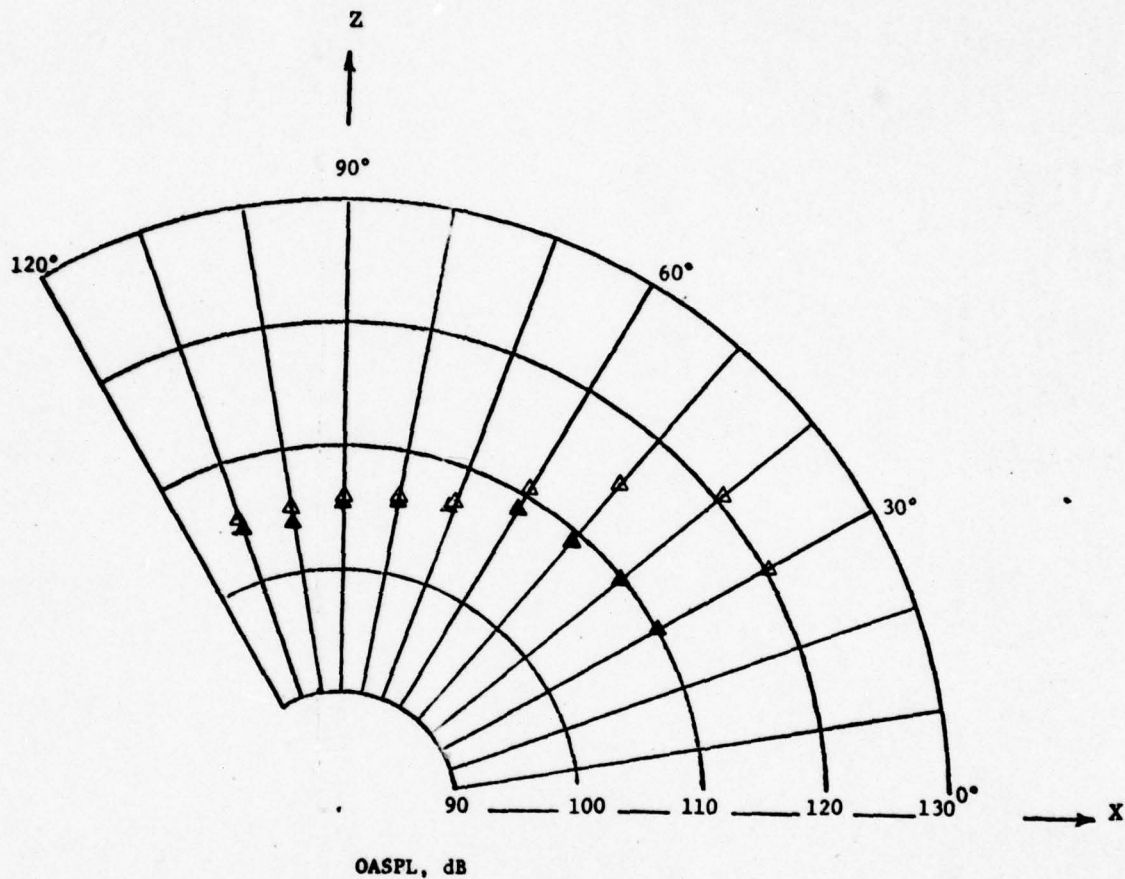
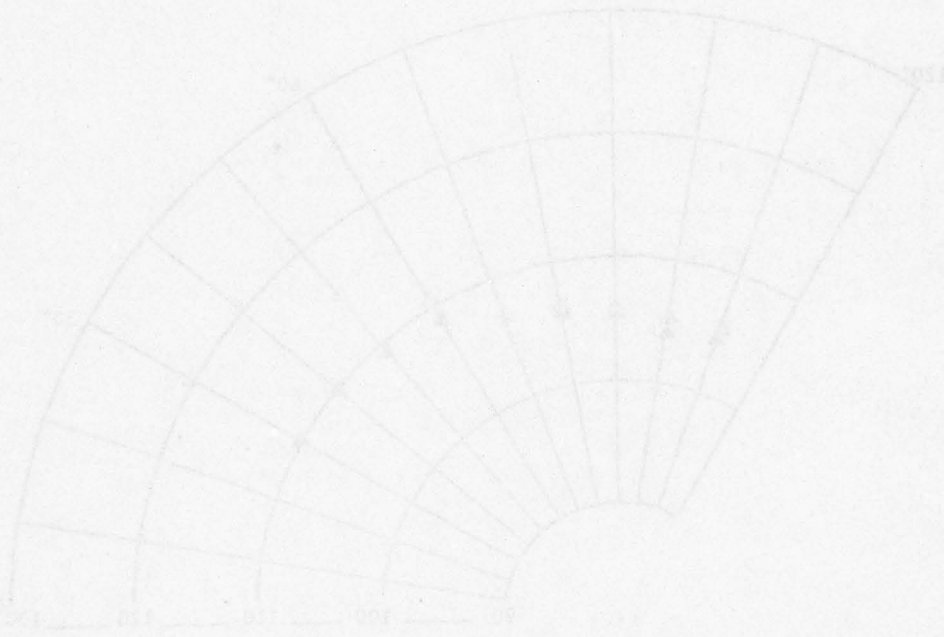


Figure 5.6. Comparison of Estimated OASPL Directivities for Conventional and Inverted JT8D Conditions with a Forward Velocity of 300 ft/sec.

profile over the conventional engine not only at static conditions but also at forward speed of the aircraft. It is interesting to note that the calculation for the inverted profile indicates very little difference in noise received by the observer when the noise is emitted when the aircraft is at position P or at position Q.



6.0 FLUID DYNAMIC MEASUREMENTS FOR CONVENTIONAL AND INVERTED PROFILES.

In order to gain further insight into the noise generation mechanism of coannular flows, fluid dynamic measurements were carried out in the flow field of a coannular nozzle using a Laser Velocimeter (LDV). Since it was desired to make these measurements for a heated flow where the difference in noise measured for the standard and inverted profiles is greatest, it was necessary to conduct the experiments in the free field facility where heated flow can be produced. A special support structure was fabricated to mount the LDV in a position to make measurements in this facility. Figure 6.1 shows the free field facility with the support structure in position and with laser and optics mounted on a rail-platform assembly. The support structure was designed to accommodate a traversing system with two degrees of freedom so that velocity and turbulence profiles can be obtained at several axial stations in the flow field. Figure 6.2 shows a close-up view of LDV optics system in position to make the velocity measurement near the nozzle exit plane.

The Laser Velocimeter used in these experiments was recently developed by the Gas Diagnostics Division at UTSI, and the measurements were carried out in collaboration with Dr. M. W. Farmer and Mr. J. O. Hornkohl of that Division. The coannular measurements described here were the first in which this instrument was employed and the signal processing system was continually being modified and improved during the course of the experiments.

A schematic of the LDV optical system used for measurements on the coannular aeroacoustic jet is shown in Figure 6.3. Light from a 15 milliwatt HeNe laser ($\lambda = 632.8 \text{ NM}$) is split into two beams of equal intensity. A lens of variable focal length brings the two beams to a simultaneous cross-focus in the region of measurement. During typical operation the optical system was adjusted such that the conversion constant, δ , from signal frequency to flow velocity was 70-100 microfeet/sec/MHz. Light scattered from the cross-focus region was collected in the forward scatter direction by an F/4 observation lens and focused to a variable slit covering a photomultiplier tube. This slit was usually adjusted to yield a minimum spatial resolution of 2-3 mm along the optical system axis, 0.5 mm

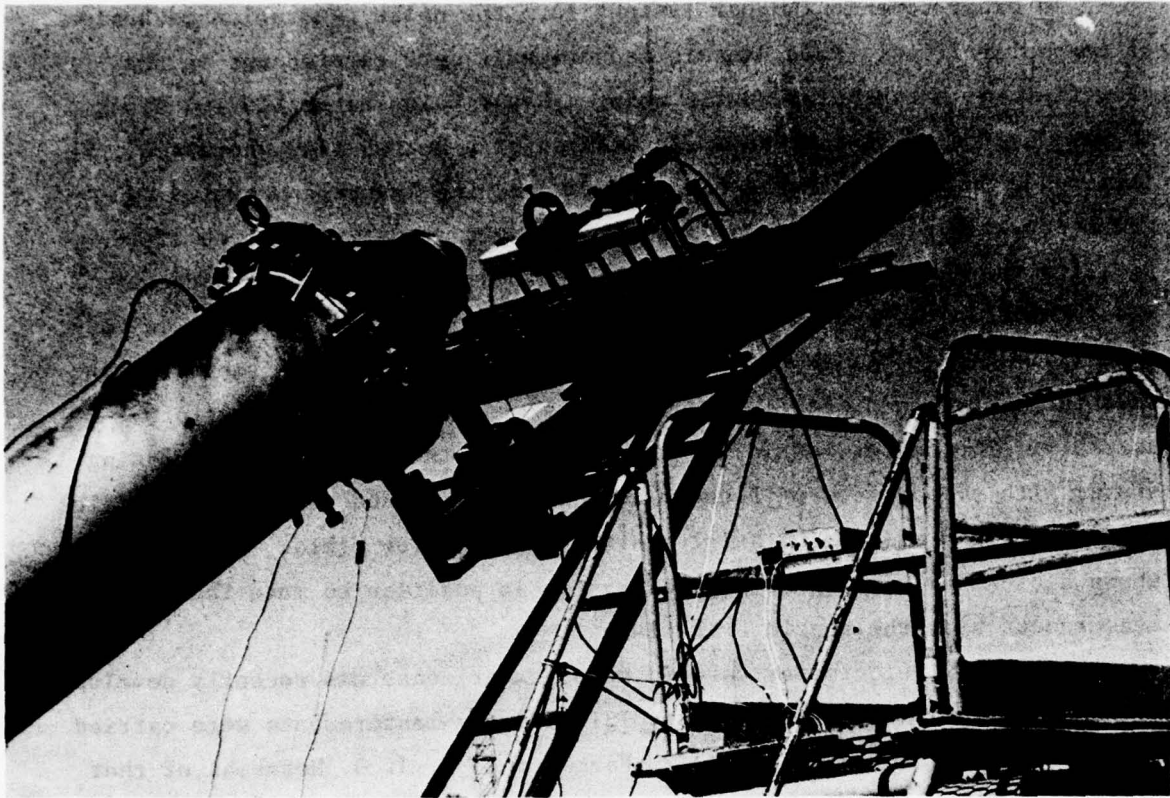


Figure 6.1 Photograph of LDV System Mounted on the Free Field Facility.

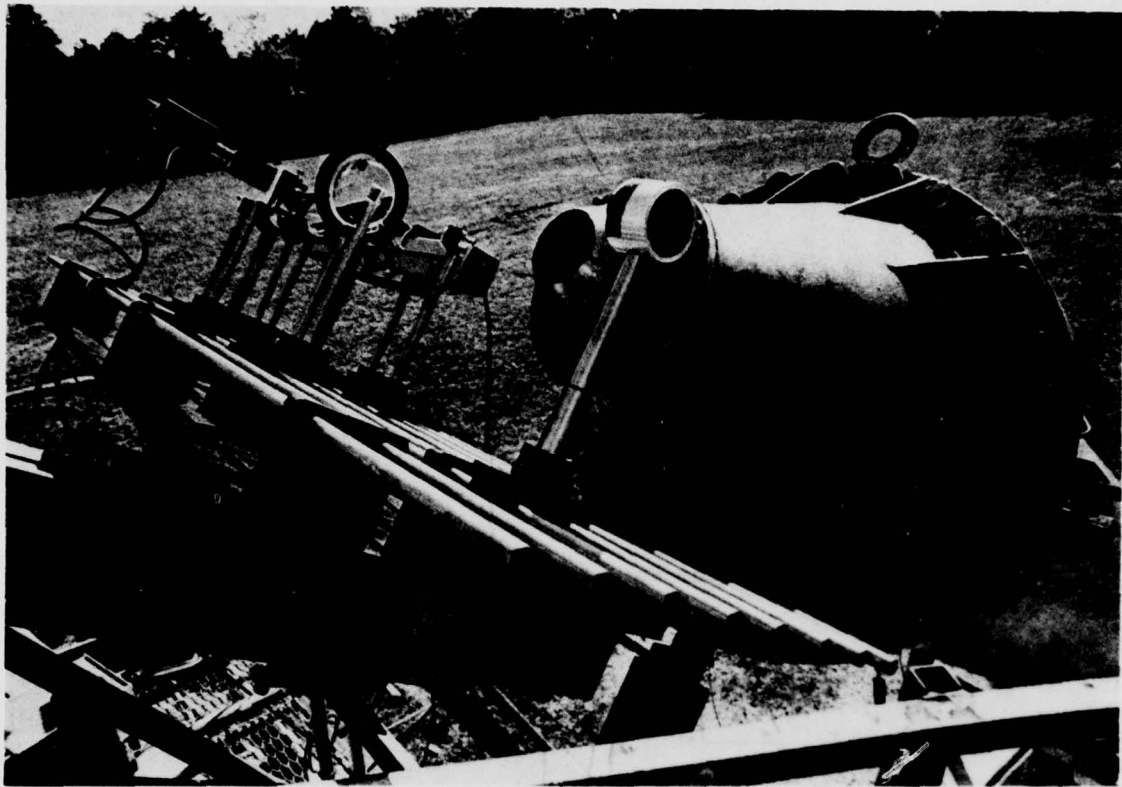


Figure 6.2. Photograph of Laser and Optics Mounted on Rail-Platform Assembly.

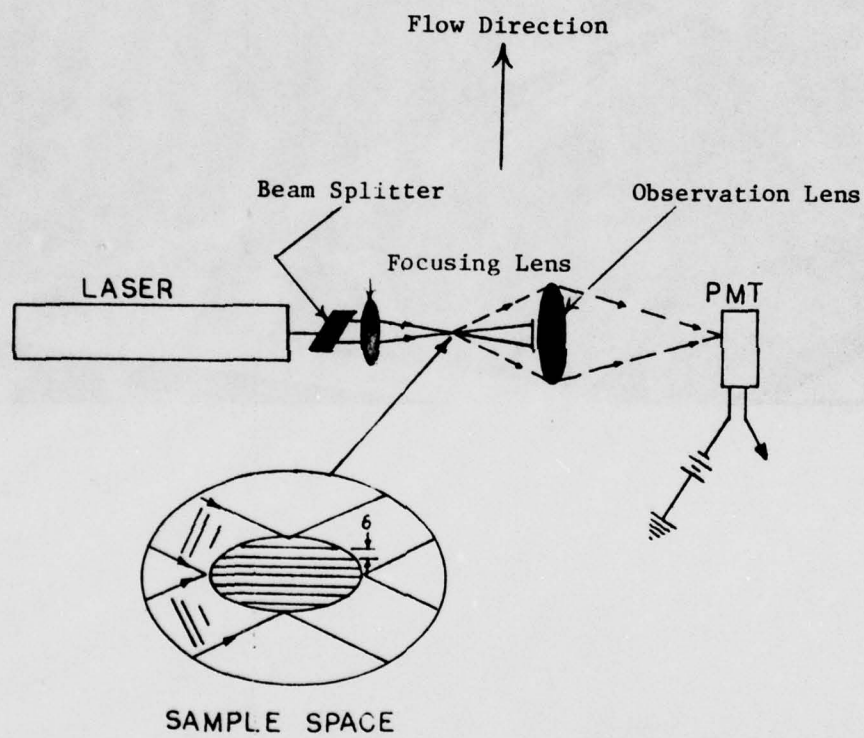


Figure 6.3. Schematic Diagram of Laser Velocimeter Optics.

parallel to the centerline of the flow, and 0.3 mm perpendicular to the direction of flow. A preamp with a gain of twenty was used to drive the LDV signal to the signal processing electronics located in the laboratory 70 m away from the jet. The entire optical system was mounted to a planar, two-dimensional transverse system for manually scanning the flow during a test.

The signal processing system consists of the instrument used to measure the time period of the LDV signal (a so-called burst processor) and a micro-computer system for storing and manipulating a data sample. After the incoming signal is low-pass filtered, the device measures the LDV signal time period by computing two averages of the time period over a pre-set number of signal cycles. For operation in these measurements one average was computed for 16 cycles of signal and one for 10 cycles. These averages are compared to determine if the signal is periodic within some pre-set limit. This limit ultimately determines the processor resolution and upper limit on system accuracy. Both signal time averages are stored in computer memory until a software program tests the averages for signal periodicity. Those measurements which pass the periodicity test are used to compute mean flow speed, standard deviation, and the kurtosis of the speed distribution. This information is recorded by a digital printer for hardcopy.

Should the operator choose, all measurements forming the distribution can be recorded to form histograms of the velocity distribution. The system operator is also free to instruct the system in the number of measurements which should enter a particular data sample. During typical runs, this was 200-400 measurements per sample and 2-5 samples were obtained per spatial position.

Two flow conditions were selected for the LDV measurements corresponding to simulated approach conditions for the JT8D engine with conventional and inverted velocity and temperature profiles. In order to allow sufficient run time to obtain profile data, the experiments were carried out using the 4-inch coannular nozzle. The flow parameters for these two conditions are listed in Tables 4.3 and 4.3a as conditions C and F. Comparative acoustic data are shown in Figures 4.11 and 4.12.

The profile data taken for the approach condition C with hot, high velocity inner flow and cold, low velocity outer flow are shown in Figures 6.4 and 6.5. Unfortunately, the traversing device used for these experiments did not have sufficient lateral range to traverse across the entire jet width. The LDV probe volume was initially set up near the centerline of the jet and the traverse was made through the jet center to the boundary of the outer shear layer. It was discovered during the course of the experiments that there could be up to 1/2-inch error in the location of the lateral position of the probe volume. This error combined with the uncertainty in the exact location of the jet centerline, an uncertainty which increases with distance from the jet exit plane, resulted in a lateral displacement of some of the profiles. Thus, some of the mean velocity and turbulence profiles shown in Figures 6.4 and 6.5 have been adjusted laterally so that axial momentum is approximately conserved.

The stepped profile shown in Figure 6.4 represents the exit velocity as calculated from the stagnation conditions assuming isentropic flow. The difference between the calculated maximum exit velocity and the measured exit velocity represents an error of between 3 and 5% and is probably associated with the uncertainty in the fringe pattern spacing in the sample volume (see Figure 6.3).

The LDV processor was being continually improved during the course of the experiments. Early in the measurement program when the profiles very close to the nozzle exit plane were being taken, the LDV processor had not been programmed to deliver turbulence information. Thus, the first turbulence intensity profile shown in Figure 6.5 was obtained at $x/D_0 = 2.25$.

The turbulence intensity values in Figure 6.5 are computed from the standard deviation of the individual velocity measurements,

$$u' = \frac{1}{N - 1} \sum_{i=1}^N (u_i - U)^2$$

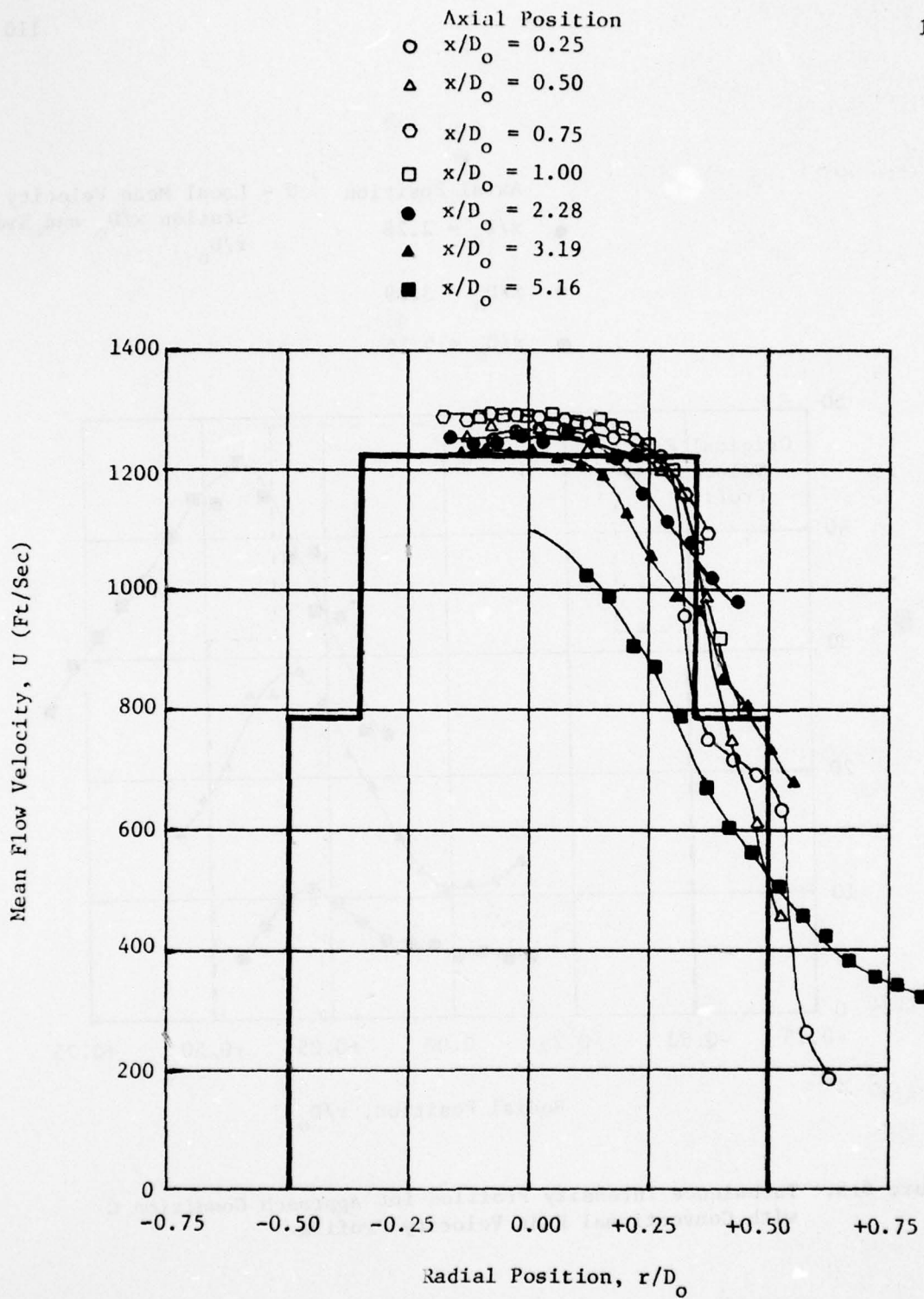


Figure 6.4. Mean Velocity Profiles for Approach Condition C with Conventional Exit Velocity Profile.

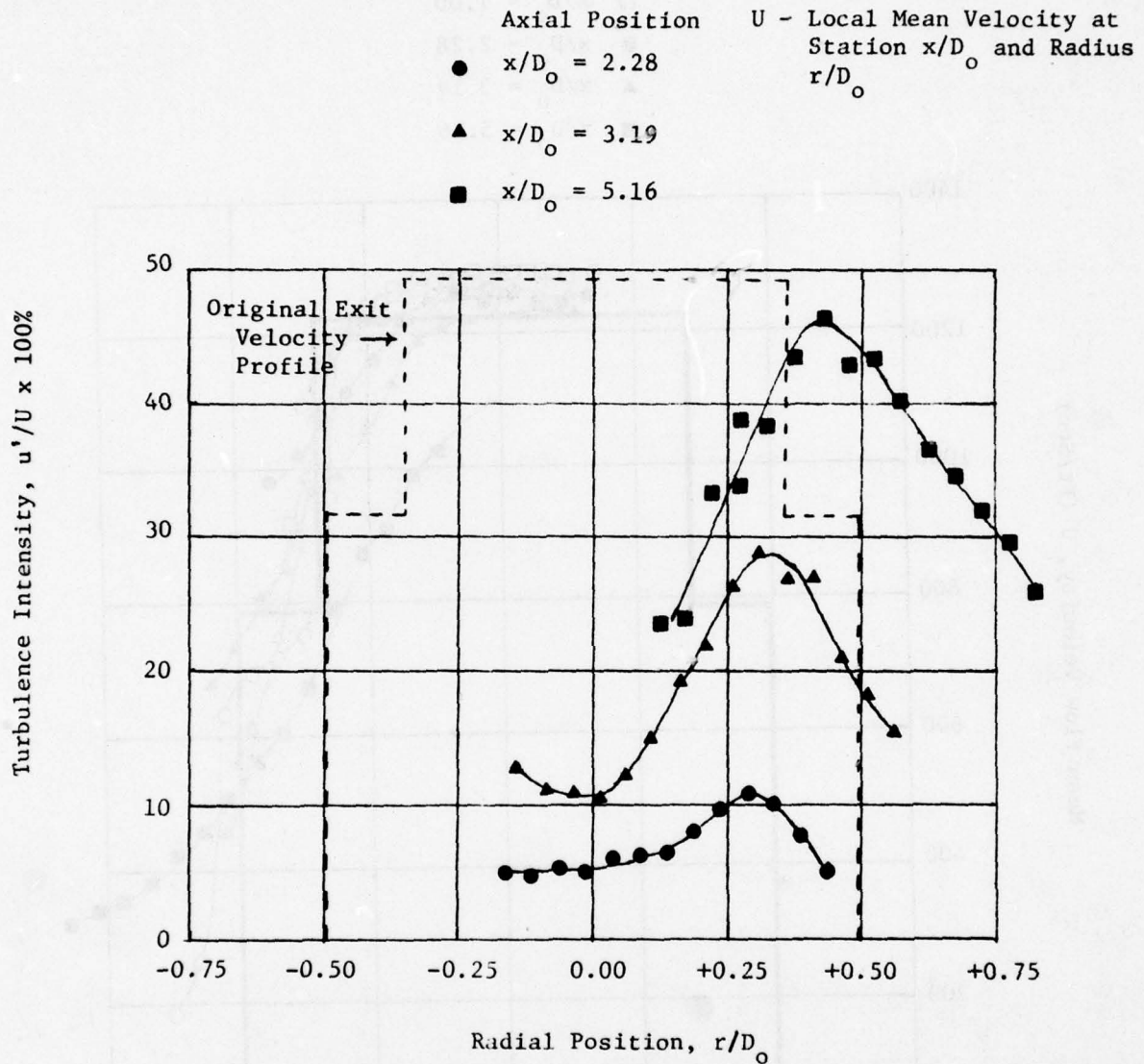


Figure 6.5. Turbulence Intensity Profiles for Approach Condition C with Conventional Exit Velocity Profile.

where

$$U = \frac{1}{N} \sum_{i=1}^N u_i$$

These values are normalized with respect to the local average velocity, U , yielding somewhat higher values than would be obtained by normalizing with centerline velocity or the jet exit velocity. Figure 6.5 shows that the turbulence level is increasing with distance from the jet downstream of $x/D = 2$; it may be speculated that further upstream this trend is reversed.

Figures 6.6 and 6.7 show profile data for the approach condition F with inverted velocity profiles. Unfortunately, the experimental program had to be curtailed before data could be obtained for axial positions greater than $x/D_0 = 2$. However, the data obtained is in the most interesting region. The mean velocity profiles in Figure 6.6 show that the maximum mean velocity decreases much more rapidly than occurs for the standard velocity profile. Also, Figure 6.7 shows that the turbulence level for the inverted profiles is much higher than that for the conventional profiles in the region $x/D_0 \approx 2$. The two results are certainly consistent. The very high turbulence level caused by the steep velocity gradients in the outer shear layer of the inverted profile indicate very large turbulent shear stress which would quickly reduce the velocity in the annular region.

Figure 6.8 and 6.9 are summary graphs showing the decay of the maximum mean velocity and the change in maximum turbulence intensity. Note in Figure 6.9 that the turbulence velocity is now normalized with respect to the maximum exit velocity so that the values can be compared directly. These graphs reveal dramatically the difference between the conventional and inverted profiles in the first few diameters. It is expected that if the measurements were taken further downstream the curves for the standard and inverted profiles would gradually come together. Both the maximum mean velocity and the maximum turbulence velocity should asymptotically approach the $1/x$ decay rate predicted by turbulence jet theory.

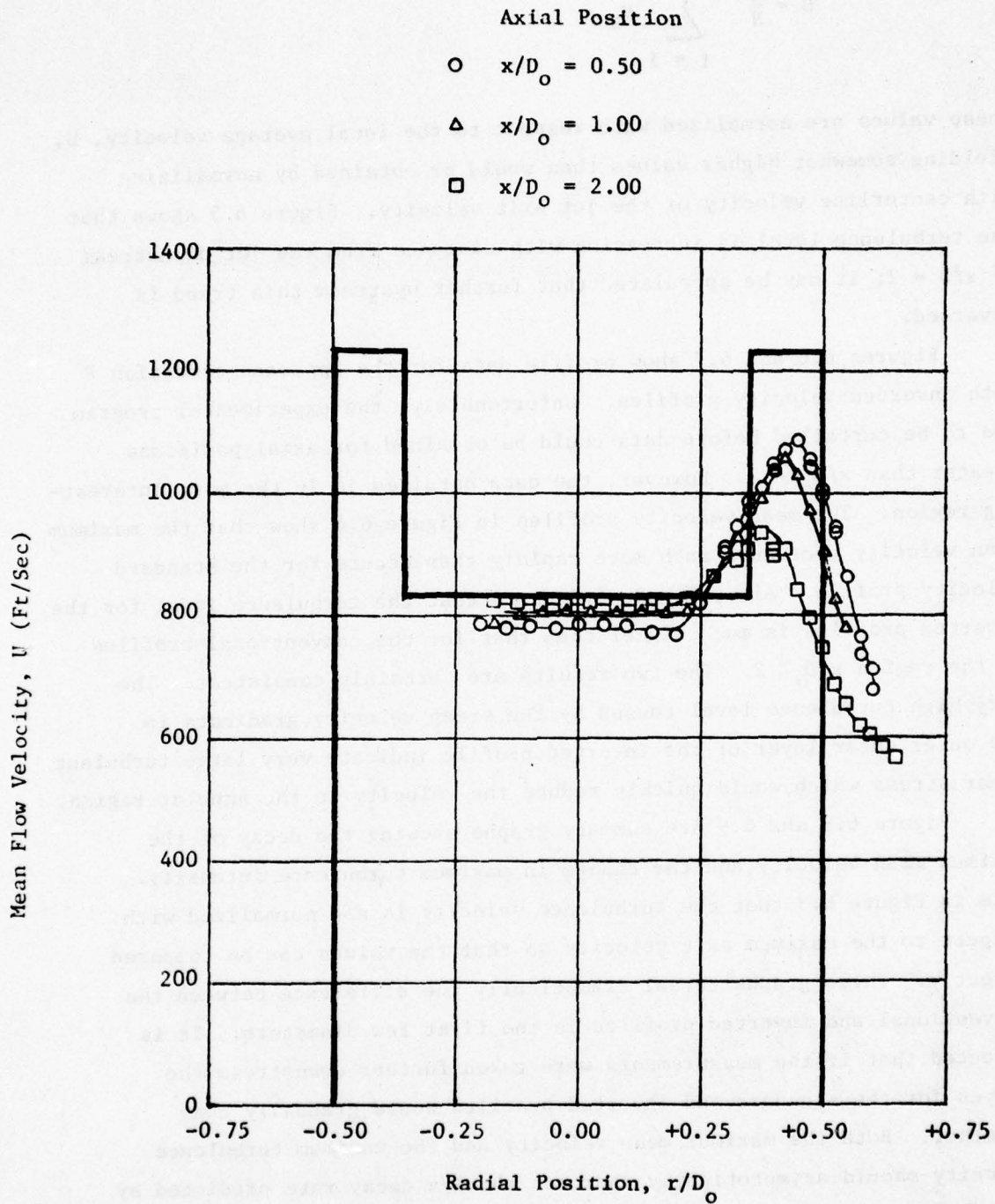


Figure 6.6. Mean Velocity Profiles for Approach Condition F with Inverted Exit Velocity Profile.

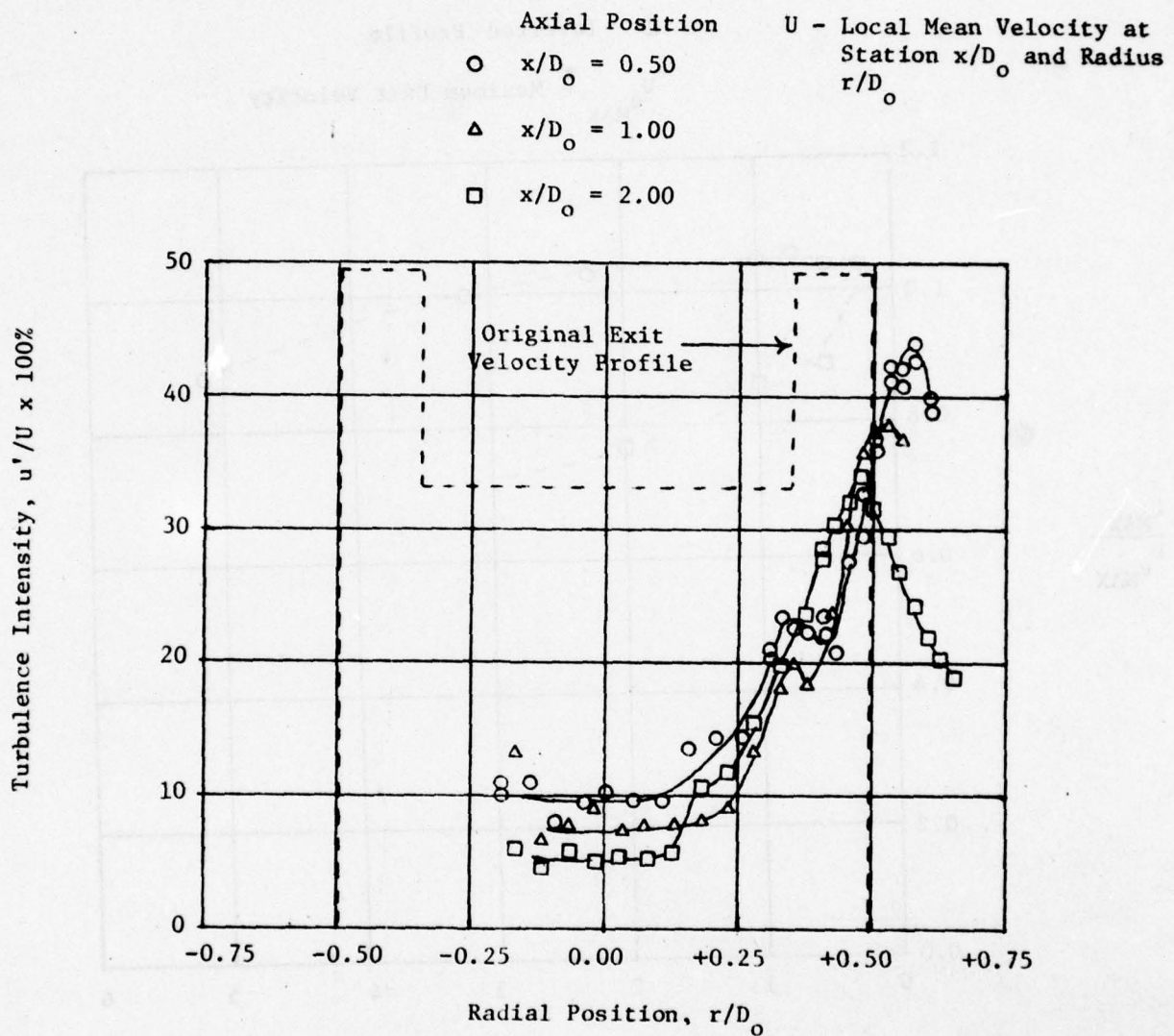


Figure 6.7. Turbulence Intensity Profiles for Approach Condition F with Inverted Exit Velocity Profile.

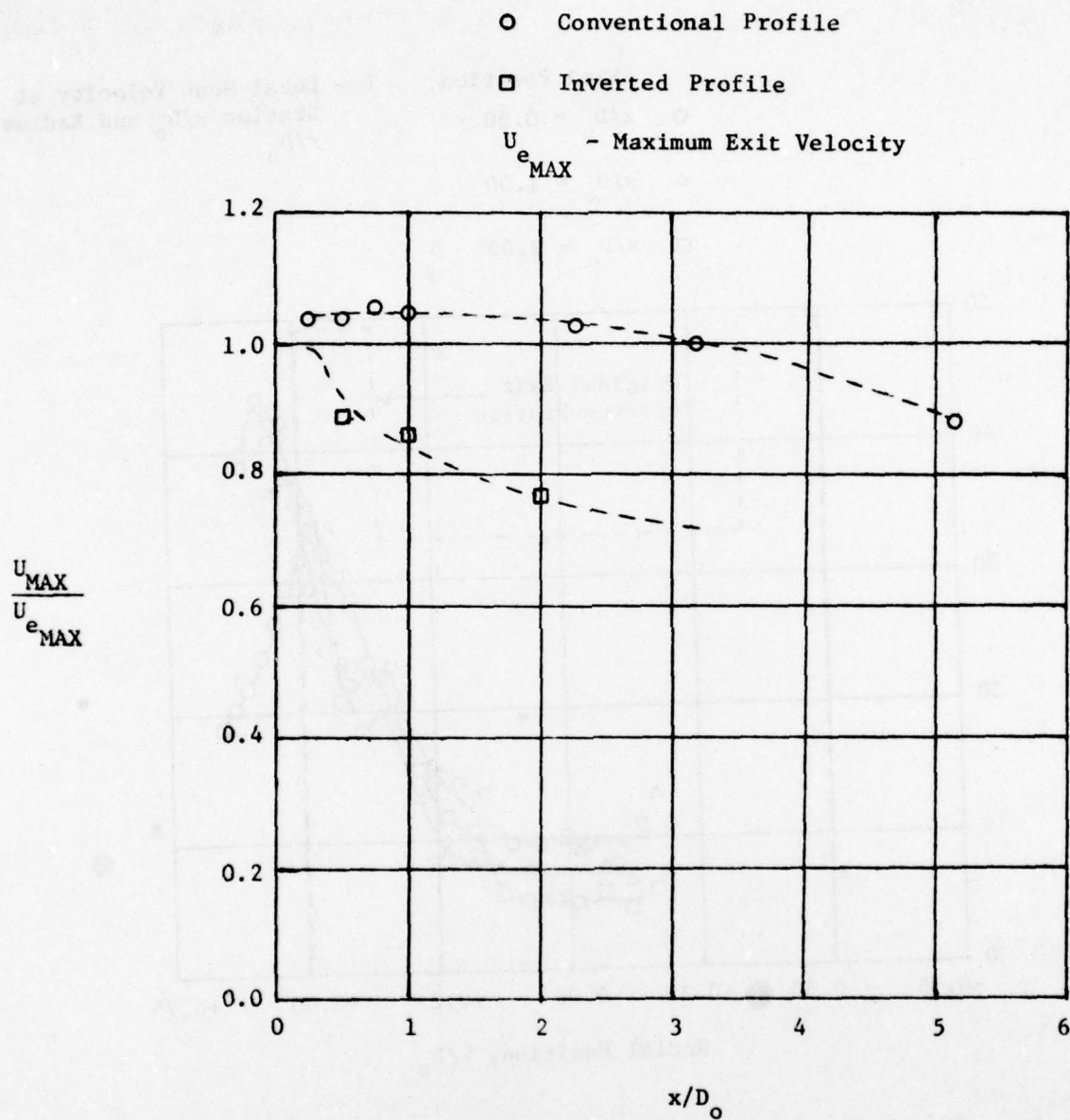


Figure 6.8. Comparison of Maximum Mean Velocities for Standard and Inverted Conditions. (LDV Data).

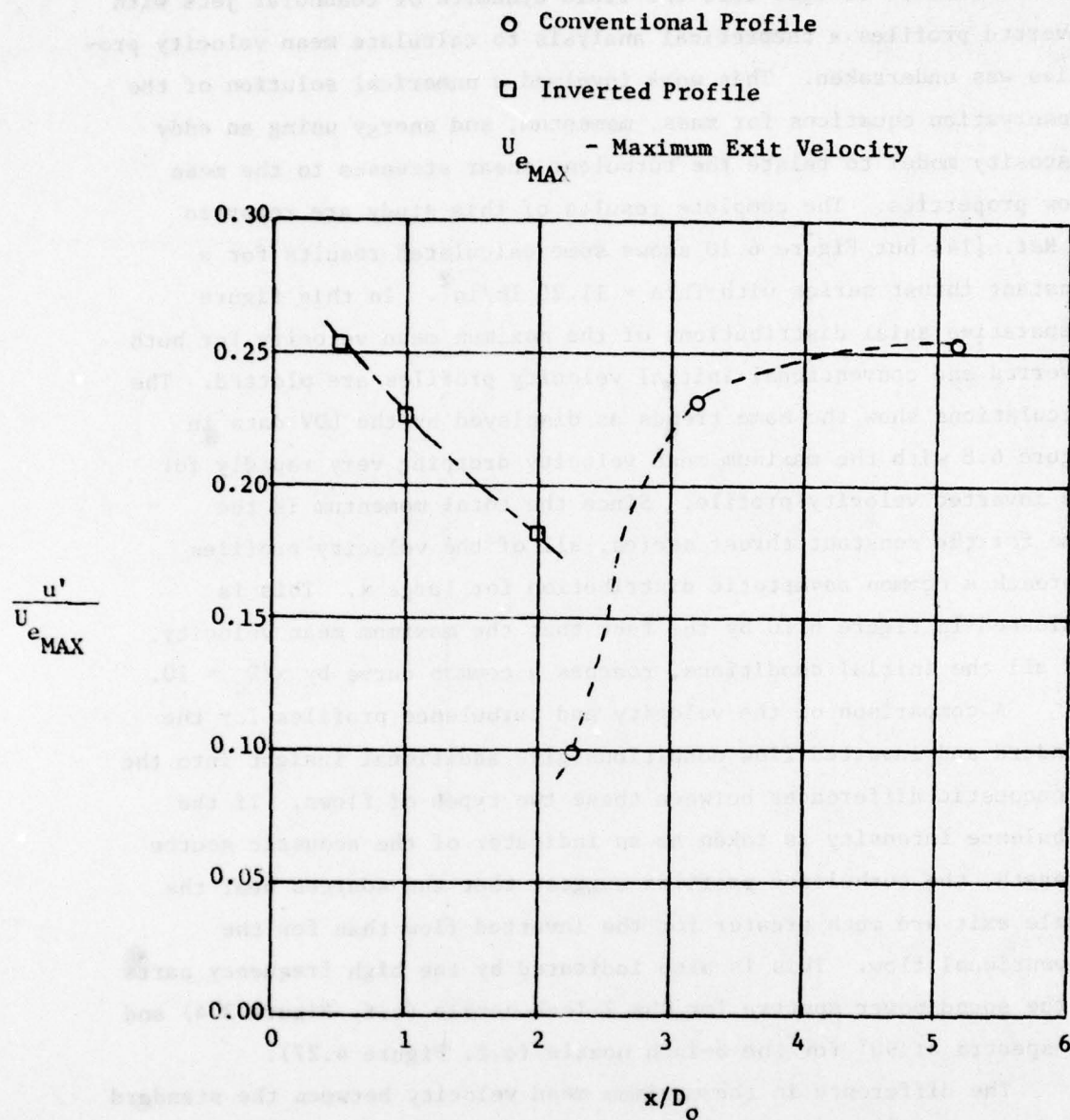


Figure 6.9. Comparison of Turbulence Velocities for Standard and Inverted Conditions. (LDV Data).

In order to supplement the limited laser data obtained and to achieve further insight into the fluid dynamics of coannular jets with inverted profiles a theoretical analysis to calculate mean velocity profiles was undertaken. This work involved a numerical solution of the conservation equations for mass, momentum, and energy using an eddy viscosity model to relate the turbulent shear stresses to the mean flow properties. The complete results of this study are reported in Ref. [14] but Figure 6.10 shows some calculated results for a constant thrust series with $Th/A = 11.20 \text{ lb/in}^2$. In this figure comparative axial distributions of the maximum mean velocity for both inverted and conventional initial velocity profiles are plotted. The calculations show the same trends as displayed by the LDV data in Figure 6.8 with the maximum mean velocity dropping very rapidly for the inverted velocity profile. Since the total momentum is the same for the constant thrust series, all of the velocity profiles approach a common asymptotic distribution for large x . This is indicated in Figure 6.10 by the fact that the maximum mean velocity, for all the initial conditions, reaches a common curve by $x/D_0 = 10$.

A comparison of the velocity and turbulence profiles for the standard and inverted flow conditions give additional insight into the aeroacoustic differences between these two types of flows. If the turbulence intensity is taken as an indicator of the acoustic source strength, the turbulence profiles suggest that the sources near the nozzle exit are much greater for the inverted flow than for the conventional flow. This is also indicated by the high frequency parts of the sound power spectra for the 2-inch nozzle (c.f. Figure 3.4) and the spectra at 90° for the 8-inch nozzle (c.f. Figure 4.27).

The difference in the maximum mean velocity between the standard and inverted flows shown in Figure 6.8 is thought to be one of the most significant results of the Laser Velocimeter measurements. The fact that the maximum velocity for the inverted flow is substantially less than that for the conventional flow over a considerable portion of the jet means that the convective amplification factor $(1 - M_c \cos \theta)^{-5}$ is smaller for the inverted by as much as a factor of 5 for $\theta = 30^\circ$. This difference is probably responsible for much of the noise reduction achieved by the inverted as compared to the standard profile.

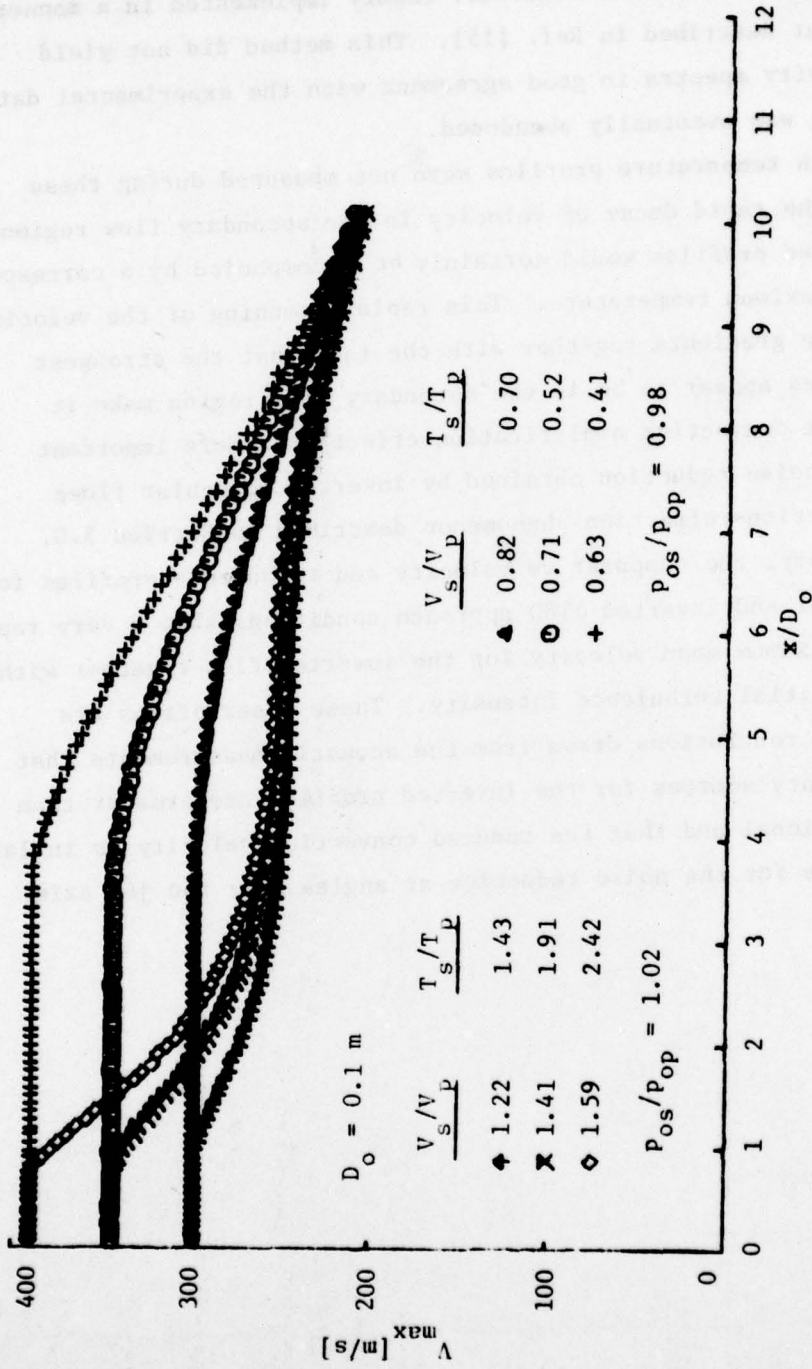


Figure 6.10. Decay of maximum velocity, comparison of standard and inverted configuration, constant thrust series, 11.1 lb/in².

An attempt was made to compute the sound field for standard and inverted profiles based on the mean flow calculations of Ref. [14]. This effort was based on the Lighthill theory implemented in a manner similar to that described in Ref. [15]. This method did not yield sound directivity spectra in good agreement with the experimental data and the effort was eventually abandoned.

Although temperature profiles were not measured during these experiments, the rapid decay of velocity in the secondary flow region for the inverted profiles would certainly be accompanied by a corresponding decay of the maximum temperature. This rapid smoothing of the velocity and temperature gradients together with the fact that the strongest acoustic sources appear to be in the secondary flow region make it likely that the convective amplification effect is a more important factor in the noise reduction obtained by inverted coannular flows than the reflection-refraction phenomenon described in Section 5.0.

In summary, the comparative velocity and turbulence profiles for the conventional and inverted JT8D approach conditions show a very rapid decay of the maximum mean velocity for the inverted flow together with a very large initial turbulence intensity. These observations are consistent with conclusions drawn from the acoustic measurements that the high frequency sources for the inverted profiles are greater than for the conventional and that the reduced convection velocity is in large part responsible for the noise reduction at angles near the jet axis.

7.0 SUMMARY AND CONCLUSIONS.

7.1 Overview of the Investigation.

An in-depth investigation of the noise characteristics of the exhaust jets from coannular nozzles with conventional and inverted profiles has been carried out. The investigation consisted of five principle phases listed below:

1. Reverberation Chamber Tests on a 2-inch nominal diameter coannular nozzle under cold flow conditions.
2. Free Field Tests on a 4-inch nominal diameter coannular nozzle under cold flow conditions.
3. Free Field Tests on the 4-inch diameter nozzle with either primary or secondary flow heated.
4. Free Field Tests on an 8-inch diameter coannular nozzle with either primary or secondary flow heated.
5. Laser Doppler Velocimeter measurements on the exhaust flow from the 4-inch nozzle with conventional and inverted profiles.

All tests were performed using circular coannular nozzles with equal primary and secondary area ($A_s/A_p = 1$).

The majority of the acoustic tests were carried out holding either the total thrust or the total mass flow of the jet exhaust constant while varying the velocity ratio, V_s/V_p . In the cold flow tests the change in the velocity ratio was accomplished by changing the stagnation pressure ratio of the primary and secondary stilling chambers. In the heated flow tests, the velocity ratio was varied primarily by changing the stagnation temperature of either the primary or secondary flow.

In the free field test facility, which was used for the bulk of the testing in this program, capability presently exists to heat only one flow stream. For this reason it was not possible to maintain both the thrust and mass flow simultaneously constant while varying the velocity ratio. In addition, for consistency, all tests for velocity ratio of one ($V_s/V_p = 1$) were performed with both streams

unheated. This constraint usually resulted in the equal velocity condition yielding the minimum noise level in a constant thrust or constant mass flow series. This condition corresponds to very low energy input and is not very meaningful for practical applications.

Since the primary and secondary exit areas for the nozzles tested were the same, inverse run conditions where stagnation pressures and temperatures of the primary and secondary streams were interchanged resulted in comparable conventional and inverted profiles with the same thrust and the same mass flow at equal energy input. Most of the comparisons cited in the report are made between these types of profiles, where $V_s/V_p)_{Inv.} = V_p/V_s)_{Std.}$

In addition to the constant thrust and constant mass flow series a number of tests were made on the 4-inch and 8-inch nozzles simulating the take-off, cut back, and approach conditions of the JT8D engine. Corresponding inverse flow conditions were also tested for direct comparisons.

The final phase of the investigation involved Laser Doppler Velocimeter measurements to determine mean velocity and turbulence data on the simulated approach conditions for the JT8D engine with standard and inverted velocity and temperature profiles. These measurements were made with an LDV recently built at UTSI by the Gas Diagnostics Division.

7.2 Summary of Major Results.

Unless otherwise noted all acoustic comparisons cited in this summary will refer to comparisons between conventional and inverted profile flows at the same total thrust, the same total mass flow, and at equal energy input.

7.2.1 Cold Flow Results.

Reverberation chamber measurements in the cold-flow tests on the 2-inch coannular nozzle revealed very little difference in the overall sound power produced by the standard and inverted profiles at the same thrust and mass flow. Comparison of sound power spectra (Figure 3.4) showed that the high frequency noise generated by the inverted profile was greater and that the low frequency noise was reduced.

Similar cold flow comparisons in the free field on the 4-inch coannular nozzle showed (Figure 3.7) a moderate reduction (< 5 dB) in the intensity in the direction of maximum noise radiation for the inverted profile. The sound pressure level at 90° to the jet axis was only slightly different for the conventional and inverted profiles. Comparison of the sound pressure levels in the region of maximum noise radiation at about 30° (Figures 3.10 and 3.11) indicate that the noise reduction achieved by the inverted velocity profile improves as the thrust level and velocity ratio increases. The sound pressure spectra at 30° (Figure 3.9) show that the inverted velocity profile has a much flatter spectra with more high frequency noise radiated and less low frequency noise compared to conventional profile at the same mass flow and the same thrust.

7.2.2 Hot Flow Results.

Free field tests on the 4-inch coannular nozzle where either the primary or secondary flow stream was heated yield trends which are generally similar to those obtained in cold flow. However, the difference between the noise levels of the conventional and the inverted profile flows is much greater in the case of heated flow. A comparison of hot and cold flows, at the same thrust and the same velocity ratio (Figure 3.10 and Figure 4.7) show that the noise reduction achieved by the inverted profile where the outer flow is heated is much greater than when both flows are cold. A direct comparison between the maximum sound radiated at 30° for the simulated JT8D conditions and the corresponding inverted flow conditions show a 10 dB advantage for the inverted profiles over the entire thrust range.

A comparison of the sound pressure spectra at 30° to the jet axis (Figure 4.4) show that the spectrum for the inverted velocity profile is much flatter than that for the conventional profile. At very high thrust levels, the sound pressure spectra for the inverted profile develops a double peaked character such as shown in Figure 4.10.

The noise reduction exhibited by the inverted profile flows is greatest in the region of maximum noise radiation, that is, at angles

less than 45° to the jet axis. For radiation angles greater than 60° there is very little difference between the noise radiated by conventional and inverted profiles with the same thrust and total mass flow. A comparison of spectra at 90° , in fact, shows only an increase in the high frequency noise for the inverted profile without the decrease in low and mid-frequency noise that occurs at 30° , (Figure 4.17). This result suggests that the noise reduction observed at the lower angles may not be due primarily to a decrease in the strength of the acoustic sources in the inverted flow. It is thought that the principal mechanisms of noise reduction may be the reduced convection effect in the inverted flow and an increase in the interaction between the radiated sound and the high velocity, high temperature outer mean flow.

7.2.3 Comparison with Synthesized and Mixed Flow.

The acoustic results for both the conventional and inverted profile flows have been compared with semi-empirical estimates for synthesized flow and fully mixed flows. The synthesized flow estimates were determined by converting the secondary flow annulus to a circular area and adding the sound intensities of the two circular flows without considering mutual interference. This technique has been recommended [Ref. 5] for estimating the noise output of standard profile coannular flows. In the present study, the results of the synthesized calculations were found to agree reasonably well with measured acoustic data for standard velocity profiles, although somewhat overpredicting the noise output at high thrust and high velocity ratio (V_p/V_s). The synthesized sound level is a somewhat arbitrary standard and to assess the noise reduction potential of the inverted profile flows it is much more meaningful to compare with an equivalent fully mixed exhaust flow. Any coannular flow with conventional or inverted velocity profile can theoretically be converted to a fully mixed flow with the same total thrust and the same total mass flow. The computed sound pressure level for the fully mixed flow generally fell approximately mid-way between measured values for the standard profile and the inverted profile. These results indicate that the noise reduction obtainable by mixing the standard coannular profile is only about one-half of that achievable by inverting the velocity profile.

7.2.4 Effect of Nozzle Size.

Comparison of the acoustic data for the 4-inch and 8-inch coannular nozzles show that the overall sound pressure level scales very well with nozzle area (Figure 4.23). Applying standard Strouhal scaling to the observed sound frequencies reduced the 4-inch and 8-inch sound pressure spectra to comparable curves (Figures 4.15, 4.16). Although there is some discrepancy in the location of the peak frequency and some deviation in the high frequency sound levels, the overall agreement is considered to be reasonably good.

7.2.5 Results of LDV Measurements.

The mean velocity and turbulence measurements taken on the 4-inch coannular nozzle reveal clearly the great differences in the flow fields of the conventional and inverted conditions in the first few diameters. For the inverted flow the maximum mean velocity drops very rapidly initially and quickly reaches a plateau value at about the inner jet velocity. On the other hand, the maximum mean velocity of the conventional profile flow remains near the inner jet exit velocity for several diameters before beginning to decay. Thus there is a region of several diameters where the maximum velocity of the conventional flow is substantially higher than that of the inverted flow. This result supports the suggestion that differences in the convective effect between the two flows is contributing to the differences in the noise radiation.

The turbulence intensity profiles indicate that, as expected, near the nozzle exit plane the turbulence level for the inverted profile is much higher than for the standard profile. This suggests that the noise sources in that region are greater for the inverted profile and is consistent with the increase of high frequency noise observed for that type flow.

Some results from a theoretical investigation of the free turbulent mixing of coannular jets are reported to give additional insight into the comparative evolution of coannular flows with conventional and inverted profiles. Complete results of this study are given in a Master's thesis by Dathe [14].

7.3 Conclusions.

The results of this study show that coannular flows with inverted velocity profiles are quieter than standard velocity profiles at the same thrust and mass flow. The acoustic differences between these two types of flow are much greater when the velocity differences between the inner and outer streams are caused by changes in the stagnation temperatures rather than by changes in the stagnation pressure ratios of the primary and secondary flows. The major differences in the sound fields occur at angles less than 45° from the jet axis, where the greatest noise is radiated, and result from a reduction of the peak frequency noise of the standard profile.

The reduction in noise obtained by the inverted velocity profile is thought to be largely due to the rapid decay of the maximum mean velocity that occurs compared to the standard velocity profiles. This implies that the source convection velocity is reduced with a corresponding reduction in sound radiated near the jet axis. The fact that the effect is enhanced when the secondary flow is heated is due to the fact that the low density, high temperature secondary air loses its momentum more rapidly by mixing with the cold ambient air.

The noise reduction obtainable by mixing a standard profile coannular flow to produce a uniform velocity profile with the same thrust is less than that attainable by inverting the standard profile.

Standard jet noise scaling techniques can be applied to coannular flows with inverted velocity profiles to determine large scale noise levels from model tests provided the area ratios are the same.

7.4 Limitations of the Study.

In the present test series only one flow stream, either primary or secondary, could be heated. This limitation prevented the investigation of intermediate conditions between hot primary - cold secondary and hot secondary - cold primary. By controlled heating of both streams it would be possible to investigate the influence of varying velocity ratio over a wide range of value while holding both the total thrust and the total mass flow constant.

In the present study only coannular nozzles with area ratios of one were tested. While this provided a convenient way of directly comparing the standard and inverted profile flows it may not be near the optimum nozzle configuration. Additional studies investigating systematically the influence of area ratio and controlled heating of both streams would be useful.

1. ...
2. ...
3. ...
4. ...
5. ...
6. ...
7. ...
8. ...
9. ...
10. ...
11. ...
12. ...

REFERENCES

1. Packman, A. B., H. Kozlowski, and O. Gutierrez, "Jet Noise Characteristics of Unsuppressed Duct Burning Turbofan Exhaust System" AIAA Paper 76-149 January 1976.
2. Cargill, A. M. and J. P. Duponchel, "The Noise Characteristics of Inverted Velocity Profile Coannular Jets," AIAA Paper 77-1263, October 1977.
3. Goethert, B. H. et al., "Investigation of Feasible Nozzle Configurations for Noise Reduction in Turbofan and Turbojet Aircraft." FAA-RD-75-163-1 July 1975.
4. Gutierrez, O. A., "Aeroacoustic Studies of Circular Nozzles Suitable for Supersonic Cruise Aircraft Applications," Proc. of the SCAR Conference, Part 2, Nov. 1976.
5. Jet Noise Prediction. Aerospace Information Report 876 SAE, July 1965.
6. Kozlowski, H., and A. B. Packman, "Aerodynamic and Acoustic Tests of Duct Burning Turbofan Exhaust Nozzles," NASA CR 2628, December 1978.
7. Lighthill, M. J., "On Sound Generated Aerodynamically, I, General Theory" Proc. Royal Soc. London 211A, pp. 564-587, 1952.
8. Lighthill, M. J., "Jet Noise" AIAA Journal, v. 1, pp. 1507-17, 1963.
9. Ffowcs-Williams, J. E., "The Noise from Turbulence Convected at High Speed," Phil. Trans. Roy. Soc. (London) A255, pp. 469-503, 1963.
10. Ribner, H. S., "Quadrupole Correlations Governing the Pattern of Jet Noise." J. Fluid Mechanics, v. 38, pp. 1-24, 1969.
11. Ahuja, K. A. and D. S. Dosanjh, "Heated Fluid Shroud for Noise Reduction - An Experimental Study" AIAA Paper 77-1286, October 1977.
12. Champagne, F. H. and I. J. Wignanski, "An Experimental Investigation of Coaxial Turbulent Jets" International Journal of Heat and Mass Transfer, v. 14, pp. 1445-64, Sept. 1971.
13. Packman, A. B. and K. W. Ng., "Effect of Simulated Forward Speed on the Jet Noise of Inverted Profile Coannular Nozzles." AIAA Paper No. 77-1329, October 1977.

14. Dathe, Ingo, "A Theoretical Investigation of the Free Turbulent Mixing of Coannular Jets." Master's Thesis, The University of Tennessee Space Institute, June 1978.
15. Larson, R. S., "Theoretical Jet Exhaust Model for Duct Burning Turbofan" AIAA Paper 77-1264, October 1977.